Studies on Fluorescent Probe Composed of Artificial Nucleic Acids for Detection of Natural Nucleic Acids

(天然核酸検出に向けた人工核酸を有する蛍光プローブに関する研究)

Yanglingzhi Chen

2022

Contents

Chapter 1. Natural Nucleic Acids

1.1 An introduction to natural nucleic acid

1.1.1 Fundamental characterization

Since Watson & Crick revealed double-helix structure (Figure 1.1.1a) of deoxyribonucleic acid (DNA) from X-ray diffraction image,[1] natural nucleic acid has gradually became the most popular oligomer all over the world. In the natural nucleic acids, such as DNA, four kinds of base-group (adenine, thymine, guanine, and cytosine) are modified on the ribose. Monomers of the ribose are linked through 3', 5'-phosphodiester bonds and form nucleotides. Base group in the nucleotides specifically from hydrogen bonds to corresponding base-group, following the principle of complementary base pairing: the adenine/thymine and guanine/cytosine (Figure 1.1.1b). High sequence specificity of nucleotides enables orthogonal recognition of DNA, enabling storage of genetic information.

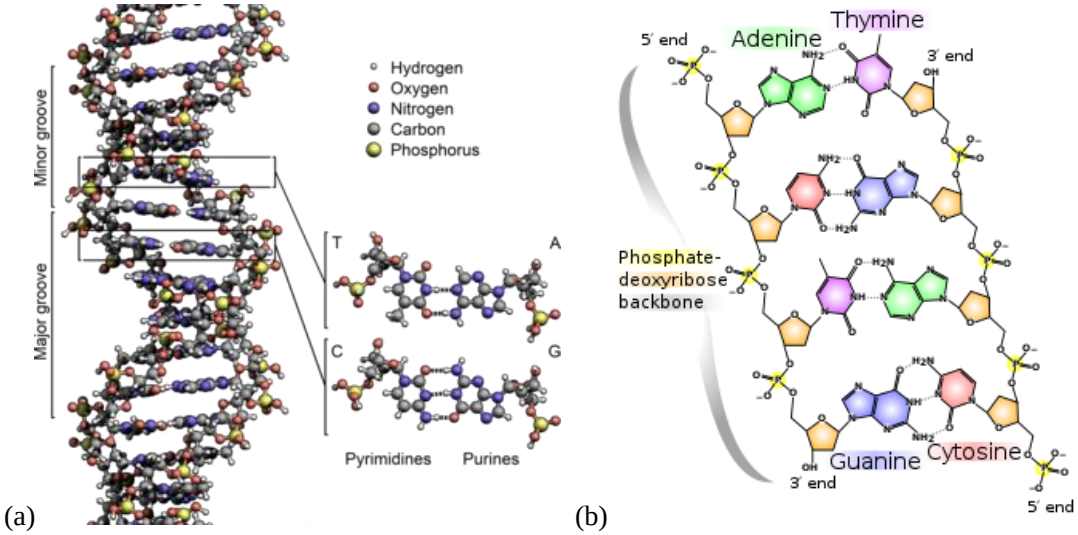

Figure 1.1.1 (a) DNA in double helix structure. (b) Chemical structures of ribose and bases.

In cellular condition, DNA can be transcript to ribonucleic acid (RNA, Figure 1.1.2a), which is another natural nucleic acid with versatile applications in the cell. For example, transfer RNA (tRNA, Figure 1.1.2b) serves as carrier of amino acid enable translation of message RNA (mRNA) to protein with complicated functions;[2] small interfering RNA (siRNA) regulate the gene silencing (Figure 1.1.2c);[3] micro RNA length in 21 to 23 base pairs (bps) attracts wide concern due to its crucial role for the inhabitation of

mRNA translation (Figure 1.1.2d).[4] All of these applications above have indicated the important role of natural nucleic acids.

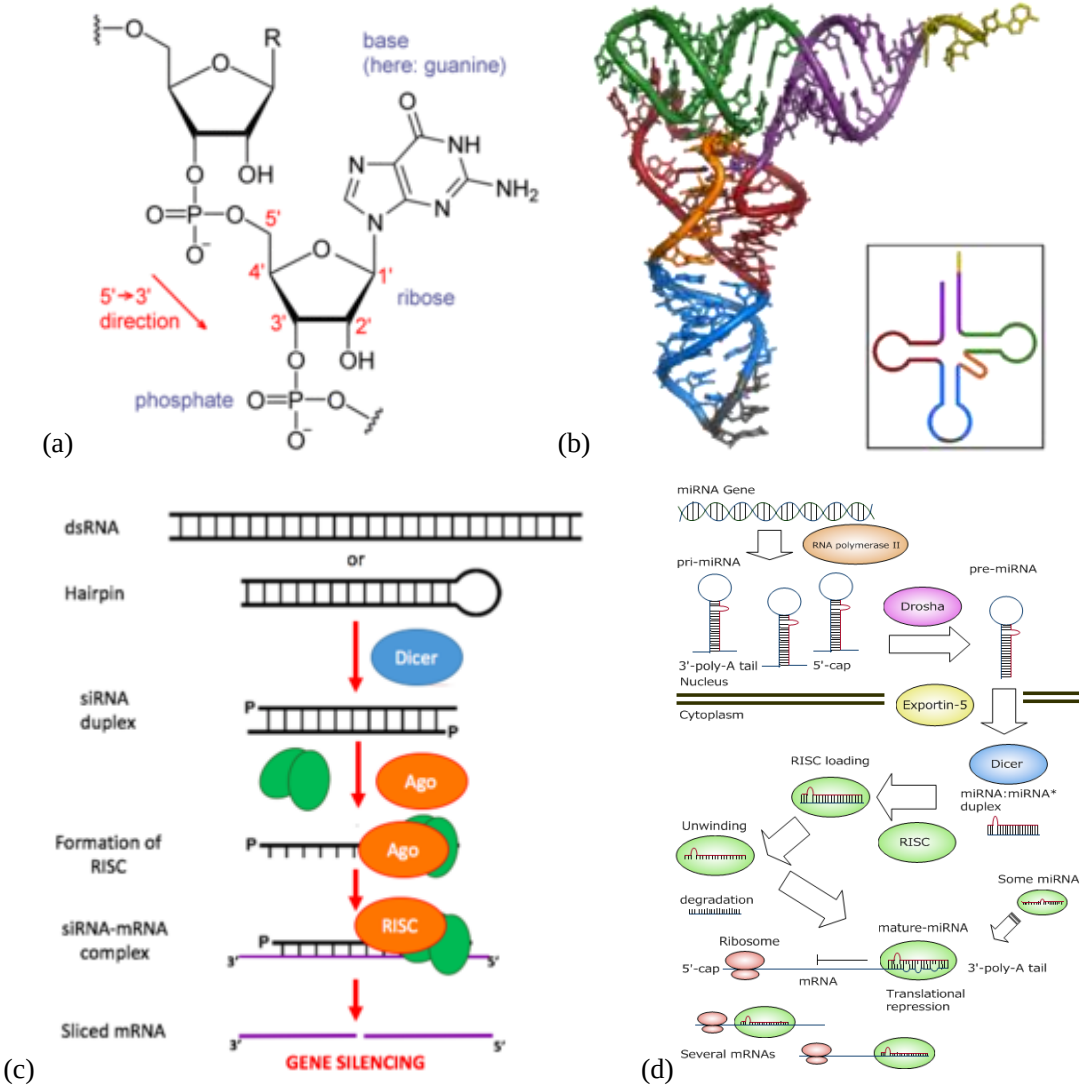

Figure 1.1.2 (a) Chemical structure of RNA. (b) Sturcture of tRNA, and the schematic illustrations of (c) siRNA in gene silencing (d) miRNA in translation repression.

1.1.2 Potential application

Because of wide distribution, conserved sequence, and sequence-dependent orthogonality, natural nucleic acids (DNA and RNA) are regarded as an ideal molecule for labeling in the organism. Detection of unique DNA or RNA fragments in the organism is regarded as an efficiency way for characterizing its existence, providing reliable diagnosis. For example, nucleic acid test provided an effective approach for determining infection of coronavirus-19 (COVID-19).[5] RNA extracted from tissues is firstly reverse-transcribed to cDNA, which will serve as template for further amplified

and checked by quantitative polymerase-chain reaction (qPCR, schematic is shown in Figure 1.1.3).

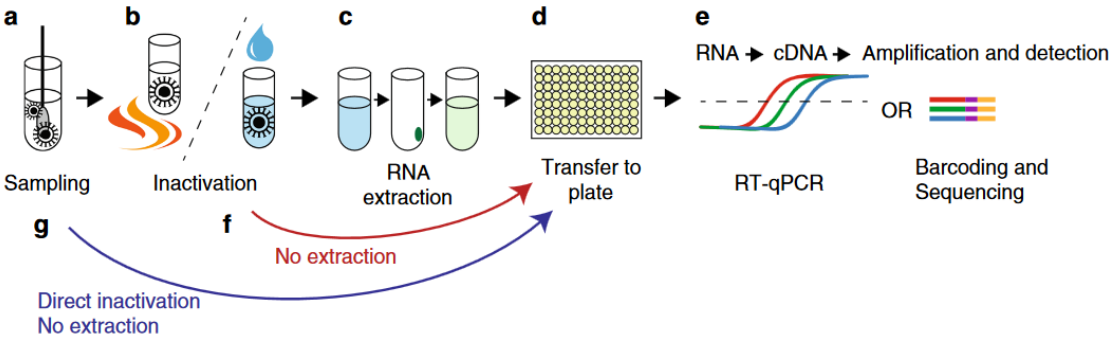

Figure 1.1.3 Schematic overview of nucleic acid test for COVID-19.

RNA detection in vivo is also regarded as an important approach for cell imagination, such as fluorescence in situ hybridization (FISH, schematic is shown in Figure 1.1.4).[6] To fixed cell, fluorophore-labeled DNA probes are added. After incubation, location of target DNA will be confirmed by hybridization of florescent probes. By analyzing the existence of target DNA (or mRNA), it is possible for us to identify the function of cells. [7] Moreover, detection in living cells can provide us more information, such as the behaviors and metabolism. Refer to the analysis, we will have a better understanding to the cell.

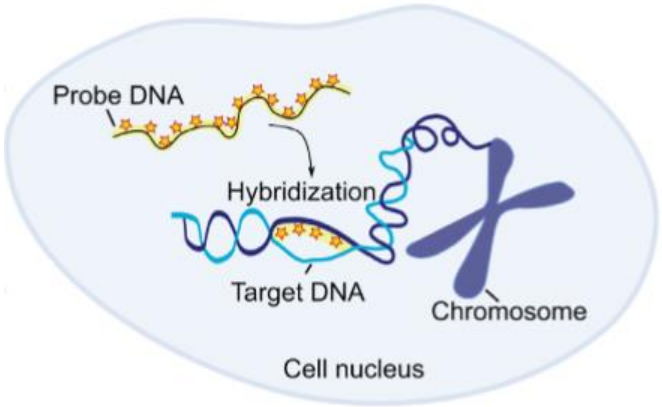

Figure 1.1.4 Schematic overview of fluorescence in situ hybridization.

Based on the sequence orthogonality, nucleic acid probe with complementary sequence design enables precise detection of target nucleic acid with high specificity. Molecular beacon might be the most used fluorescent probe in the nucleic acid detection.[8] Basically, DNA with partly self-complementary region is designed to form a hairpin structure, divided to stem and loop part (Figure 1.1.5a). At each terminal of stem, fluorophore and quencher are modified, respectively (Figure 1.1.5b). In the

single-stranded state, molecular beacon maintain in hairpin structure, herein the fluorescence will be quenched due to interaction between fluorophore and quencher. While target nucleic acid exist, molecular beacon/Target duplex formed, because of the separation of quencher, fluorescence will recover. By utilizing this simple concept, molecular beacon has achieved a clear ON-OFF switch for nucleic acid detection.

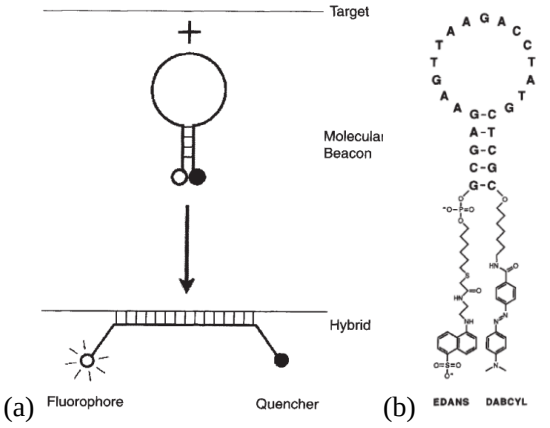

Figure 1.1.5 (a) Schematic illustration of molecular beacon. (b) Design of molecular beacon.

Except for the applications of the fluorescent detection, DNA also exhibit great potential as material of nano-assemble. Under a programmable designed of DNA sequences, molecular assemble in two-dimension (2D, Figure 1.1.6a) or even three-dimension (3D, Figure 1.1.6b) structure will be able to form under a gradual annealing process.[9][10] Free shapes of DNA origami enable wide range of application in nano environments, including logic computation[11], secure communication[12], drug deliverly,[13] molecular-level rotation tracking[14] and so on.

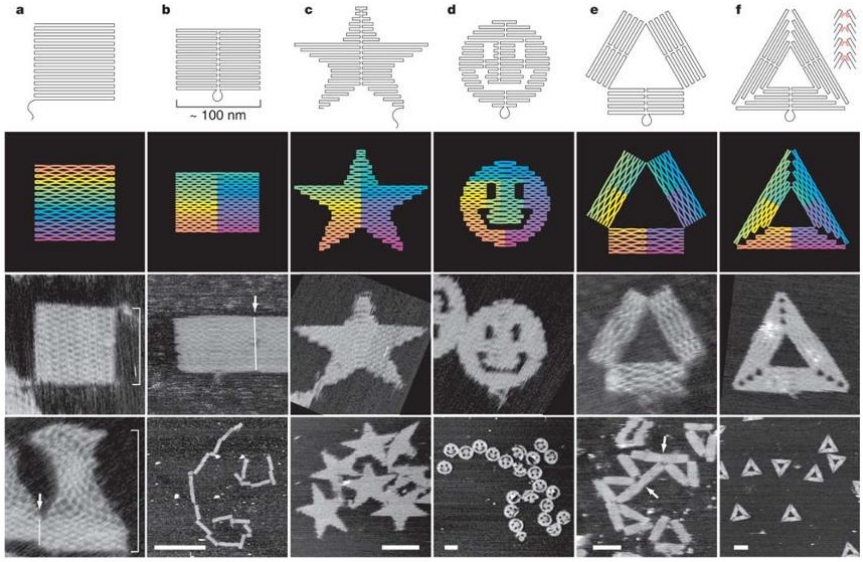

(a)

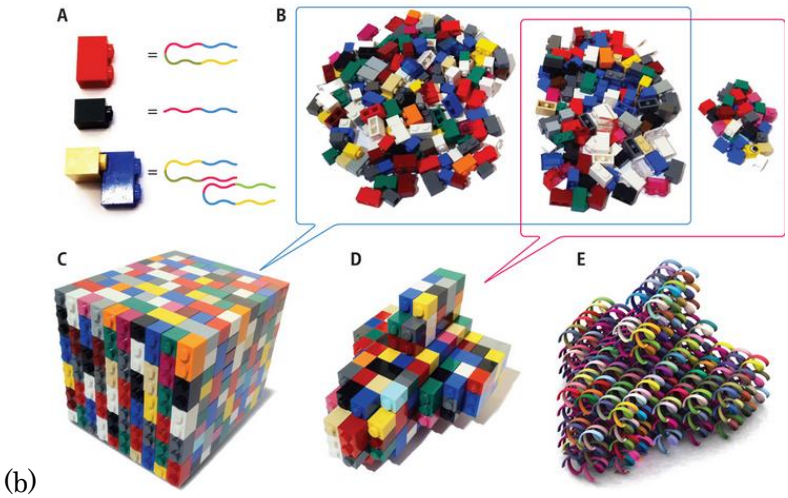

Figure 1.1.6 (a) 2D and (b) 3D DNA origami structures

Dynamic control of DNA strand under molecular level has also been confirmed, such as DNA walker,[15] DNA tweezer,[16] and DNA circuit. [17] Spontaneous process of DNA achieved under an overall consideration of concentration, distance, and length of DNA duplex. For example, DNA circuit implement algorithm in molecular level by utilizing a simple concept of strand displacement, achieving a logic computation. A large amount of these computing unit forms a huge network (Figure 1.1.7), which is potential for further construction of biological computer.

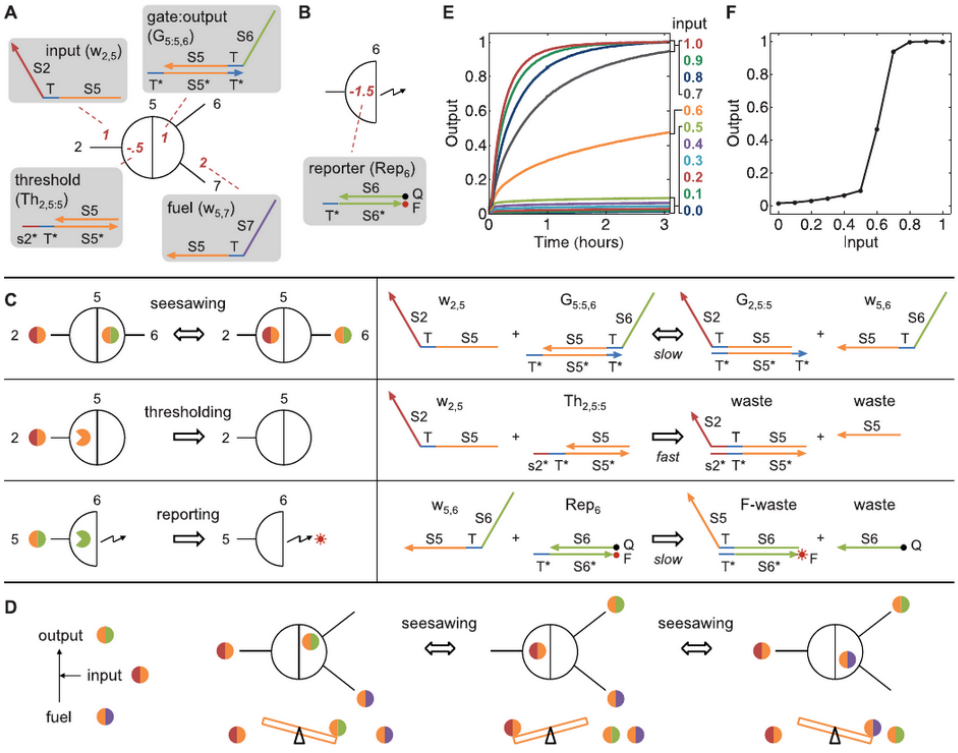

Figure 1.1.7 Basic unit of the biomimetic neural network composed of DNA.

1.2 Artificial nucleic acid

1.2.1 General introduction

Unique characters of DNA ensure versatile applications. However, applications of DNA strands/nanostructure *in vivo* are limited, due largely to the lack of nuclease-resistance. Ribose scaffold of DNA can be easily recognized by nuclease, thereby being decomposed in the cell. Aim at these problems, substitutes of the ribose scaffold have been widely considered. Therefore artificial nucleic acid, also known as Xeno-nucleic acid (XNA) has been developed.[18][19][20][21][22][23]Firstly, similar to ribose scaffold, XNAs with a cyclic scaffold have been raised up (Figure 1.2.1). Like natural nucleic acid, it has been confirmed that cyclic XNAs can also form a double helix structure according to sequence complementary principle. Some cyclic XNAs have shown relatively strong enzymatic tolerance against nuclease, although digestion sometimes happened. Moreover, since the monomer units of cyclic XNAs are hard to synthesize, cyclic XNA has not been widely used.

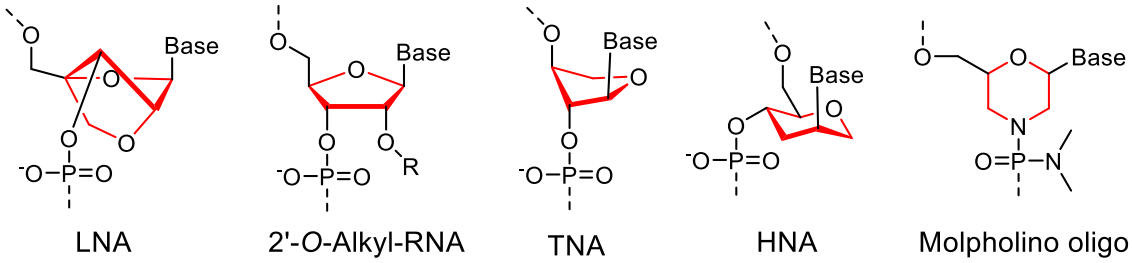

Figure 1.2.1 Chemical structure of cyclic artificial nucleic acids.

Begin form the Glycol nucleic acid (GNA in Figure 1.2.2),[24] which formed stable homo-duplex. It has been confirmed that cyclic scaffold is not necessary for XNA, enabling a higher freedom degree for molecular design. A serious of acyclic XNAs have gradually been developed (Figure 1.2.2a).[25][26][27][28] Completely different scaffold to natural nucleic acid impart acyclic XNA extremely high nuclease resistance, and ease of chemical synthesis ensure future applications with low cost.

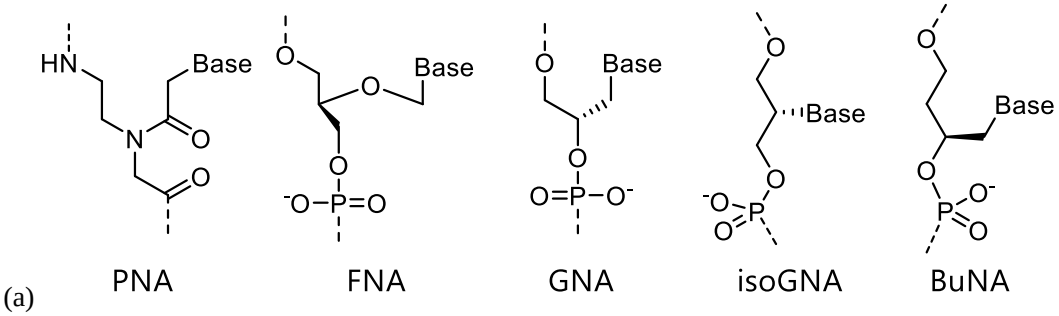

(a)

(b)

	DNA	PNA	FNA	GNA	isoGNA	BuNA
Charge	–	Neutral	–	–	–	–
Homo-duplex	○	◎	△	◎	△	△
Hetero-duplex with DNA	○	◎	×	×	×	×
Hetero-duplex with RNA	○	◎	×	△	×	×

◎>○>△>×

Figure 1.2.2 (a) Chemical structure of acyclic artificial nucleic acids. (b) Biocompatibility among the acyclic XNA and natural nucleic acids (DNA, RNA).

However, acyclic XNA still face some problems: 1. almost all the acyclic XNAs hardly form stable hetero duplex with natural nucleic acids (Figure 1.2.2b), which greatly limited the application (ie. DNA detection) of XNA. 2. Although peptide nucleic acid (PNA) forms stable hetero duplex to DNA or RNA, it suffers low water solubility due to its neutral scaffold. Herein, hydrophilic modification is highly required, especially in long PNA strand.

1.2.2 Acyclic D-theroninol nucleic acid

Previously, our laboratory has newly developed D-threoninol as novel substitute of the main scaffold.[29] While D-threoninol modified with dyes (or other molecules) incorporated to DNA oligonucleotides (Figure 1.2.3a), this molecule will intercalated between the DNA base-pair, instead of causing a hindrance to the base pairing (figure 1.2.3b). Under proper modification (ie. perylene), intercalation of fluorophore through D-threoninol has been proved to stabilize the duplex formation, due to stacking interaction between fluorophores and base groups.

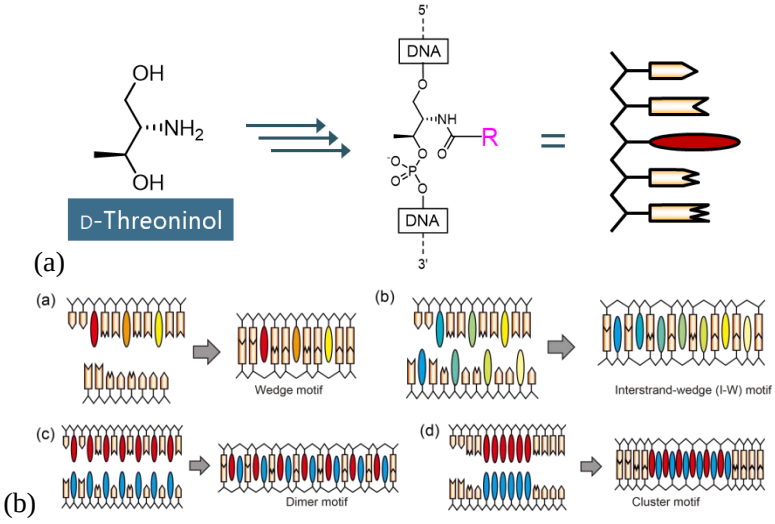

Figure 1.2.3 (a) Schematic illustration of D-threoninol in DNA oligonucleotides. (b) Multiple

D-threoninol intercalated to DNA duplex.

Besides, strand composed of D-threoninol with modification of base groups have also been discussed, which is named acyclic D-threoninol nucleic acid (D-*a*TNA, Figure 1.2.4a).[30] We have confirmed stable homo-duplex of D-*a*TNA. Compare to DNA homo-duplex in same sequence design, D-*a*TNA duplex formed duplex with higher melting temperature (T_m) of 62.7 ^{o}C (Figure 1.2.4b). We attribute the reason to low electronic repulsion among the phosphate groups in D-*a*TNA duplex. Furthermore, We also found that D-*a*TNA is hard to form hetero duplex to natural nucleic acids. We attribute the problem to the helicity of D-*a*TNA in left handed duplex, which is orthogonal to natural nucleic acid in right handed duplex.

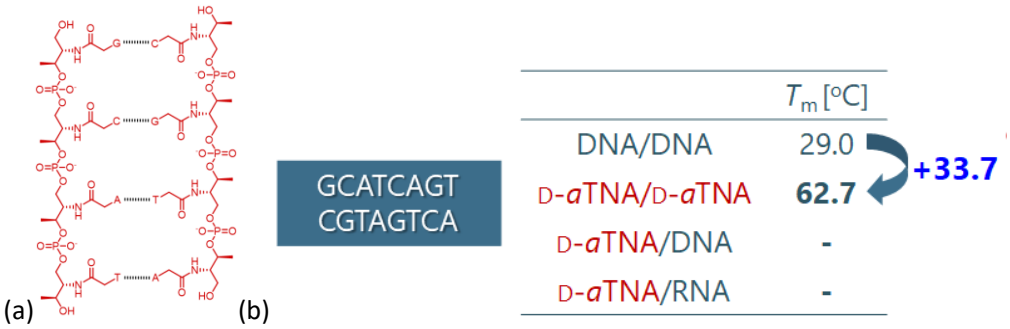

Figure 1.2.4 (a) Chemical structure of D-*a*TNA duplex. (b) T_m of homo- and hetero- D-*a*TNA duplex, and DNA homo duplex in same sequence deisgn. T_m that is undetectable marked with dash (-) in the table. Condition: [XNA] = 2.0 mM, [NaCl] = 0.1 M, 10 mM phosphate buffer pH 7.0

1.2.3 Serinol nucleic acid

We consider the orthogonality of D-*a*TNA is caused by methyl group in the scaffold. Next we have developed another acyclic nucleic acid with a 2-amino-1,3-propanediol (serinol) scaffold, named serinol nucleic acid (SNA).[31] Since methyl group is no longer modified at the scaffold, we assumed SNA strand would be biocompatible to natural nucleic acid. As a result, SNA successfully hybridized to both DNA and RNA (Figure 1.2.5). Both homo SNA and SNA/RNA duplex are stable, while SNA/DNA duplex showed relatively low T_m.

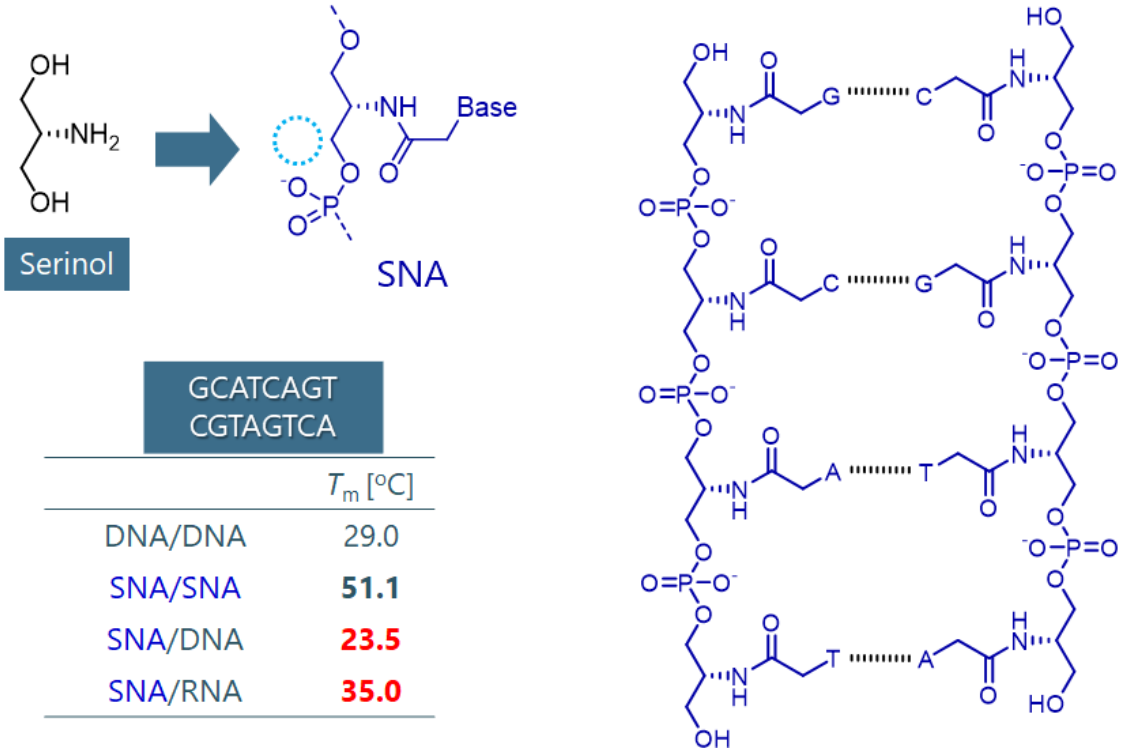

GCATCAGT
CGTAGTCA

	T_m [°C]
DNA/DNA	29.0
SNA/SNA	**51.1**
SNA/DNA	**23.5**
SNA/RNA	**35.0**

Figure 1.2.5 Overview of SNA, including chemical structure of monomer, T_m in different duplexes, and chemical structure of homo-duplex. Condition: [XNA] = 2.0 mM, [NaCl] = 0.1 M, 10 mM phosphate buffer pH 7.0

Since SNA is composed of achiral scaffold, the helicity of SNA is alternative, mainly depends on the sequence design of SNA. While a palindrome sequence is designed in the SNA, racemization will be confirmed in the solution, without significant circular dichroism (CD) absorbance around 240 nm to 260 nm (Figure 1.2.6). Different design in the SNA causes different helicity. Because of flexible scaffold, we conclude that SNA has no helical preference in the duplex-hybridization.

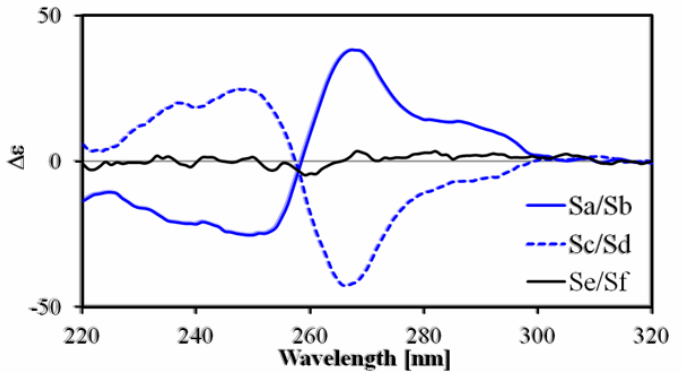

Sa (*S*)- GCATCAGT -(*R*)
Sb (*R*)- CGTAGTCA -(*S*)

Sc (*S*)- CGTAGTCA -(*R*)
Sd (*R*)- GCATCAGT -(*S*)

Se (*S*)- GCATTACG -(*R*)
Sf (*R*)- CGTAATGC -(*S*)

Figure 1.2.6 CD spectra of SNA. Condition:[SNA] = 4 mM, [NaCl] = 0.1 M,10 mM phosphate buffer, pH 7.0, 0 °C.

1.2.4 Acyclic L-theroninol nucleic acid

Base on L-theroninol which is enantiomer of D-theroninol, we further developed L-*a*TNA (Figure 1.2.7a).[32] L-*a*TNA can also form stable homo duplex. Contrast to the D-*a*TNA, L-*a*TNA duplex exhibit positive CD spectra around 260 nm (Figure 1.2.7b), indicating an opposite helicity.

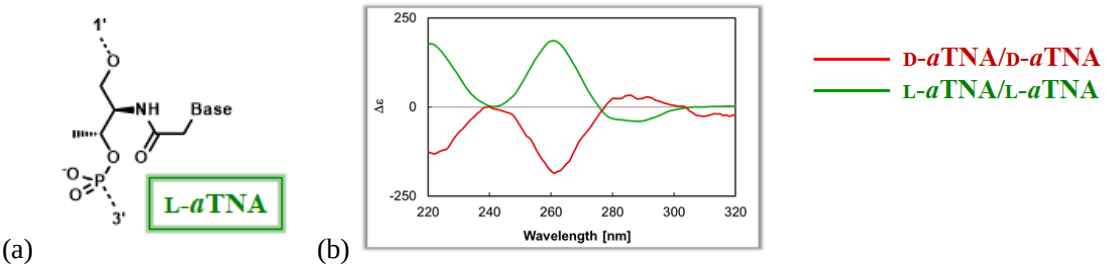

Figure 1.2.7 CD spectra of L-*a*TNA and D-*a*TNA. Conditions: [D-*a*TNA] = 1 mM, [L-*a*TNA] = 4 mM, [NaCl] = 0.1 M, 10 mM phosphate buffer pH 7.0.

L-*a*TNA in right-handed helix greatly enhances its biocompatibility to natural nucleic acids. Refer to figure 1.2.8, L-*a*TNA/RNA forms stable duplex with T_m of 41.0 °C (8-mer) and 51.5 °C (15-mer), even higher than the T_m of homo RNA duplex.

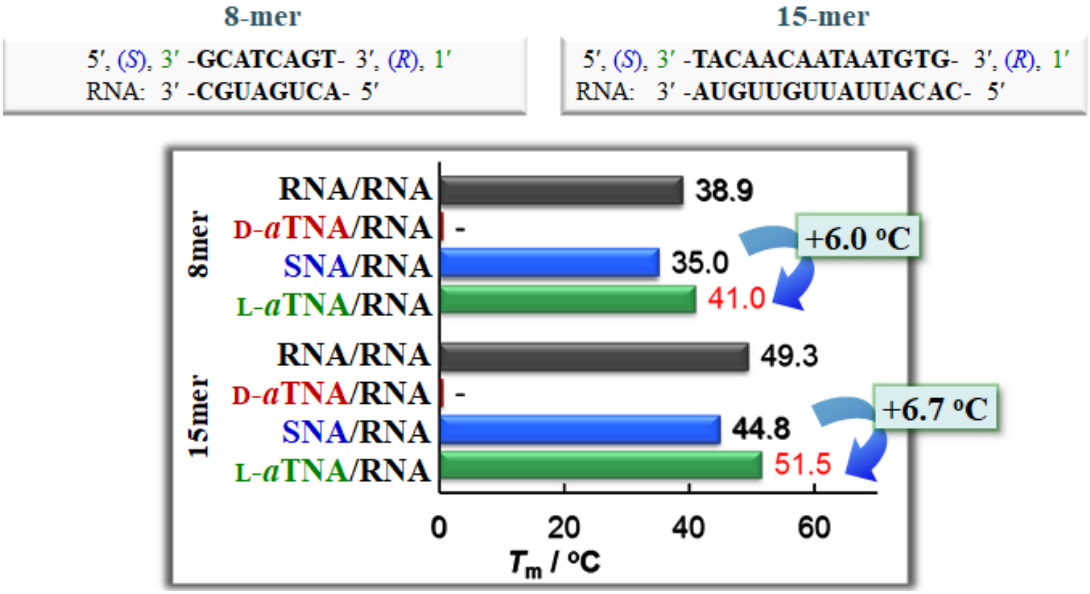

Figure 1.2.8 T_ms among the acyclic XNA and RNA. [XNA] = [RNA] = 2 mM, [NaCl] = 0.1 M, 10 mM phosphate buffer pH 7.0.

In conclusion, we have successfully developed three kinds of acyclic XNA with different characterization: SNA forms hetero duplex with natural nucleic acids, while it has no helical preference. Although D-*a*TNA cannot hybridize to natural nucleic acids

because of conformational mismatch, it serves as an ideal material for incorporating the fluorophore to the probe. L-*a*TNA also forms hetero-duplex, because of its right-handed helix conformation, duplex formation is stable with high T_m. By utilizing these XNA properly, we trust their great potential for future development of fluorescent probe, antisense drug, and molecular nano-machine.

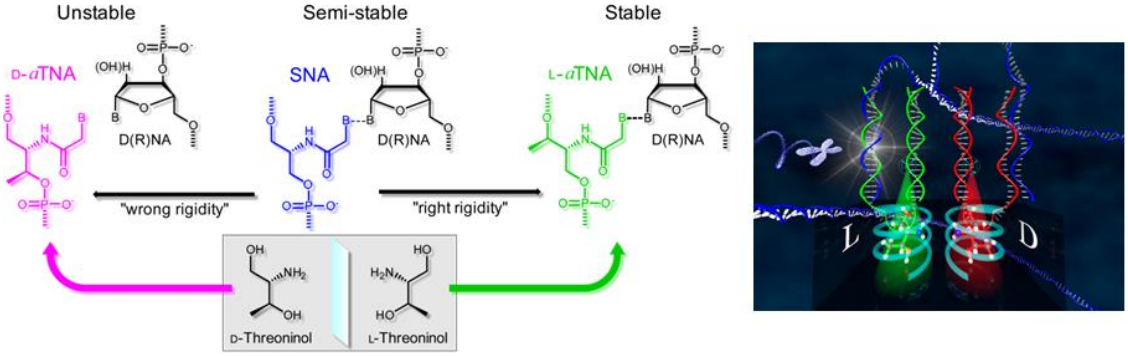

Figure 1.2.9 Chemical structures and characters of L-*a*TNA, D-*a*TNA and SNA.

1.3 Reference

[1] F. Crick, J. Watson, *Nature* **1953**, *171*, 737–738.

[2] S. H. Kim, G. J. Quigley, F. L. Suddath, A. Mcpherson, D. Sneden, J. J. Kim, J. Weinzierl, A. Rich, *Science (80-.).* **1973**, *179*, 285–288.

[3] C. P. Paul, P. D. Good, I. Winer, D. R. Engelke, *Nat. Biotechnol.* **2002**, *20*, 505–508.

[4] B. John, A. J. Enright, A. Aravin, T. Tuschl, C. Sander, D. S. Marks, *PLoS Biol.* **2004**, *2*, 1862–1879.

[5] I. Smyrlaki, M. Ekman, A. Lentini, N. Rufino de Sousa, N. Papanicolaou, M. Vondracek, J. Aarum, H. Safari, S. Muradrasoli, A. G. Rothfuchs, et al., *Nat. Commun.* **2020**, *11*, 1–12.

[6] J. M. Levsky, R. H. Singer, *J. Cell Sci.* **2003**, *116*, 2833–2838.

[7] I. B. Cohen, S. E. Morison, *Some Early Tools Am. Sci.* **2014**, *343*, 177–190.

[8] S. Tyagi, F. R. Kramer, *Nature* **1996**, *14*, 303–308.

[9] P. W. K. Rothemund, *Nature* **2006**, *440*, 297–302.

[10] Y. Ke, L. L. Ong, W. M. Shih, P. Yin, *Science (80-.).* **2012**, *338*, 1177–1183.

[11] L. Qian, E. Winfree, J. Bruck, *Nature* **2011**, *475*, 368–372.

[12] Y. Zhang, F. Wang, J. Chao, M. Xie, H. Liu, M. Pan, E. Kopperger, X. Liu, Q. Li, J. Shi, et al., *Nat. Commun.* **2019**, *10*, DOI 10.1038/s41467-019-13517-3.

[13] J. Weiden, M. M. C. Bastings, *Curr. Opin. Colloid Interface Sci.* **2021**, *52*, 101411.

[14] P. Kosuri, B. D. Altheimer, M. Dai, P. Yin, X. Zhuang, *Nature* **2019**, *572*, 136–140.

[15] J. S. Shin, N. A. Pierce, *J. Am. Chem. Soc.* **2004**, *126*, 10834–10835.

[16] M. Liu, J. Fu, C. Hejesen, Y. Yang, N. W. Woodbury, K. Gothelf, Y. Liu, H. Yan, *Nat. Commun.* **2013**, *4*, 1–5.

[17] M. Turelli, R. A. Watson, L. Chao, G. Tkacik, J. B. Plotkin, T. L. Parsons, G. P. Wagner, J. B. Plotkin, R. E. Lenski, S. P. Miller, et al., **2011**, *99*, 1196–1202.

[18] J. Summerton, D. Stein, S. Ben Huang, P. Matthews, D. Weller, M. Partridge, *Antisense Nucleic Acid Drug Dev.* **1997**, *7*, 63–70.

[19] S. Obika, D. Nanbu, Y. Hari, J. I. Andoh, K. I. Morio, T. Doi, T. Imanishi, *Tetrahedron Lett.* **1998**, *39*, 5401–5404.

[20] C. Hendrix, H. Rosemeyer, I. Verheggen, F. Seela, A. Van Aerschot, P. Herdewijn, *Chem. Eur. J.* **1997**, *3*, 110–120.

[21] A. Eschenmoser, *Science (80-.).* **1999**, *284*, 2118.

[22] S. K. Singh, P. Nielsen, A. a. Koshkin, J. Wengel, *Chem. Commun.* **1998**, 455–456.

[23] P. R. Sanders, J. A. Winter, A. R. Bamason, S. G. Rogers, R. T. Fraley, **1987**, *15*, 1543–1558.

[24] L. Zhang, A. Peritz, E. Meggers, *J. Am. Chem. Soc.* **2005**, *127*, 4174–4175.

[25] K. C. Schneider, S. A. Benner, **1990**, *606*, 453–455.

[26] P. E. Nielsen, M. Egholm, R. H. Berg, O. Buchardt, *Science (80-.).* **1991**, *254*, 1497–1500.

[27] P. Karri, V. Punna, K. Kim, R. Krishnamurthy, *Angew. Chemie - Int. Ed.* **2013**, *52*, 5840–5844.

[28] V. Kumar, K. R. Gore, P. I. Pradeepkumar, V. Kesavan, *Org. Biomol. Chem.* **2013**, *11*, 5853–5865.

[29] H. Asanuma, H. Kashida, K. Yukiko, *Chem. Rec.* **2014**, *14*, 1055–1069.

[30] H. Asanuma, T. Toda, K. Murayama, X. Liang, H. Kashida, *J. Am. Chem. Soc.* **2010**, *132*, 14702–14703.

[31] H. Kashida, K. Murayama, T. Toda, H. Asanuma, *Angew. Chemie - Int. Ed.* **2011**, *50*, 1285–1288.

[32] K. Murayama, H. Kashida, H. Asanuma, *Chem. Commun.* **2015**, *51*, 6500–6503.

Chapter 2. Triplex-forming Linear Probe

2.1 Introduction

DNA-triplex, a special DNA structure which forms the hoogsteen pairs with purine of the Watson-Crick base-pairs has been regarded as one of the most powerful techniques for the control of gene expression (Figure 2.1.1).[1] Triplex-forming oligonucleotides that can recognize and hybridize to duplex DNA in sequence-specific manner are ideal agents for targeted genome modification and gene therapy: agents are capable of promoting site-directed mutagenesis and site-specific homologous recombination, inducing sequence-specific silencing at target gene via triplex formation, thus achieving therapeutic alternation of gene expression (Figure 2.1.2). [2]

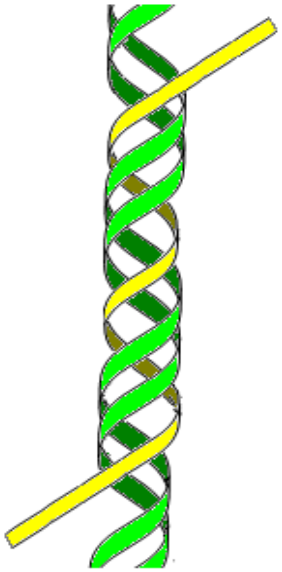

Figure 2.1.1 Illustration of DNA triplex formation

Besides, since the hybridization of triplex does not require DNA denaturation, triplex forming oligonucleotides (TFO) is also regarded as potential biomarker with modification of fluorophore.[3] However, as triplex-forming biomarkers targeting duplex DNA (dsDNA), there are several problems remains: 1. Conventional biomarkers composed by natural nucleic acids are easy to be digested by nuclease in the cell, which is one of the reasons for false-positive signal for the detection *in vivo*. 2. Since the protonation is necessary for cytosine in the hoogsteen base-pair, natural TFOs are found stable in acidic conditions,[4] stability in physiological condition (pH neutral) is one issue to be considered on the construction of artificial TFO agents. 3. Generally, to ensure efficient quenching of fluorophore, self-hybridization in the fluorescent probe is designed. For instance, stem in the molecular beacon forms energy-barrier for hybridization, making the detection time-consuming. Herein, a triplex-forming fluorescent probe with high nuclease-tolerance, stable duplex affinity with fast kinetics of fluorescence emission is desirable for the detection of dsDNA.

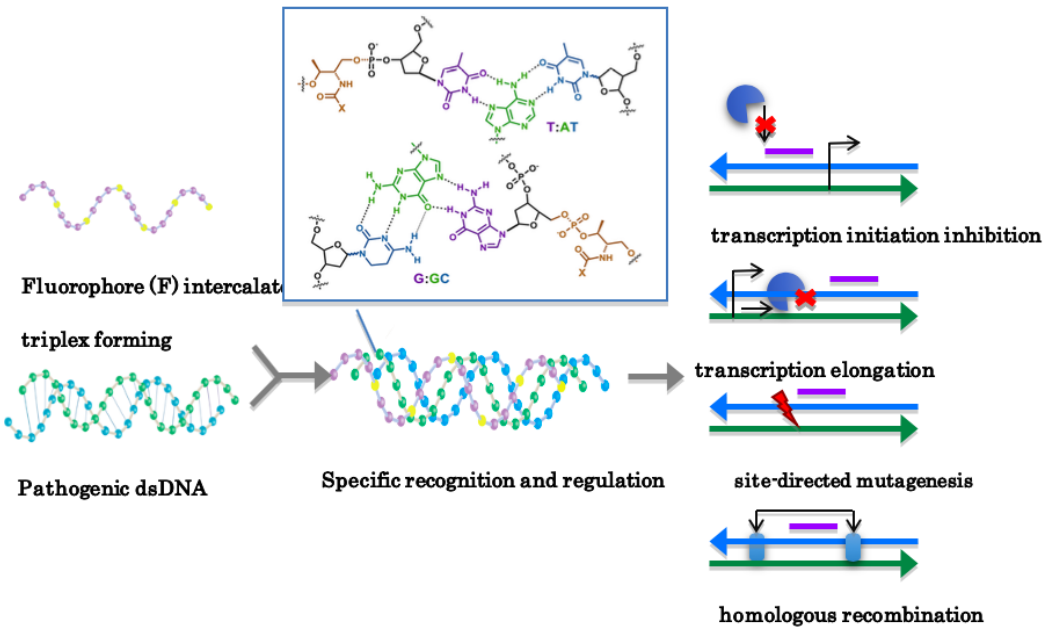

Figure 2.1.2 Potential therapeutic applications of triplex forming oligonucleotides.

2.2 Method

2.2.1 Aggregation caused quenching

Aggregation-cause quenching (ACQ) is known as a phenomenon of quenching among aromatic compounds, which was firstly discovered by Foster and Kasper about seventy years ago.[5] Under high concentration, aromatic compounds were quenched, which was cause by collisional interactions from sandwich-shaped excimers. This ubiquitous and notorious concentration-dependence quenching greatly limited the applications of aromatic fluorophores, the sensitivity and the fluorescence intensity are weak due to low concentration. [6]

Even under low concentration of fluorophore, concentration-dependent quenching can still be observed in the solution. Some methodology enable accumulation of fluorophores, herein fluorescence are quenched.[7] Generally, concentration-dependent quenching occurs among the aromatic molecules with planar structure, like pyrene and perylene (Figure 2.2.1): π-π stacking interactions among these fluorophores cause H-aggregation among the fluorophores, thereby quenching the emission, which is also known as aggregation-caused quenching (ACQ). [8]

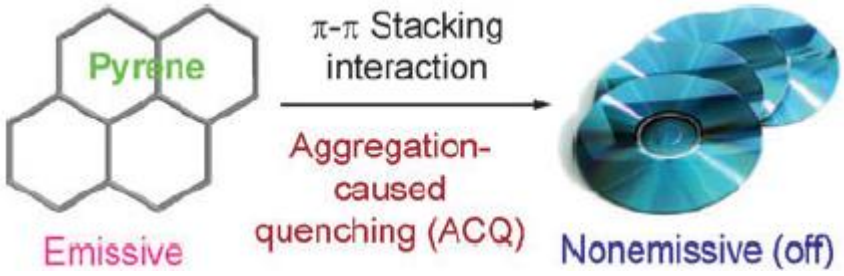

Figure 2.2.1 Simple concept of Aggregation caused quenching.

We have designed a quencher-free fluorescent probe by utilizing ACQ.[9] D-threoninol with modification of perylene molecules are incorporated to DNA oligonucleotides, named linear probe due to its stem-less shape (Figure 2.2.2). Because of high flexibility of DNA scaffold in the single strand state, while target mRNA did not exist, perylene approached to each other. Herein, even linear probe has not been modified with quencher, weak fluorescence would be observed due to ACQ. While sequence complementary mRNA was added, linear probe/RNA duplex formed. Therefore, separation of suppress ACQ, and fluorescence of perylene molecules recovered. Without modification of quencher, linear probe no longer needs hairpin-loop structure like molecular beacon, achieving fast kinetics in the detection.

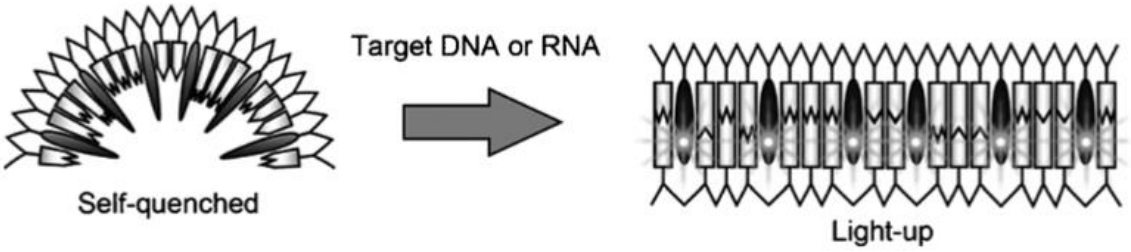

Figure 2.2.2 Schematic illustration of linear probe targeting mRNA.

2.2.2 Triplex-forming linear probe

We newly design a triplex-forming fluorescent linear probe tethering multiple fluorophores at intervals of native oligonucleotides with D-threoninol as scaffold, which enables simple detection of the double-stranded DNA (dsDNA) without denaturation.[10] The principle of the linear probe is schematically illustrated in Figure 2.2.3: At single-stranded state, similarly, triplex forming linear probe self-quenches due to hydrophobic interaction among fluorophores, while the linear probe sequence-specifically forms triplex with target dsDNA via hoogsteen base-pairing. As a result, fluorescence will remarkably recover because weakly stacked fluorophores are separated by their intercalation between the base-pairs. Unlike conventional fluorescent

probe, like molecular beacon, that was modified by one fluorophore. Since multiple fluorophores are incorporated to linear structure, we assume the linear probe would achieve strong fluorescence emission with high efficiency.

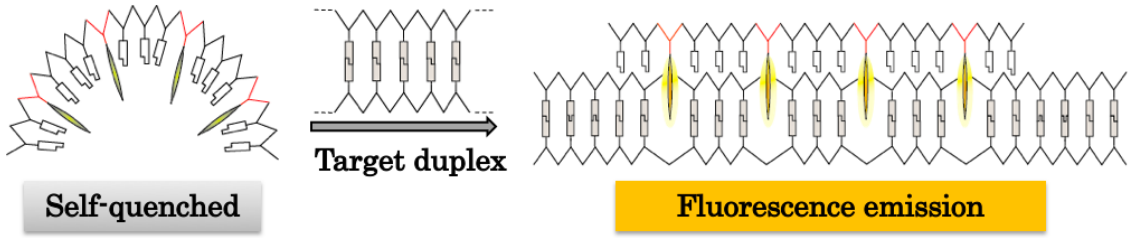

Figure 2.2.3 Illustration of triplex-forming linear probe targeting dsDNA.

Agenda of current investigation are: 1. Confirm the linear probe incorporated with fluorophore on the artificial XNA scaffold can actually from the triplex as our assumption; 2. whether and how the introduction number and intervals of fluorophores would affect the properties of linear probe; 3. Suitable chemical structure of dye for triplex.

Base on the regular pattern we have concluded, an optimal linear probe with high emission efficiency is expected to be synthesized. Then, to test its feasibility, the linear probe will be further applied to cell imagination and detection of PCR products (nucleic acid test).

2.3 Characterization of linear probes

2.3.1 Sequence design/evaluation

Table 2.3.1 The sequences of the probes and the target DNA

Target DNA duplex	**DNA-A**	5’-CGTCGGTTT-AAAAAAAAAAAAA-TTTCGTGGC-3’
	DNA-T	3’-GCAGCCAAA-TTTTTTTTTTTTT-AAAGCACCG-5’
Probes	**0F-T**	5’-TTTTTTTTTTTTT-3’
	1F-T	5’-FTTTTTTTTTTTT-3’
	2F-T	5’-FTTTFTTTTTTTTT-3’
	3F-T	5’-FTTTFTTTFTTTTTTT-3’
	4F-T	5’-FTTTFTTTFTTTFTTTT-3’

Here are the sequences we have designed. Duplex of poly A and poly T region were selected as model target sites. Next, we designed poly T probe that was expected to hybridize with target by forming triplex. D-threoninol condensed to perylene derivatives

was selected as fluorophore because of its high quantum yield and planar structure (Figure 2.3.1). Initial number (nF-T) indicates the number of fluorophores F (Table 2.3.1). Refer to our previous work, incorporation of fluorophore F every 3 base-groups proved the most efficient design for the linear probe [9]. This time, in order to further Figure out the optimal number of perylene for linear probe. Refer to our previous protocol (for DNA synthesis), I have synthesized 5 kinds of design including the probe without modification of fluorophore F as negative control (0F-T).

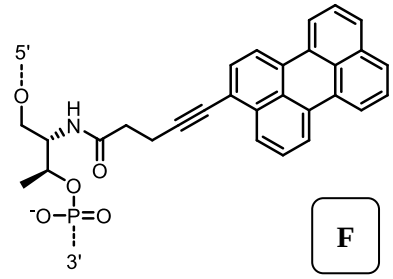

Figure 2.3.1 Chemical structure of F type perylene

We mainly evaluate the detecting ability of triplex-forming linear probes targeting dsDNA base on 2 indexes: 1. The melting temperature (T_m), which represent to the temperature when absorbance reach the midpoint due to hyperchromic effect, which is an important character to evaluate the thermal stability of the nucleic acid triplex. In another words, it can evaluate how current linear probe can stabilize the triplex formation. 2. The signal/background emission (S/B) ratio, which represent the ratio of intensity in the triplex state to single-stranded state. S/B ratio indicates the fluorescence change after linear probe successfully detect the target duplex, it can help us to evaluate the emission efficiency of current linear probe.

2.3.2 Thermal stability

Melting curves showed in the Figure 2.3.2. Here, we could clearly find two sigmoid which represent to Watson-Crick base pair and Hoogsteen base pair respectively. Therefore the formation of triplex was confirmed within the triplex-forming linear probe.

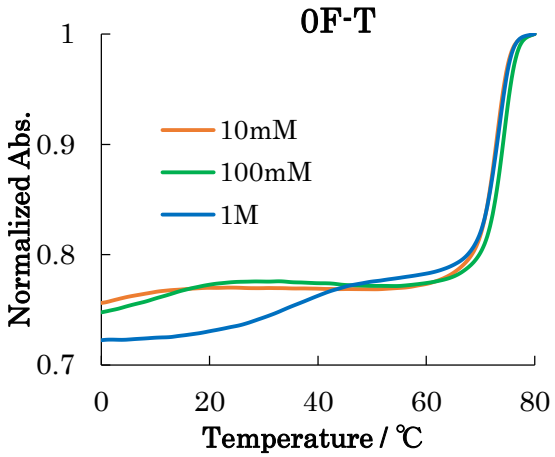

Figure 2.3.2 Melting curve of triplex-forming linear probe in the triplex formation. Conditions: 1.0 μM 0F-T, DNA-A, 1.1 μM DNA-T, 90 mM TB buffer ([$MgCl_2$] = 10 mM, 100 mM and 1M, pH 7.0), 80 ℃-0 ℃, 0.5 ℃ / min.

Next, we evaluated the thermal stability of the triplex. T_ms of triplexes at different Mg^{2+} concentrations are plotted in the Figure below (Figure 2.3.3). As for the control group, 0F-T without F was hard to form triplex, so it required high cation concentration of Mg^{2+} in Tris/Borate (TB) buffer to maintain its formation. For the triplex with triplex-forming linear probe, interestingly, introduction of F residue significantly stabilized the triplex. Moreover, as number of F increased initially, T_m of triplex also increased. For example, T_m of 3F-T was 44 ℃ higher than 0F-T. However, the tendency stopped while more fluorophores are incorporated: the 4F-T had little decreased the T_m. We assume it was caused by the interaction among the perylene even though the fluorescence recovered in the triplex formation. In conclusion, we can find that triplex-forming linear probe with fluorophore could successfully form triplex with remarkably high stability, and the probe with 3 fluorophores every 3 base-pair (3F-T) showed the highest melting temperature.

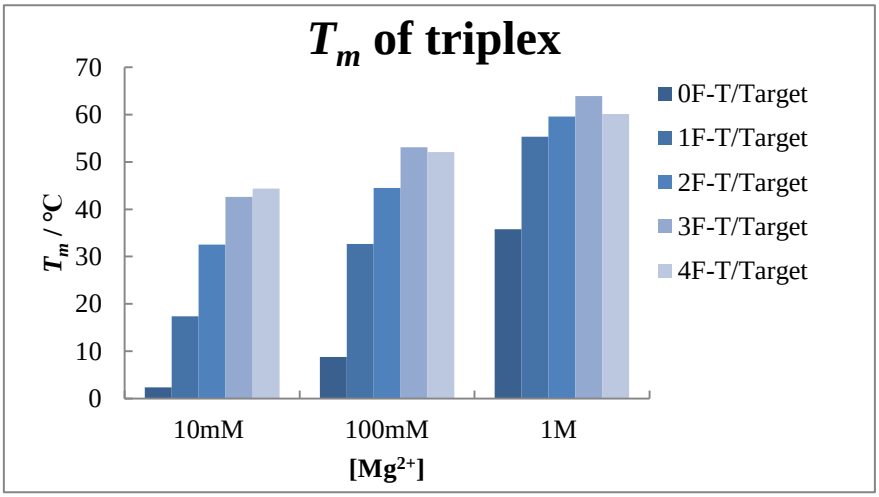

Figure 2.3.3 Melting temperatures (hoogsteen base pair) of linear probe (1F-T, 2F-T, 3F-T, 4F-T). Conditions: 1.0 μM DNA, 90 mM TB buffer ([$MgCl_2$] = 10 mM, 100 mM, and 1M, pH 7.0), 80 ℃-0 ℃, 0.5 ℃ / min.

2.3.3 Fluorescence emission efficiency

At first, I measured the fluorescence emission of single stranded probes. Here, take the fluorescence spectra under 100 mM Mg^{2+} TB buffer as an example. The intensities (472nm) at 20 ℃ among different triplex-forming linear probe were summarized in Figure 2.3.4.

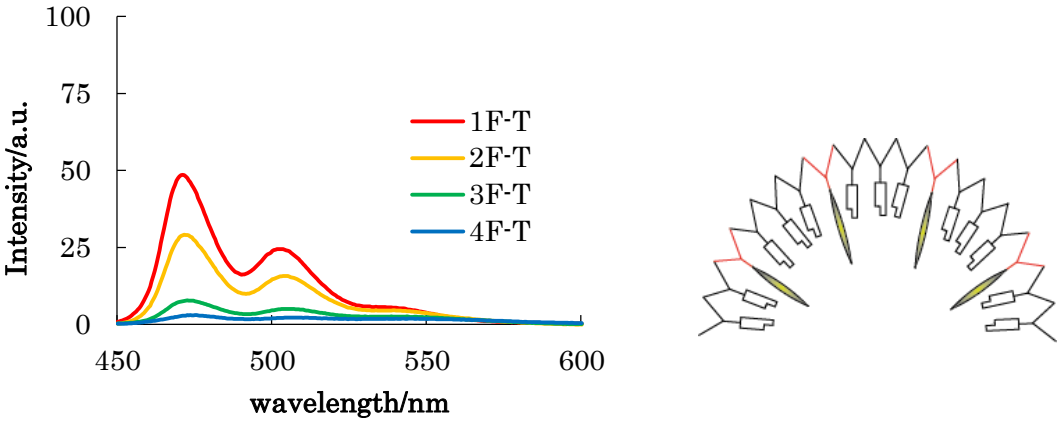

Figure 2.3.4 Fluorescence spectra for each single strand probe (1F-T, 2F-T, 3F-T, 4F-T). Conditions: Excitation wavelength: 440nm; response: 0.1 sec.; Linear probe 1.0 μM in 90mM TB buffer ([$MgCl_2$] = 100mM, pH 7.0). 20 ℃

As increasing number of F, multiplied perylene caused strong self-quenching effect. Hence, the background emission gradually decreased. About the self-quenching behavior under different cation concentration, in my report, I found no relationship between magnesium concentration and fluorescence behavior in single stranded state, which indicate reliability of ACQ in the fluorescent probe.

Next, I measured the fluorescence emission in the triplex formation (Figure 2.3.5). Since no self-quenching occurred in 1F-T, emission intensity was same to single strand, which was consistent with our assumption. With increasing number of fluorophore F in the linear probe, the fluorescence emission intensity increased. However, emission in triplex formation was not proportional to the number of the fluorophore F, which was likely cause by the interaction among the fluorophores.

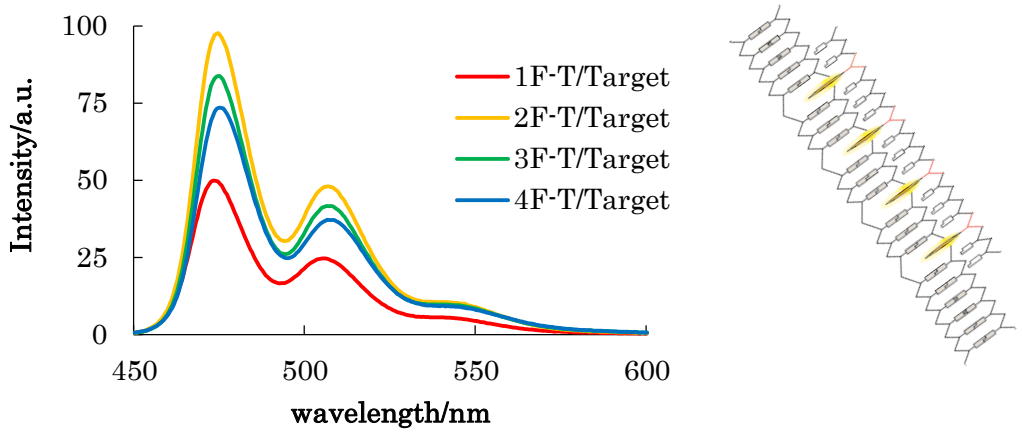

Figure 2.3.5 Fluorescence emission of each linear probe (1F-T, 2F-T, 3F-T, 4F-T) at triplex formation. Conditions: Excitation wavelength: 440nm; Linear probe 1.0 μM, DNA-A 1.0 μM, DNA-T 1.1 μM in 90mM TB buffer ([$MgCl_2$] = 100mM, pH 7.0). 20 ℃

The fluorescence intensities at 472 nm for triplex formation among different linear probes were showed in Figure 2.3.6. While concentration of the Mg^{2+} increased, because of stable triplex formation, the fluorescence intensity increasing (Figure 2.3.6). Followed by the fluorescence emission, I have calculated the S/B ratio in order to Figure out the best design for linear probe.

The 2F-T cannot self-quench very well. Comparing with the fluorescence intensity emitted from the triplex, the S/B ratio at the 472nm was only 2~3. It could not satisfy us much, which makes the result of detection very hard to judge whether the triplex had been formed when we apply it to the practice.

In the same case, the probe 3F-T showed more effective way to be distinguished. It was above 10-fold comparing with the fluorescence intensity when only the linear probe exists. And the process of forming the triplex is almost same to the 2F-T probe (after 10mM concentration of the Mg^{2+}, their fluorescence intensity become constant). Obviously, the linear probe 3F-T was more suitable than 2F-r the application.

Although the S/B value of 4F-T (triplex) became higher and it self-quenched better than other probes. It was obviously that 4F-T emitted weak fluorescence intensity under the low concentration (10mM) of cation comparing to other probes (Figure S2.3.1, Figure S2.3.2). The intensity of 4F-T should be one fourth of 1F-T but it emitted weaker fluorescence than our expectation. Theoretically, the more fluorescence molecule was, the stronger intensity should be emitted. Hence, we assumed that a strong interaction existed among fluorophores in the 4F-T.

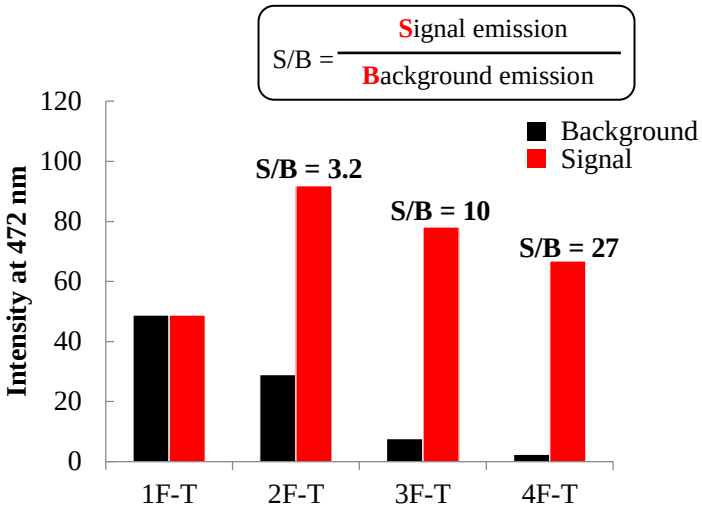

Figure 2.3.6 S/B ratio of each linear probe (1F-T, 2F-T, 3F-T, 4F-T). Conditions: Excitation wavelength: 440nm; 90mM TB buffer ([$MgCl_2$] = 100mM, pH 7.0). 20 ℃

In conclusions of this section, triplex-forming linear probes successfully hybridized with duplex, forming triplex as we designed. Especially, 3F-T always showed the highest melting temperature and S/B ratio, it should be the most suitable design for the practice.

2.3.4 UV/Vis analyze

In order to get a better understand on the fluorophore interaction in both single strand state and triplex state, we measure their UV/Vis spectra. For instance, I would like to show the spectra for 3F-T in the 100mM Mg^{2+} (Figure 2.3.7).

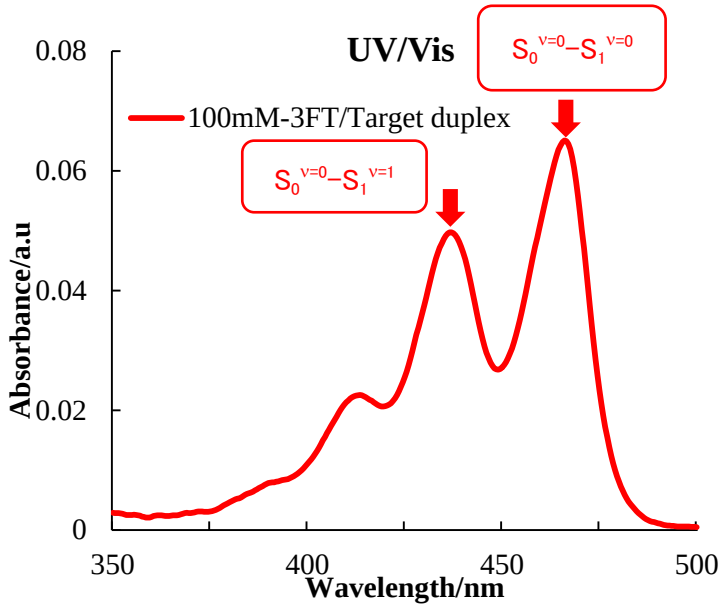

Figure 2.3.7 UV spectra of each linear probe. Conditions: [Linear probe] = 1 μM, DNA-A 1 μM,

DNA-T = 1.1 μM; 90 mM TB buffer ([$MgCl_2$]=100 mM, pH 7.0, 20℃).

In the UV/Vis spectra, the absorption at 467 nm was mainly consist of $S_0^{v=0}$-$S_1^{v=0}$ transition of fluorophore F, and the absorption at 437 nm was mainly consist of $S_0^{v=0}$-$S_1^{v=1}$ transition of fluorophore F. Hence, the intensity ratio of between them indicated the interaction among the fluorophores. We have concluded the intensities in the Figure 2.3.8, the less A467/A437 ratio was, the strong interaction remains among the fluorophores would be.

In the single strand state, because of the self-quenching, the interaction increased with the fluorophore F increased, which was reasonable and same to the experiment data.

In the triplex state, the ratio was higher than the ratio in the single strand state totally, although it gradually decreased with the number of F increased. Besides, it suddenly decreased when F increase from 3 to 4, which could also explain the relatively low melting temperature and emission intensity for the 4F-T.

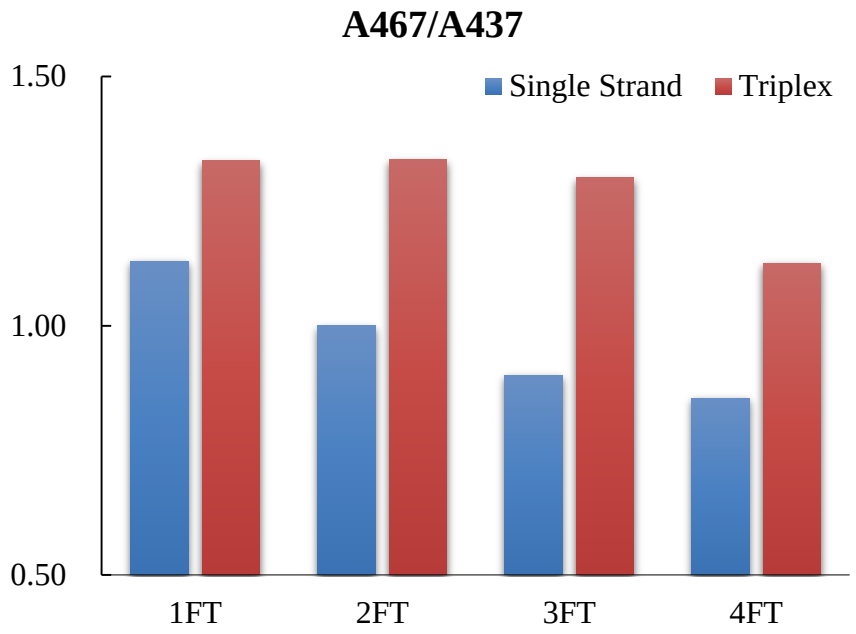

Figure 2.3.8 A467/A437 for different linear probes (1F-T, 2F-T, 3F-T, 4F-T) at 100mM Mg^{2+}.1 μM, DNA-A 1 μM, DNA-T = 1.1 μM, pH=7.0, 20℃

Next, in order to increase the emission efficiency of linear probe, there are two ways that we can do: 1. Addition of quencher, quencher in the linear probe can quench fluorophore, the decrease of background emission might increase S/B ratio; 2. A more suitable fluorophore for the triplex formation. Because the design had been determined, it seems like the most direct way for development of triplex-forming linear probe.

2.4 Optimization of sequence design

2.4.1 Incorporation of quencher Q

Firstly, we have newly incorporated anthraquinone Q condensed with D-threoninol as the quencher in linear probes, structures were shown in Figure 2.4.1.

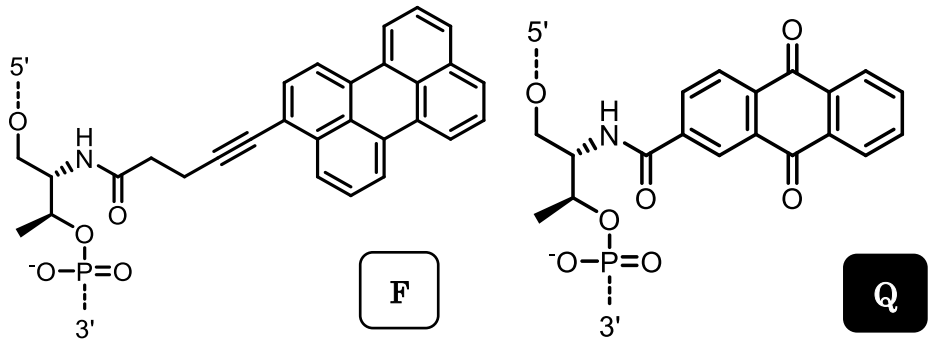

Figure 2.4.1 Chemical structure of F type perylene and Q type anthraquinone.

Refer to our pervious study, quencher Q can both stabilize the duplex formation and enhance the quenching effect when it is introduced in the linear probe targeting single strand mRNA. The S/B ratio had even reached to 1000 during the experiment. Hence, this time we also expected the quencher Q could show great quenching efficiency in the triplex-forming linear probe.

The new linear probe design showed in the Table 2.4.1, this time I chose to locate the Q at the 5-prime terminal and 3-prime terminal. We assumed quencher Q at terminal can perform its quenching ability in the single strand state and cause a slight quenching effect to the fluorophores at the triplex formation. Besides, the triplex could also be further stabilized due to the intercalation in the duplex target. After synthesizing them in the DNA synthesizer and purified by HPLC. Evaluations among 1Q3F, 2Q3F and 2Q3F-2 have been done.

Table 2.4.1 Sequence of linear probes with incorporation of quencher Q

Target DNA duplex	**DNA-A** **DNA-T**	**5’-CGTCGGTTT-AAAAAAAAAAAAA-TTTCGTGGC-3’** **3’-GCAGCCAAA-TTTTTTTTTTTTT-AAAGCACCG-5’**
Probes	**1Q3F**	5’-QTTTFTTTFTTTFTTTT-3’
	2Q3F	5’-QTTTFTTTFTTTFTTTTQ-3’
	2Q3F-2	5’-QTTTFTTTFTTTFTTTQT-3’

Melting curves shows in the Figure 2.4.2. Refer to the T_m of triplex included the probe with quencher Q (1Q3F, 2Q3F, 2Q3F-2) and without quencher Q (3F-T). Unfortunately,

quencher Q showed destabilizing effect to the triplex formation. After introduction of Q, the melting temperature at least decreased 14 ℃, which might indicate that the quencher Q have not perfectly intercalated into the duplex target as our assumption, or some interaction occurred between the quenchers and fluorophores.

Next, compare 2Q3F to 2Q3f-2, modification of quencher Q at 3'- end has not cause significate effect on T_m. Besides, the linear probe with near location of quencher Q relatively destabilized the triplex, which was caused by interaction between Q and F. In conclusion, interaction might be an important factor for regulating the stability of triplex-forming linear probe.

It may give us some advice in the sequence design that we should leave quencher Q from the fluorophore F away in order to decrease interaction affection.

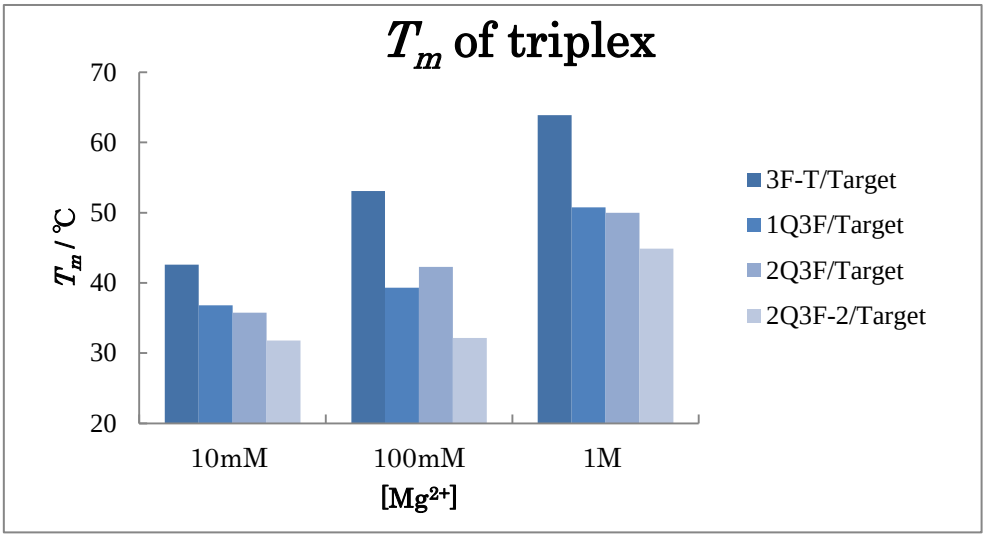

Figure 2.4.2 Melting temperatures (hoogsteen base pair) of new linear probe (3F-T, 1Q3F, 2Q3F, 2Q3F-2). Conditions: 1.0 μM DNA, 90 mM TB buffer ([$MgCl_2$] = 10 mM, 100 mM, and 1M, pH 7.0), 80 ℃-0 ℃, 0.5 ℃ / min.

Next, I measured the fluorescence emission of single stranded probes, which was same to the former process. The intensities (472nm) at 20 ℃ among different linear probe (3F-T, 1Q3F, 2Q3F, 2Q3F-2) were summarized on Figure 2.4.3.

At single strand state, probes with quencher Q showed a strong quenching ability comparing to the 3F-T as control group. Especially the sequence with 2 quencher Q, the background emission dramatically decreased, which was almost 0. It indicates anthraquinone is an ideal quencher for the perylene in the linear probe. Although I expected low back ground emission, the signal emission should be considered at the same time. These results have not satisfied us a lot.

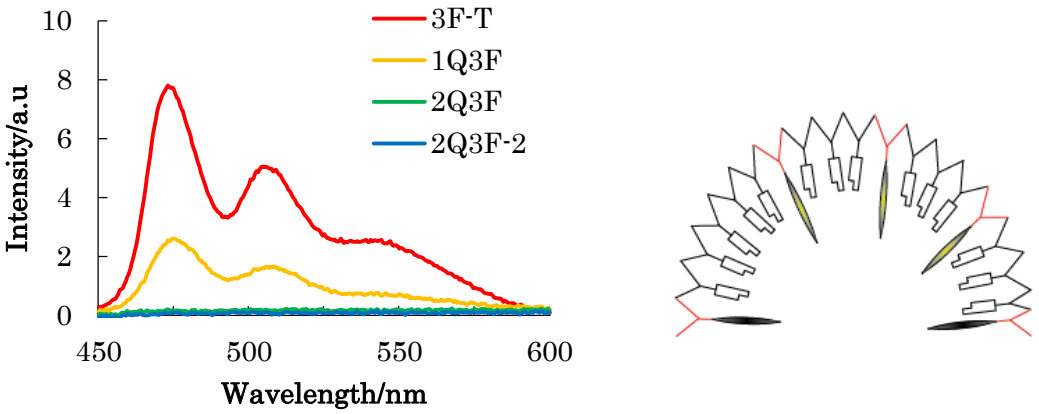

Figure 2.4.3 Fluorescence emission from each single strand probe (3F-T, 1Q3F, 2Q3F, 2Q3F-2). Conditions: Excitation wavelength: 440nm; response: 0.1 sec.; Linear probe 1.0 μM in 90mM TB buffer ([$MgCl_2$] = 100mM, pH 7.0). 20 ℃

At triplex formation, the fluorescence spectra of these linear probes (3F-T, 1Q3F, 2Q3F, 2Q3F-2) in 100mM Mg^{2+} showed in Figure 2.4.4. When DNA triplex gradually formed and emitted fluorescence with the Mg^{2+} concentration increasing. The maximum intensity of linear probes were much lower than the control group 3F-T, 1Q3F decrease about 50%, the 2Q3F and 2Q3F-2 even decrease about 80%.

There are two possibilities which might cause low emission in the triplex: 1. Interaction between anthraquinone and perylene; 2. Anthraquinone's destabilize affection on the triplex formation which can make the triplex forms incompletely. Or both of the reasons exist, quencher Q with a short chemical structure could not intercalate into the triplex perfectly. At the same time, the sequence design with only 3 or 4 base pairs might not enough for the anthraquinone-perylene pair, quencher Q still cause a huge quenching effect in the triplex formation. Hence, the triplex formed with low emission and stabilization.

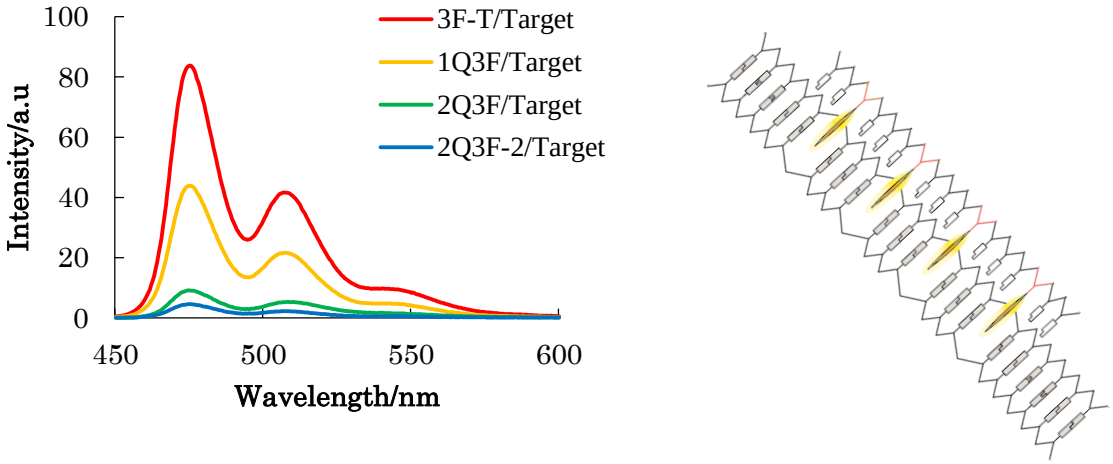

Figure 2.4.4 Fluorescence emission of each linear probe (3F-T, 1Q3F, 2Q3F, 2Q3F-2) at triplex formation. Conditions: Excitation wavelength: 440nm; response: 0.1 sec.; Linear probe 1.0 μM, DNA-A 1.0 μM, DNA-T 1.1 μM in 90mM TB buffer ([$MgCl_2$] = 100mM, pH 7.0). 20 ℃

The S/B ratio among the linear probes (3F-T, 1Q3F, 2Q3F, 2Q3F-2) showed in Figure 2.4.5. This time, although the S/B ratio increased a lot due to the extreme low background emission. The interaction resulted in low fluorescence intensity in triplex and melting temperature indicated quencher Q was not a suitable quencher for the linear probe development. Although I failed during this attempt, it might direct us that a fluorophore with longer chemical structure or quencher were suitable for the triplex formation. For the next step, we plan to prove this assumption.

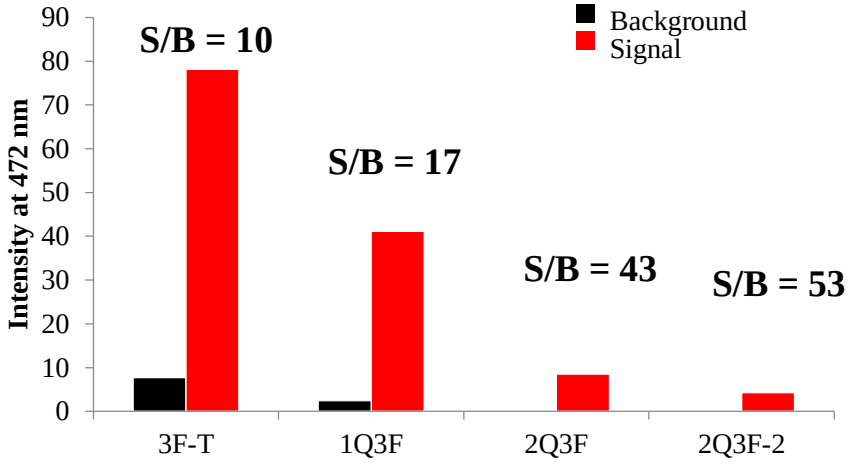

Figure 2.4.5 S/B ratio of each linear probe (3F-T, 1Q3F, 2Q3F, 2Q3F-2). Conditions: Excitation wavelength: 440nm; response: 0.1 sec.; 90mM TB buffer ([$MgCl_2$]= 100mM , pH 7.0). 80 ℃-0 ℃, 0.5 ℃ / min.

2.4.2 Incorporation of fluorophore L

Inspired by the consideration that use a fluorophore with longer linker, I chose the L type perylene derivative as new fluorophore to replace the F type perylene (Figure 2.4.6). Refer to the pervious studying in our laboratory, fluorophore L significantly destabilized duplex, because L was too large to intercalate into DNA duplex.[11] However, for the triplex formation, the expanded base pairing system in triplex might accept such large molecule and stabilize the triplex structure by stacking interaction. Hence, we expected this fluorophore L would show great performance in the triplex formation. The sequence design of new triplex-forming linear probe showed in Table 2.4.2, optimal sequence and a control group with only one fluorophore L (1L-T) have been synthesized.

Table 2.4.2 Sequences of new linear probes (1L-T, 3L-T) with fluorophore L and target DNA

Target DNA duplex	**DNA-A** **DNA-T**	**5'-CGTCGGTTT-AAAAAAAAAAAAA-TTTCGTGGC-3'** **3'-GCAGCCAAA-TTTTTTTTTTTTT-AAAGCACCG-5'**
Probes	**1L-T**	5'-LTTTTTTTTTTTTT-3'
	3L-T	5'-LTTTLTTTLTTTTTTT-3'

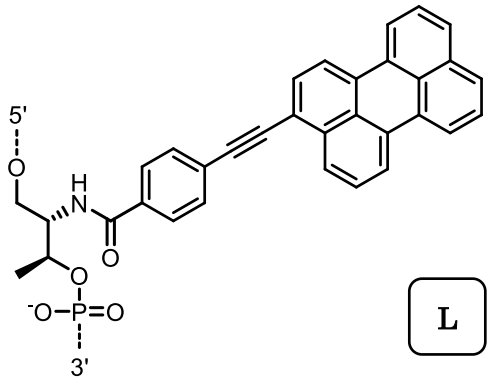

Figure 2.4.6 Chemical structure of L type perylene

As our expectation, L-type perylene showed great performance for stabilizing the triplex formation. While multiple fluorophore L was introduced into probe, linear probe could extremely stabilize the triplex formation with high T_m (71.6 ^{o}C) even at the low concentration of Mg^{2+} (10mM, Figure 2.4.7). This character proved our assumption that the fluorophore with relatively long linker in the triplex-forming linear probe could intercalate into triplex tightly and stabilize it.

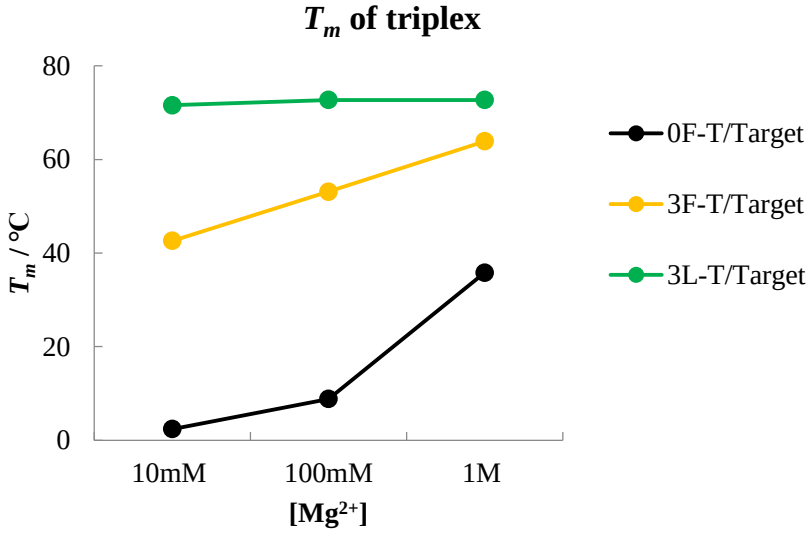

Figure 2.4.7 Melting temperatures (hoogsteen base pair) of new linear probe (0F-T, 3F-T, 3L-T). Conditions: 1.0 μM DNA-A and linear probes, 1.1 μM DNA-T, 90 mM TB buffer ([$MgCl_2$] = 10 mM, 100

mM, and 1M, pH 7.0), 80 ℃-0 ℃, 0.5 ℃ / min.

In case of 1L-T, fluorescence intensity remained in certain value because self-quenching does not exist (Figure S2.4.1). And we could find a red shift in the Fluorescence spectra, which is reasonable because it indicates the formation of complex (triplex or duplex).

For the probe 3L-T, strong self-quenching effect was found in the low concentration. As a result, the S/B ratio also increased from 10 to 28 comparing to the linear probe with fluorophore F (Figure 2.4.8). Hence, the fluorophore L exhibit great performance both in melting temperature and emissions efficiency, which was regard as suitable fluorophore for development of triplex-forming linear probe.

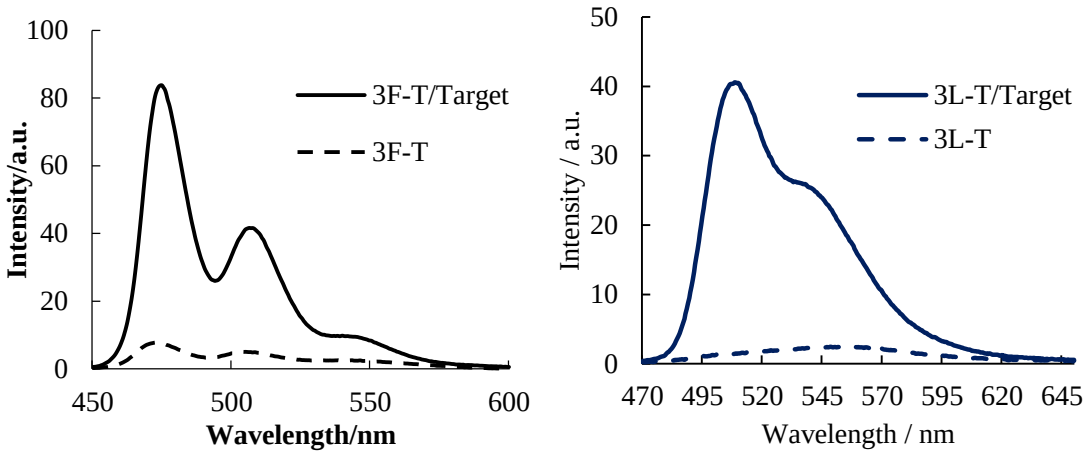

Figure 2.4.8 Fluorescence emission of each linear probe (3F-T, 3L-T) at triplex formation. Conditions: Excitation wavelength: 440nm; Linear probe 1.0 μM, DNA-A 1.0 μM, DNA-T 1.1 μM in 90mM TB buffer ([$MgCl_2$] = 100mM, pH 7.0). 20 ℃

2.4.3 Duplex binding specificity

Next, we evaluated the specificity on triplex formation against duplex. The T_m of duplex and triplex at 10mM magnesium shows Figure 2.4.9. Comparing to the duplex formation, triplex of F-type perylene (3F-T) was slightly unstable, which indicated low specificity on triplex formation. In contrast, the linear probe with L-type perylene (3L-T) showed excellent stabilizing effect on the triplex comparing the T_m in duplex. Which indicated linear probe containing fluorophore L preferred triplex formation to duplex formation. This situation satisfied us a lot, the linear probe with high specificity on triplex could avoid the unspecific binding with complementary mRNA, which might be the reason of unspecific background emission while we apply them in the cell detection.

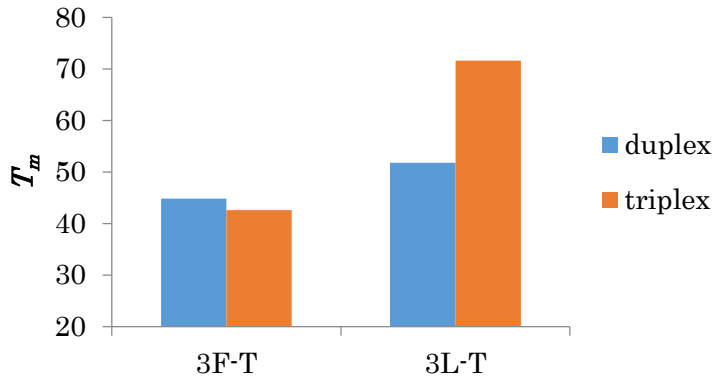

Figure 2.4.9 Melting temperature of duplex and triplex (3F-T, 3L-T). Conditions: Linear probe 1.0 μM, DNA-A 1.0 μM, DNA-T 1.1 μM (if needed) in 90mM TB buffer ([$MgCl_2$] = 10mM, pH 7.0). 20 °C.

2.5 Detection of androgen receptor gene

2.5.1 Sequence optimization

Linear probe for detection of human androgen receptor (AR) gene designed. AR gene as nuclear receptor, always serves as important regulate gene and maintained male sexual phenotype.[12] Hence, it is necessary to apply our linear probe in its detection.

Because AR gene duplex was longer than template duplex, it was worried that the quenching efficiency might decrease due to the steric hindrance from long tail. Hence, two linear probes were synthesized, the 3LX1 with 3 base pair intervals and the 3LX2 with four base pair intervals. A control group (triplex-forming oligonucleotides X, TFO X) was also prepared for further evaluation (Table 2.5.1).

Table 2.5.1 Sequences of the linear probes with fluorophore L targeting AR dsDNA

AR DNA duplex	**AR antisense**	5’-CTACT-AAAGAAGAAAAGAGAGAA-GAATC-3’
	AR sense	5’-GATTC-TTCTCTCTTTTCTTCTTT-AGTAG-3’
Probes	**3LX1**	5’-LTTTLCTTLCTTTTCTCTCTT-3’
	3LX2	5’-LTTTCLTTCTLTTTCTCTCTT-3’
	TFO X	5’-TTTCTTCTTTTCTCTCTT-3’

Since linear probes contained the cytosine, which needed to be protonated before forming hoogsteen base pair, acidic condition was highly required for the detection. However, we assumed the stabilization effect caused by intercalation of fluorophore would maintain triplex formation, herein the evaluation of triplex forming linear probe targeting AR dsDNA was performed under physical condition (pH=7.0).

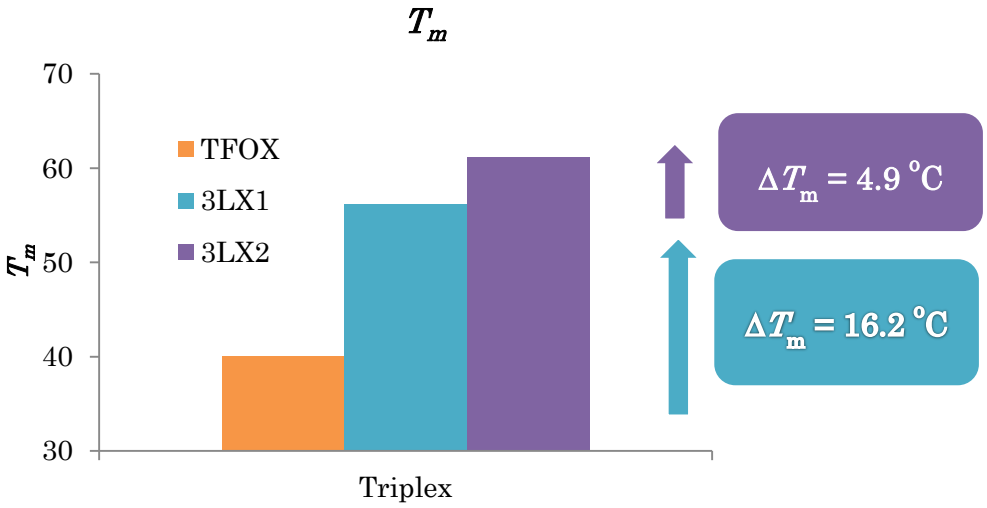

Figure 2.5.1 Melting temperatures of triplex containing linear probes (3LX1, 3LX2, TFO X). Conditions: 1.0 μM DNA, AR antisense 1.0 μM, AR sense 1.1 μM 90 mM TB buffer ([$MgCl_2$] = 100 mM, pH 7.0).

The melting temperatures of triplex containing linear probes (3LX1, 3LX2, TFO X) showed in Figure 2.5.1. This time, linear probes again formed stable triplex under pH 7.0. Comparing to the control linear probe (TFO X), melting temperature of triplex increased at least 16.2 ℃, which helped us to confirm the feasibility of linear probe for detection of dsDNA.

The fluorescence spectra were shown in Figure 2.5.2, we could clearly find the linear probes with sufficient emission efficiency for AR dsDNA detection, and the S/B ratio was also very high. Compare two designs, the 3LX2 in the single strand state could not self-quench very well due to the long interval. S/B ratio also lower than the 3LX1 (S/B ratio: 3LX1=14.7; 3LX2=8.2). Therefore, sequence design with fluorophores incorporation every 3 base-pair was the optimal design for AR dsDNA detection.

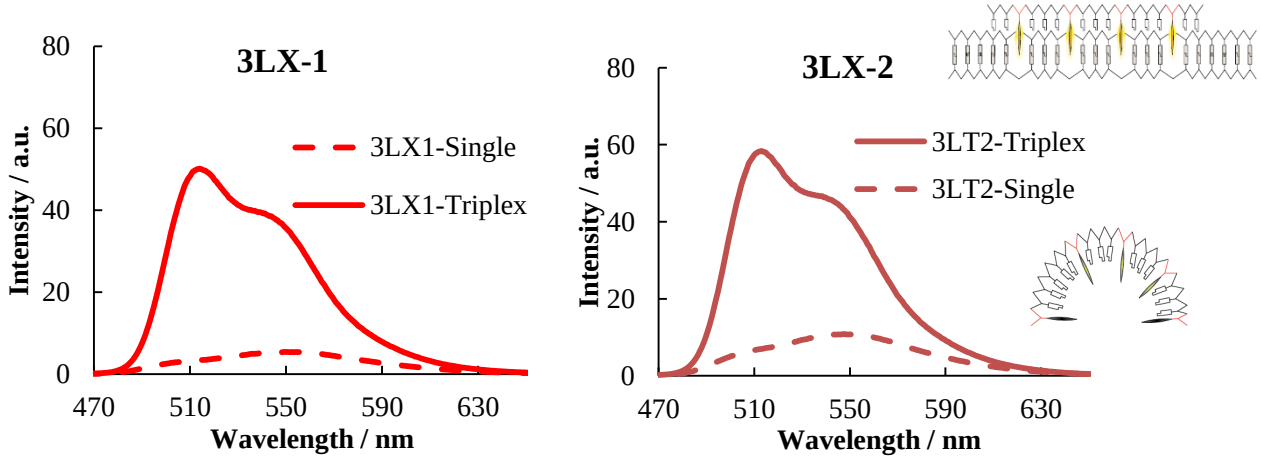

Figure 2.5.2 Fluorescence emission of linear probe for detection of AR dsDNA (3LX-1, 3LX-2). Solid

line: triplex emission; Dash line: single strand emission. Conditions: Excitation wavelength: 455nm; r Linear probe 1.0 uM, AR antisense 1.0 μM, AR sense 1.1 μM in 90mM TB buffer ([$MgCl_2$] = 100mM, pH 7.0). 20 ℃

2.5.2 Incorporation of quencher gQ

To further suppress the background emission of linear probe. Quencher gQ, which was condensed by D-threoninol and anthraquinone derivative with glycel-like linker (Figure 2.5.3), was subsequently incorporated into linear probe. Since gQ has long structure, we supposed that quencher gQ could quench the background emission without significant interaction to the fluorophore L.

About the sequence design, referred to pervious experiments, anthraquinone can caused strong quenching effect on the perylene. Hence, this time I incorporated the gQ with 6 and 11 base pairs interval for the new linear probe (Table 2.5.2).

Table 2.5.2 Sequences of linear probes within fluorophore L and quencher Q targeting AR dsDNA

Target DNA duplex	**AR antisense**	5’-CTACT-AAAGAAGAAAAGAGAGAA-GAATC-3’
	AR sense	3’-GATGA-TTTCTTCTTTTCTCTCTT-CTTAG-5’
Probes	**3L1gQ-1**	5’-LTTTLCTTLCTTTTCgQTCTCTT-3’
	3L1gQ-2	5’-LTTTLCTTLCTTTTCTCTCTgQT-3’

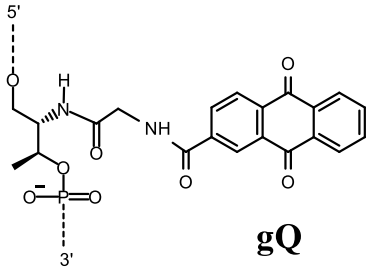

Figure 2.5.3 Chemical structure of quencher gQ

Firstly, as usual I evaluated its thermal stability both in triplex and duplex.

At triplex formation, after incorporation of quencher gQ, the stability of hoogsteen base pair was same to the triplex contain 3LX1. In duplex formation, although the T_m of duplex containing linear probe increased, low emission still indicated a strong interaction among the fluorophores and quencher (Figure S2.5.1), we also concluded that the quencher gQ was suitable for the triplex rather than the duplex (Figure 2.5.4).

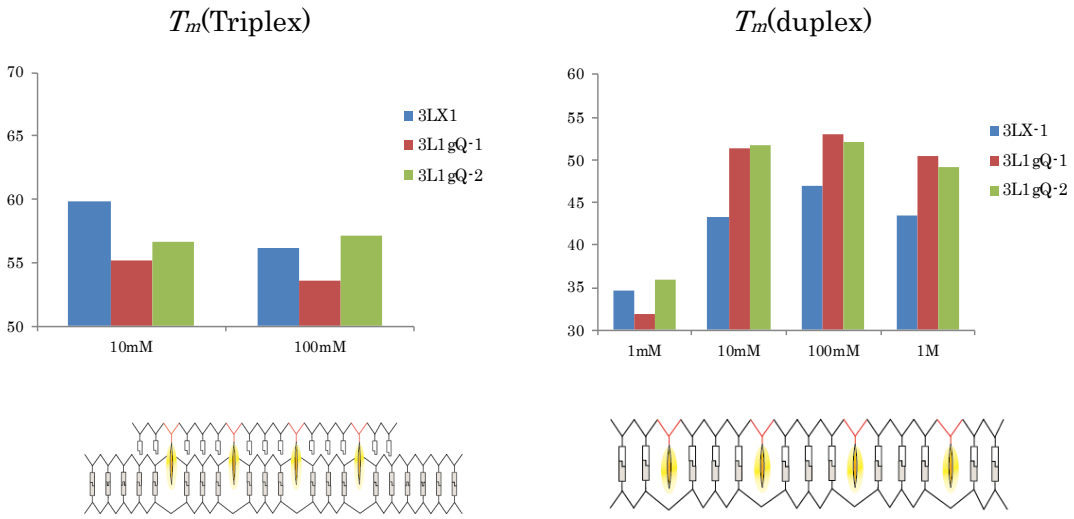

Figure 2.5.4 Melting temperatures of linear probes targeting AR dsDNA and AR antisense strand (3LX-1, 3L1gQ-1, 3L1gQ-2). Left: Triplex; Right: Duplex. Conditions: Linear probe 1.0 µM, AR antisense 1.0 µM, AR sense 1.1 µM 90 mM TB buffer ([$MgCl_2$] = 1mM, 10 mM, 100 mM, and 1M, pH 7.0).

In Figure 2.5.5, gQ showed an excellent performance in the 3L1gQ-1. Single strand state almost shows no background emission with the intensity around 0.15 at 514nm (S/B ratio almost reach to 300). At the same time, in the triplex formation, fluorescence intensity was same to the control sequence (3LX-1:5'-LTTTLCTTLCTTTTCTCTCTT-3'), indicated no interaction between quencher gQ and fluorophore L in the triplex due to long distance.

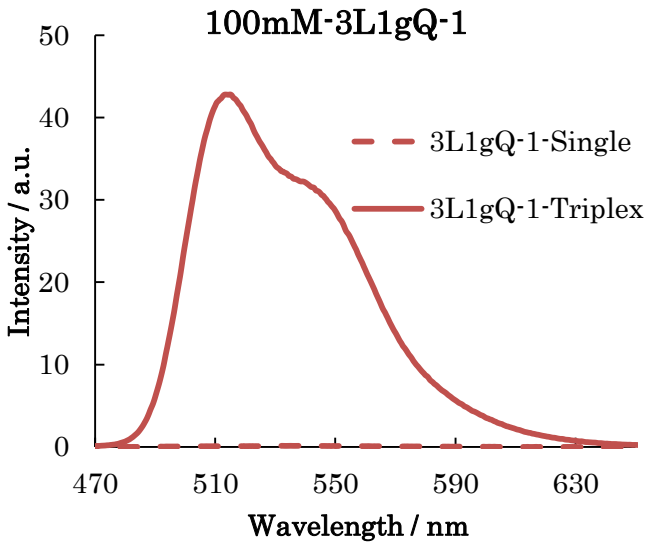

Figure 2.5.5 Fluorescence emission of 3L1gQ-1 targeting AR dsDNA. Solid line: triplex emission; Dash line: single strand emission. Conditions: Excitation wavelength: 455nm; Linear probe 1.0 uM, AR antisense 1.0 µM, AR sense 1.1 µM in 90mM TB buffer ([$MgCl_2$] = 100mM, pH 7.0). 20 ℃.

For 3L1gQ-2 (Figure 2.5.6), the quencher was located at 3'-end. Far away from fluorophores might cause a weak quenching efficiency. Hence, in the single strand state, it still emitted a weak fluorescence. Comparing to 3L1gQ-1, emission intensity of 3L1gQ-2 was lower in both duplex and triplex (Figure S2.5.1). In conclusion, the design with 6 base pairs interval (3L1gQ-1) was the optimal sequence design targeting AR dsDNA.

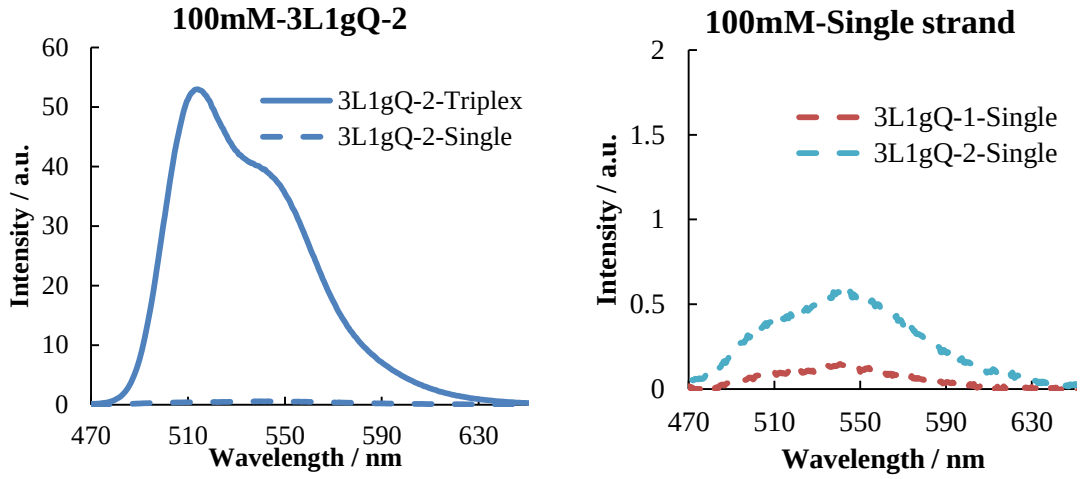

Figure 2.5.6 Fluorescence emission of linear probes. Solid line: triplex emission; Dash line: single strand emission. Left: fluorescence spectra for 3L1gQ-2; Right: Background comparison between 3L1gQ-1 and 3L1gQ-2. Conditions: Excitation wavelength: 455nm; Linear probe 1.0 uM, AR antisense 1.0 μM, AR sense 1.1 μM in 90mM TB buffer ([$MgCl_2$] = 100mM, pH 7.0). 20 ℃

2.6 Cell imagination

2.6.1 Strategy/ Plasmid construction

We planned to construct a plasmid which has target AR gene region and expression region of DsRed. DsRed region could express red fluorescence protein in the cell, which could help us to confirm the existence of the plasmid. Firstly, pcDNA 4/ myc-His C was selected as the vector to load both AR gene and DsRed, it could translate the ampicillin in E.coli, which is the antibiotic that can help us to selectively culture (map shown in Figure 2.6.1). Next, cDNA produced from another plasmid (DsRed monomer, Figure 2.6.2) was proceeded by restrict enzyme HindⅢ and EcoR Ⅰ. After work-up, the fragment would further serve as insert and incorporate into the vector by ligation. Then, based on the accessiable multiple cloning sites (MCS) in the vector (Figure 2.6.3), we have designed another insert containing AR gene dsDNA. Similarly, after ligation, the plasmid with both DsRed monomer and AR gene dsDNA was constructed.

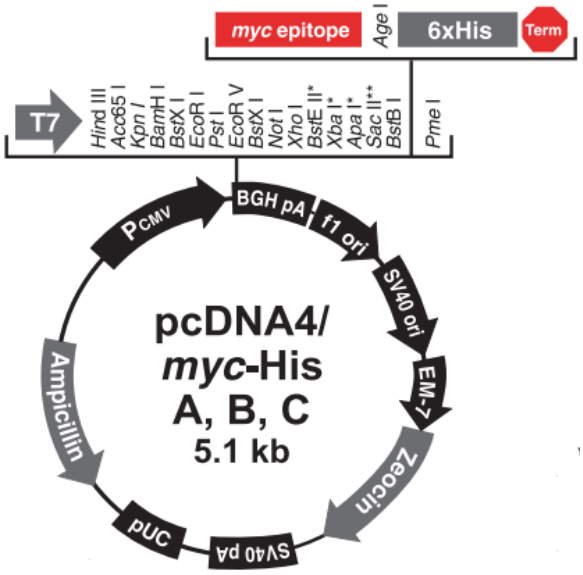

Figure 2.6.1 Plasmid map of vector (pcDNA 4/ myc-His C).

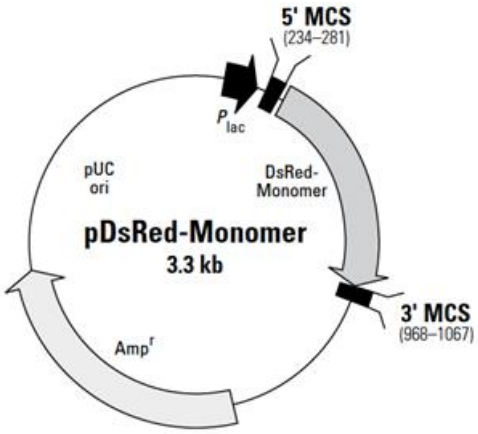

Figure 2.6.2 Plasmid map of insert (DsRed monomer)

```
                T7 promoter/priming site                                  Hind III      Acc65 I   Kpn I
861  ATTAATACGA CTCACTATAG GGAGACCCAA GCTGGCTAGT TA AGC TTG GTA CCG AGC
                                                    Ser Leu Val Pro Ser

     BamH I                          BstX I*  EcoR I          Pst I  EcoR V          BstX I*
918  TCG GAT CCA CTA GTC CAG TGT GGT GGA ATT CTG CAG ATA TCC AGC ACA GTG
     Ser Asp Pro Leu Val Gln Cys Gly Gly Ile Leu Gln Ile Ser Ser Thr Val

     Not I     Xho I     BstE II          BstB I     myc epitope
969  GCG GCC GCT CGA GGT CAC CCA TTC GAA CAA AAA CTC ATC TCA GAA GAG GAT
     Ala Ala Ala Arg Gly His Pro Phe Glu Gln Lys Leu Ile Ser Glu Glu Asp

                          Age I          Polyhistidine tag                Pme I
1020 CTG AAT ATG CAT ACC GGT CAT CAT CAC CAT CAC CAT TGA GTTTAAACCC
     Leu Asn Met His Thr Gly His His His His His His ***

                BGH Reverse priming site
1069 GCTGATCAGC CTCGACTGTG CCTTCTAGTT GC
```

Figure 2.6.3 Sequence for MCS area

As a result, we chose to insert the AR gene dsDNA with 4-mer sticky end for ligation of Xho I site. Since AR inserts were self-complementary, random number of them would be

incorporated into Xho I site, the insert sequence design showed below:

AR antisense (insert) 5'-TCGAAAAGAAGAAAAGAGAGAA-3'

AR sense (insert) 3'-TTTCTTCTTTTCTCTCTTAGCT-5'

2.6.2 Pretreatment of AR gene inserts

With the help from former students in our laboratory, I got the vector with DsRed monomer in it. Refer to the protocol (Appendix **Protocol 1**), I have transformed plasmid into E.coli and culture them. Then, we extracted the plasmid from them by the help of reagent kit. After purification the plasmid by ethanol (Appendix **Protocol 2**), finally I get 600 μL plasmid with concentration about 350ng/μL.

Next, before ligation of AR insert and vector, it was necessary to pretreat AR inserts. The process shown in Figure 2.6.4, plasmid fragment was firstly cut by restrict enzyme Xho I, then we dephosphorylated its 5-prime end to avoid its self-ligation. At the same time, phosphorylated the 5-prime end of AR insert helped the ligation with vector in the next step. The nick between 5-prime end in vector and 3-prime end in insert will be repaired in the E. coli, hence we did not to worry about this question.

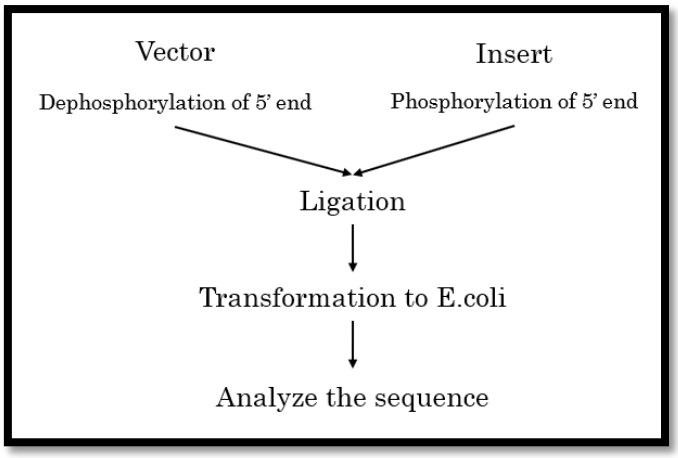

Figure 2.6.4 Experimental process of plasmid construction

Phosphorylation of insert has been finished and purified.

Dephosphorylation of plasmid also has been done and purified. Although almost all the plasmid has been cut, linear plasmid still existed. I collected them from the agarose gel (Appendix **Protocol 3**). Hence, I cut the product part on the gel and collected it for the further ligation. After transforming to E.coli and characterized by 3rd-gengeration sequencing. Finally, I have successfully constructed the plasmid I with 5 AR inserts.

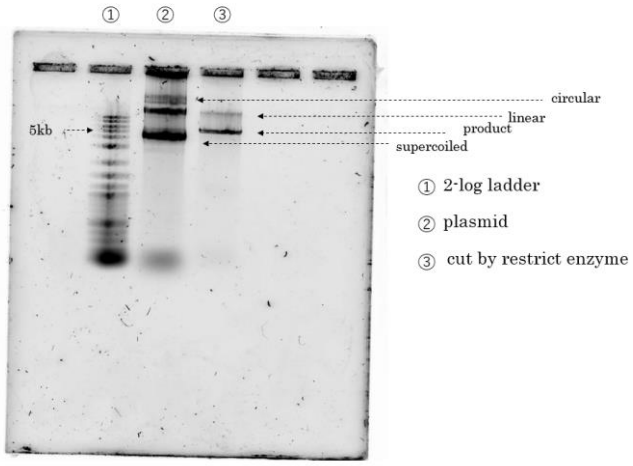

Figure 2.6.5 Agarose Gel Electrophoresis after dephosphorylation

2.6.3 Imagination of AR gene in the HeLa cell

Next, Cell imagination was performed. Firstly, the plasmid was transfected into the HeLa cell via lipofection (**Protocol 4**, lipofectamine® 2000). After incubation, the cell was fixed by formalin and 0.1 % triton X-100 (**Protocol 5**), which could increase the permeability of cell membrance. Next, fixed cell was treated by linear probes 3L1gQ-1 for further cell imagination. Finally, samples would be visualized under confocal microscope.

We have list 4 groups for cell imagination, cell containing 1. linear probe 2. plasmid 3. linear probe and plasmid. For the fourth group, we pretreated the HeLa cell with RNAse in the fixation to suppress unspecific fluorescence from linear probe and complementary RNA (ie. mRNA expressed by AR gene, the fluorescence spectra of 3L1gQ-1/AR mRNA was shown in Figure S2.6.1).

Perylene (488 nm) DsRed (561 nm) bright field Merge

Only linear probe

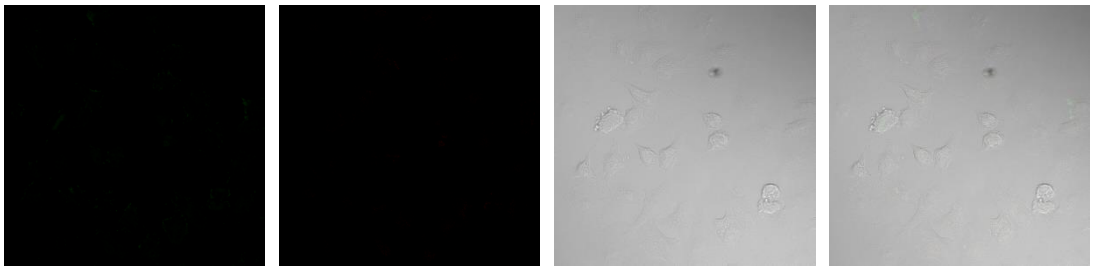

Only plasmid

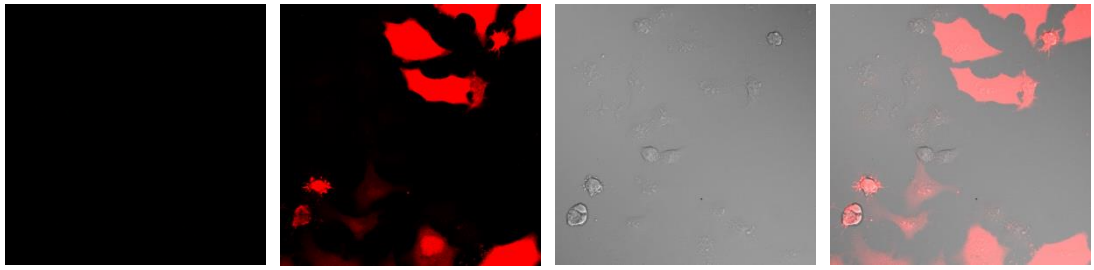

Plasmid + Linear probe

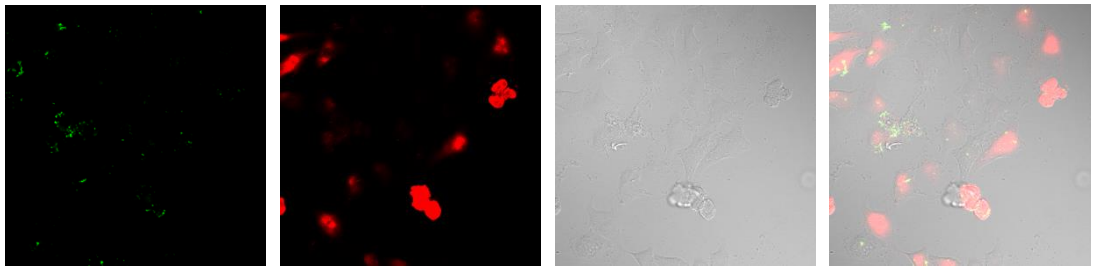

Plasmid + Linear probe (Processed by RNAse)

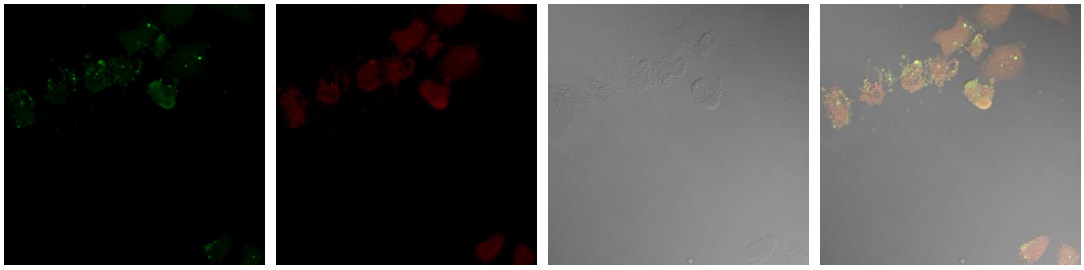

Figure 2.6.6 Visualization of mRNA transcribed from DsRed encoding plasmid by 3L1gQ-1 using confocal microscopy. DsRed: excitation at 561 nm, collected emission at 555-655 nm. Probe: excitation at 488 nm, collected emission at 500-540 nm. Magnification: 600x.

While plasmid did not exist in the cell, linear probe exhibited weak emission, indicating low background emission. After infection of plasmid containing dsRed monomer, red fluorescence protein has successfully translated in the cell as our expectation. In the cell containing plasmid, after addition of linear probe, fluorescence form fluorophore L could be visualized as our expectation. It should be noted that in group of cell which was treated by RNase, the fluorescence emission could still be visualized. Herein we could primarily conclude that linear probe successfully detected the AR gene in the plasmid in the fixed cell.

2.6.4 Imagination of beta-actin RNA in the Neuro-2a cell

As another application of linear probe, next I applied the linear probe to the mRNA detection in the neuron. Previously, we have proved the feasibility of linear probe for mRNA detection in living HeLa cells. Besides, it was known that the behavior of neuron

regulate the brain, which could help us to construct the neural network in the brain. Therefore, if the detection in the living neural succeeds, we were able to understand the neuron better.

At first, we chose to apply the linear probe to Neuro2a (N2a) cells, which can easier be handled than neurons, are selected as a model cell for beta-actin mRNA detection before the detection in living neurons. Visualization in fixed cells would be confirmed first and then apply the linear probes into the living cell. After I have confirmed the capability of linear probe in detection under neuron-like condition. I would like to further apply the linear probe into neuron detection. The procedure was almost the same as former cells.

For the sequence design, targeting beta-actin RNA, prediction of secondary structure has been done (Figure 2.6.7). For the regions where were not likely to hybridize, I have design two linear probes.

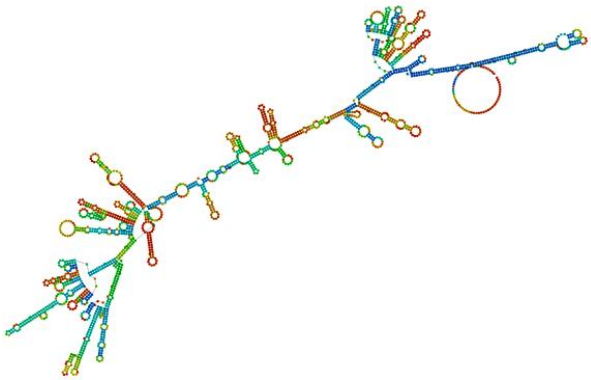

Figure 2.6.7 Prediction of secondary structure of beta-actin mRNA

As a results, I have selected 2 target binding regions in the beta-actin mRNA from positon 321 to 338(RNA1, 18mer) and 1073 to 1092 (RNA2, 20mer), here are the sequences of target RNA and linear probes. Linear probe 4e2q-1 and 4e2q-2 containing fluorophore E_2 and quencher Q has been synthesized (Figure 2.6.8, Table 2.6.1).

Table 2.6.1 Sequence of linear probe and target RNA

Target RNA	**RNA1**	5'-CCAUGGAUGACGAUAUCG-3'
	RNA2	5'-GGCAACGAGCGGUUCCGAUG-3'
Probes	**4e2q-1**	5'-C**Q**GATATC**E₂**GT**E₂**CA**E₂**TC**E₂**CATG**Q**G-3'
	4e2q-2	5'-CA**Q**TCGGA**E₂**AC**E₂**CG**E₂**CT**E₂**CGTTG**Q**CC-3'

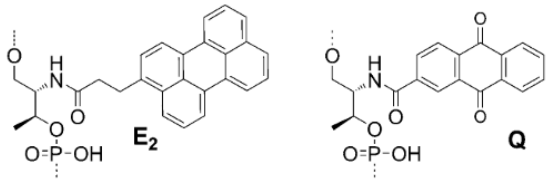

Figure 2.6.8 Chemical structure of fluorophore **E_2** and quencher **Q**.

Next the fluorescence measurements have been done. As Figure 2.6.9 showed, both of the probes showed a very high fluorescence emission at the presence of target RNA, whereas no emission observed in the single-stranded state (Signal/Background ratio: RNA1 252; RNA2 219 at 461.5 nm).

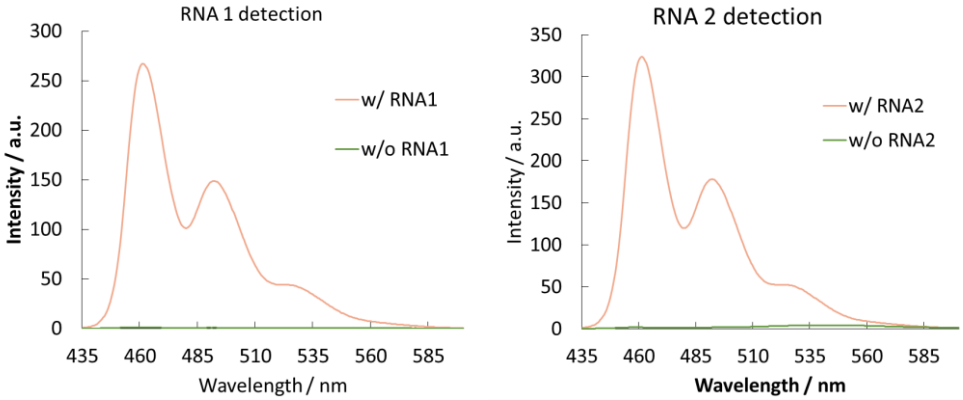

Figure 2.6.9 Fluorescence spectra of RNA1 and RNA2 detection. Condition: 1 μM indicated linear probe, 2 μM indicated RNA in 100 mM NaCl, 10 mM phosphate buffer. ex.=425 nm, pH=7.0, 20 ^{o}C.

For the negative control, I chose the HeLa cell which was easy to get in the laboratory. After checking the mRNA in the Hela cells by Basic Local Alignment Search Tool (BLAST, Figure 2.6.10), no complementary mRNA was shown to linear probe. Hence Hela cell line was regarded as great control group to the N2a cell line.

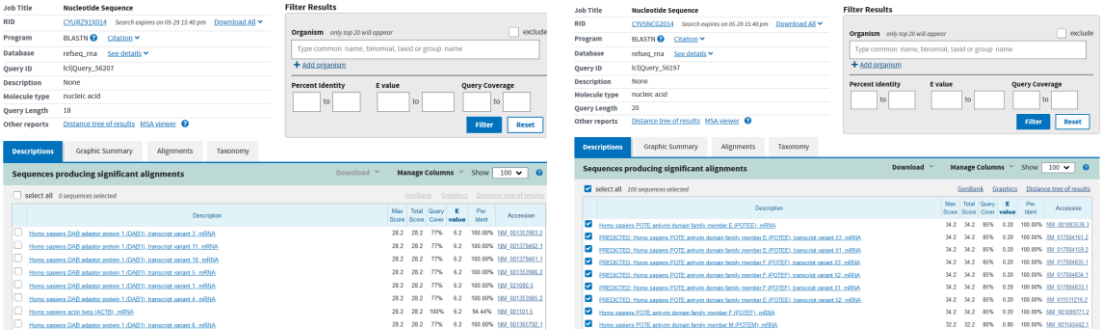

Figure 2.6.10 Blast results of probe1 (left) and probe 2 (right) in human RNA database.

Next both Hela cells and N2a cells were fixed and treated by PBS solution including different concentration of linear probes (20 pmol, 200 pmol). The imagines showed below:

4e2q-1 C**Q**GATATC**E**$_2$GT**E**$_2$CA**E**$_2$TC**E**$_2$CATG**Q**G

20 pmol HeLa cell

Condition: excitation wavelength: 445 nm; HV: 550 V; Gain: 3.25 x; offset: 10 %.

Fluorescence Emission **Bright Field** **Merge**

20 pmol HeLa cell

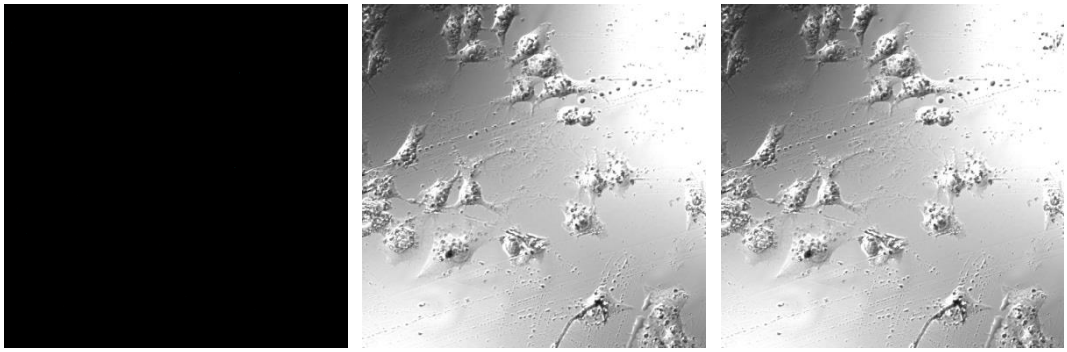

20 pmol N2a cell

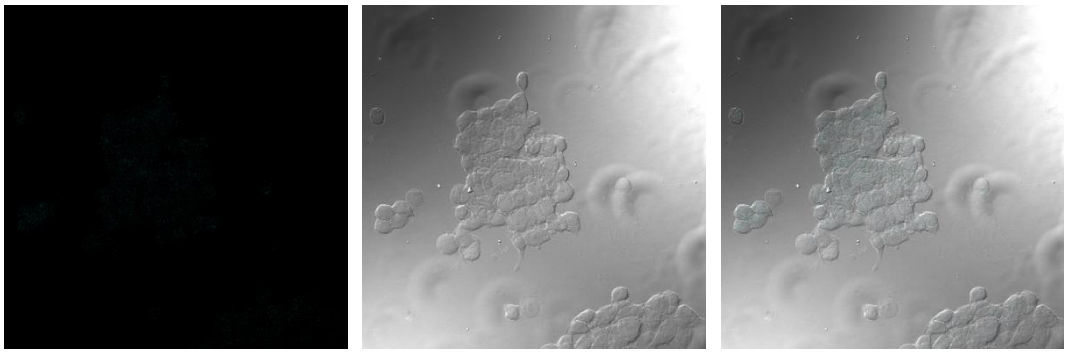

200 pmol HeLa cell

Condition: excitation wavelength: 445 nm; HV: 550 V; Gain: 3.25 x; offset: 10 %.

200 pmol N2a cell

4e2q-2 CA**Q**TCGGA**E**$_2$AC**E**$_2$CG**E**$_2$CT**E**$_2$CGTTG**Q**CC

20 pmol HeLa cell

Condition: excitation wavelength: 445 nm; HV: 570 V; Gain: 3.25 x; offset: 10 %.

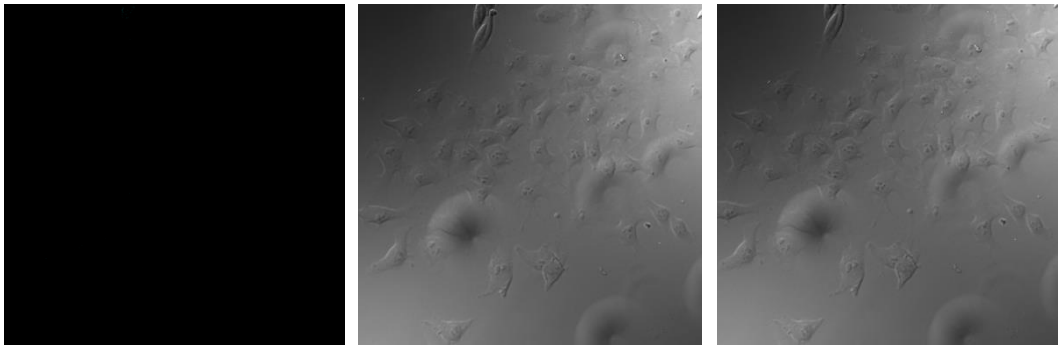

20 pmol N2a cell

200 pmol HeLa cell

Condition: excitation wavelength: 445 nm; HV: 510 V; Gain: 3.25 x; offset: 10 %.

200 pmol N2a cell

As a result, fixed N2a cell with high concentration of linear probe (200 pmole) exhibited clear emission under microcope. After comparison, 4e2q-2 showed the best S/B ratio in the N2a cell. Hence I have successfully applied the linear probe to the visualization of N2a cell line under neuron-like condition.

For the next step, the linear probe will be applied to the living N2a cell, the experiments should be continued in the future.

2.7 Nucleic acid test

2.7.1 Post-detection of PCR products

Another direction of triplex forming linear probe is the nucleic acid test, which was a method for diagnosis. In the construction of plasmid, I have finally got three plasmids within 0, 2 and 5 target regions, which would serve as the template for the subsequent PCR amplification and detection (Figure 2.7.1).

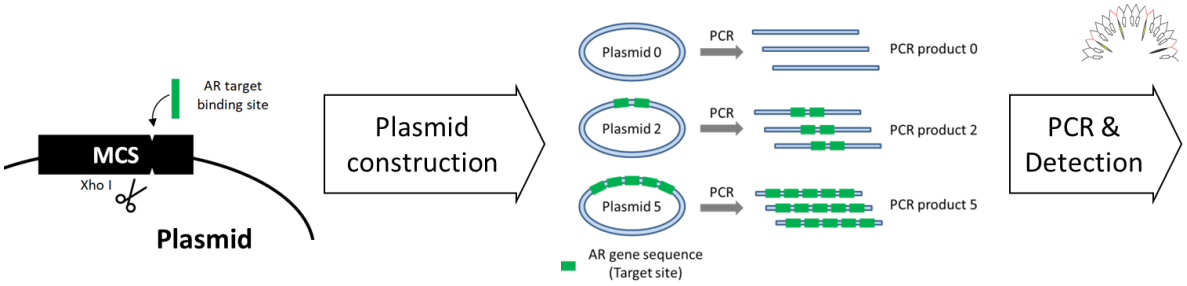

Figure 2.7.1 Schematic of nucleic acid test.

At first, native page was run to confirm the hybridization of linear probes. 1μM optimal linear probe 3L1gQ (3L1gQ-1 in the previous sections) was added into the mixture of polymerization chain reaction (PCR) products after 30 cycles amplification. In Figure 2.7.2, for the product 0 (lane 1, 2), since it did not have AR target region, no peryelene emission was visualized. For product 2 and 5 (lane 3-6), the linear probes sequence specifically hybridized to the PCR product, showing bands of triplex which were slightly higher than the duplex.

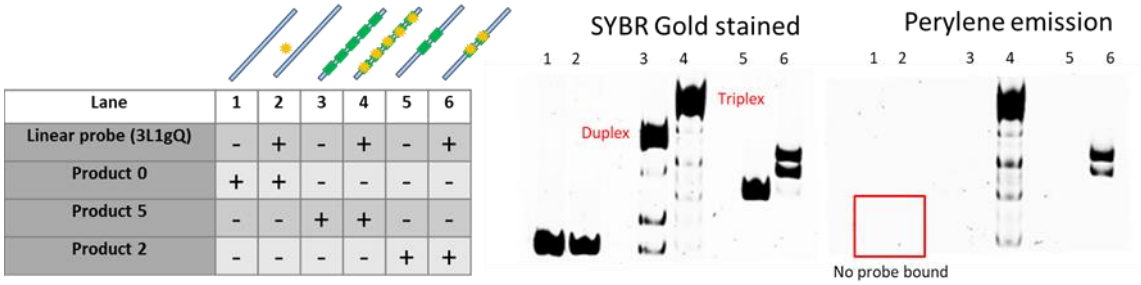

Lane	1	2	3	4	5	6
Linear probe (3L1gQ)	-	+	-	+	-	+
Product 0	+	+	-	-	-	-
Product 5	-	-	+	+	-	-
Product 2	-	-	-	-	+	+

Figure 2.7.2 Native page of post-PCR detection. Gel on the left indicated the emission of SYBR gold, gel on the right indicated the emission of fluorophore L (perylene).

Fluorescence emission of post-PCR detection was also characterized. However, linear probe exhibited unspecific emission for the detection of PCR products (Figure 2.7.3). We attribute the main reason to the interference of self-quenching in the linear probe caused by impurity in the PCR products, which was complex molecular system. Judge from the fluorescence spectra, we assumed the blue-shifted spectra caused by the transition of perylene from intramolecular charge transfer (ICT) state to locally excited (LE) state, which was also confirmed in the fluorophore with two aromatic moieties.[13] Refer to the results in the native PAGE, we cannot found unspecific emission from linear probe. It inspired us the idea to suppress the insufficient self-quenching by adding the glycerol to the sample.

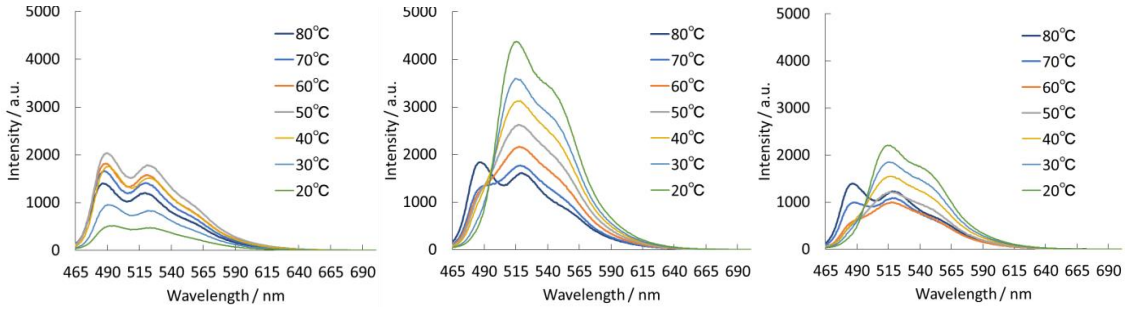

Figure 2.7.3 Comparison among different length of PCR products. Conditions: 1.0 μM linear probe, crude PCR products with 0, 5, 2 target inserts (from left to right), 90 mM TBM buffer ([$MgCl_2$] = 100 mM, pH 7.0), 20-80 °C.

We firstly test the feasibility by small scale experiments (20 uL). As our assumption, addition of glycerol could effectively suppress the unspecific background emission (Figure 2.7.4). Seems that glycerol has provided molecular crowding environment, which suppress insufficient self-quenching.

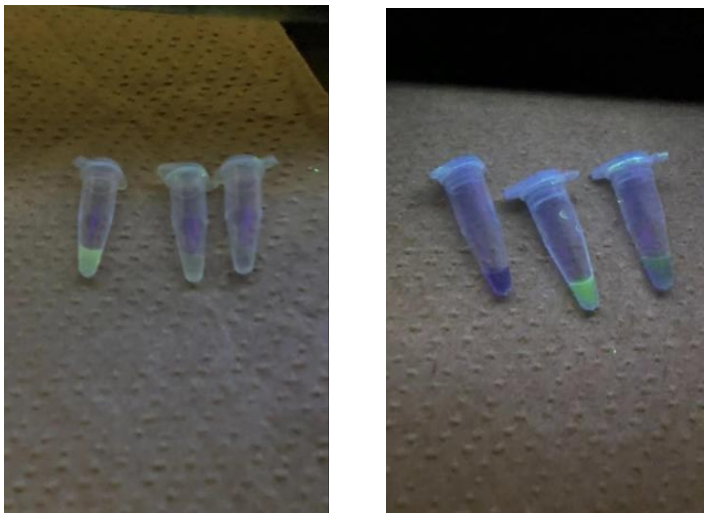

Figure 2.7.4 Image of samples under UV lamp (small scale). Left: without loading buffer; Right: within loading buffer containing 9 vol% glycerol. PCR samples from left to right: product 0, product 5 and product 2 containing 1.0 µM linear probe (3L1gQ).

Fluorescence spectra of PCR products detection containing 9 vol% glycerol were evaluated. In Figure 2.7.5, at the presence of linear probe 3L1gQ, specific fluorescence with the intensity corresponding to the target number was observed, while the product 0 without AR region exhibit limited emission. Detection of PCR product by SYBR green was designed as control group: SYBR green I was a molecular dye that can intercalated into duplex nucleic acid. Since this intercalation was sequence-unspecific, PCR product 0 still exhibited strong emission, which was not desirable.

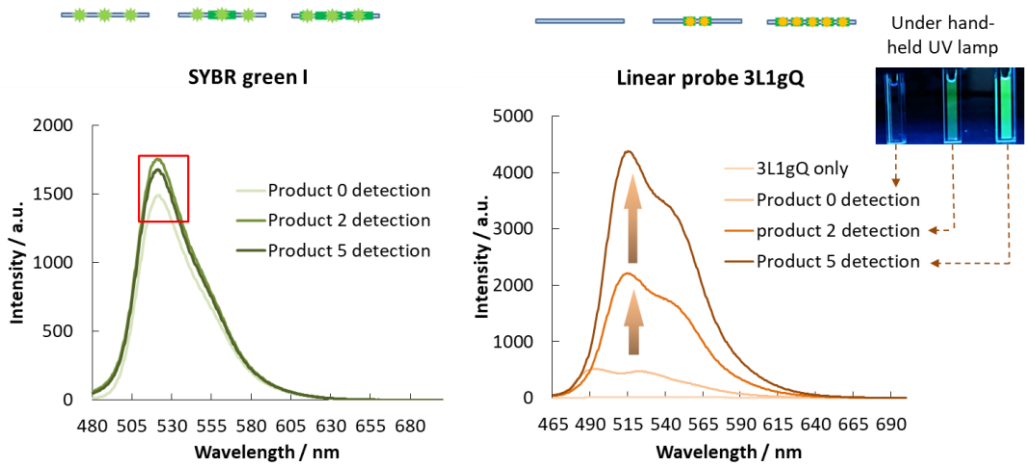

Figure 2.7.5 Direct fluorescence detection using 0.025 vol% SYBR Green I (10,000X in DMSO), ex. = 470 nm (left); 1.0 µM 3L1gQ, 50 µL crude PCR product, 9 vol% glycerol within 90 mM TBM buffer ($MgCl_2$=100 mM), pH 7.0 in a final volume of 200 µL, 20 ^{o}C. ex. = 455 nm (right); for visualization under hand-held UV lamp, ex.= 254 nm.

Because of its high S/B ratio, it should be noted that the difference of signal could be easily visualized by naked eyes under hand-held UV lamp, indicating the usefulness of linear probe for detection of PCR products.

2.7.2 Real-time PCR

Real-time PCR was subsequently performed (Figure 2.7.6). As a result, we have successfully observed the process of polymerization reaction by monitoring the emission of peryelene L. Moreover, similar quantification curves to the real-time detection by SYBR green I, which served as positive control. It indicated the accuracy of linear probe 3L1gQ in the real-time PCR.

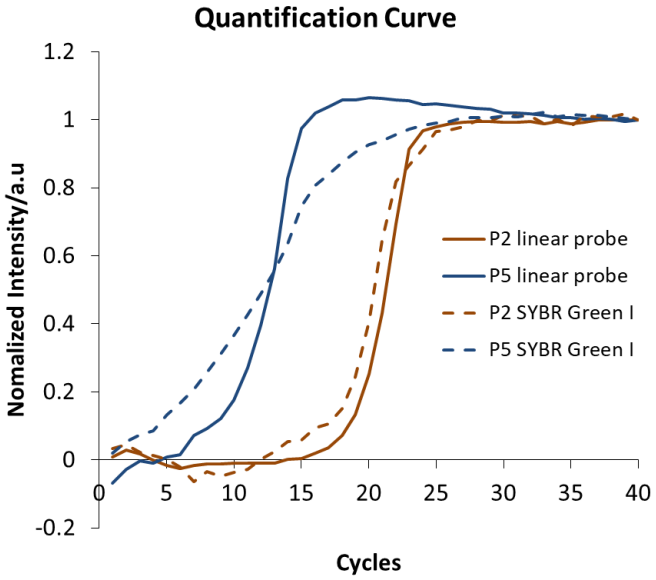

Figure 2.7.6 Amplification curves of real-time PCR. Conditions: 1 µM 3L1gQ or 0.025 vol% SYBR green I, 5 µL glycerol in 50 µl PCR sample, 9 vol% glycerol. Excitation wavelength: 470 nm, emission wavelength: 514 nm.

2.8 Summary

As a result, we have successfully proved developed triplex-forming linear probe targeting dsDNA (Figure 2.8.1): The probe conducted properly, following designed process in the schematic. Besides, with the incorporation of fluorophore, the melting temperatures of triplex raised a lot, although interaction between fluorophores still remained in the triplex. Finally, we optimized the triplex-forming linear probe with three fluorophore every three base pair which exhibited the relatively high S/B ratio (10) and highest melting temperature (T_m=53.1℃ under 100 mM $MgCl_2$).

Then, we have further optimized chemical structure of linear probe for better adaptation in the triplex formation. Fluorophore L with long and straight linker was proved to intercalate in duplex better than fluorophore F, result in an extremely stable triplex formation (T_m=72.7℃ under 100 mM $MgCl_2$). It was assumed to serve as the theoretical support for the development of high-order molecular assembly in the future.

Next, to test its detecting ability, human androgen receptor gene was selected as new dsDNA target. As a result, even though cytosine cannot be protonated in the linear probe at neutral condition. By further incorporation of quencher gQ which also has a long linker, we have successfully designed an excellent linear probe (3L1gQ-1/named 3L1gQ in section 2.7) with signal/background (S/B) ratio of as high as 280. More significantly, melting temperature of the triplex with 3L1gQ-1 (T_m=61.9 ℃) was much higher than that of native DNA (40.0 ℃), suggesting remarkably improved stability on target duplex.

I have attempted dsDNA detection in the fixed HeLa cell. After processing the fixed cell by RNase, we have successfully confirmed specific emission of linear probe. As a potential application, detection of beta-actin in the N2a cells has also performed and successfully. Although for the cell visualization, more experiments were needed to prove the usefulness of triplex-forming linear probe, we have primarily confirmed its potential feasibility for cell imagination.

Finally, as another direction of application, we applied optimal linear probe to nucleic acid test: by utilizing the constructed plasmid as template, both post-detection of PCR products and real-time PCR were conducted. As a result, both of the detection succeeded, achieving high S/B reaction which could be easily visualized by naked eyes. Such a fluorescent probe with high versatility was assumed as powerful tools for wide range of application, both *in vivo* and *in vitro*.

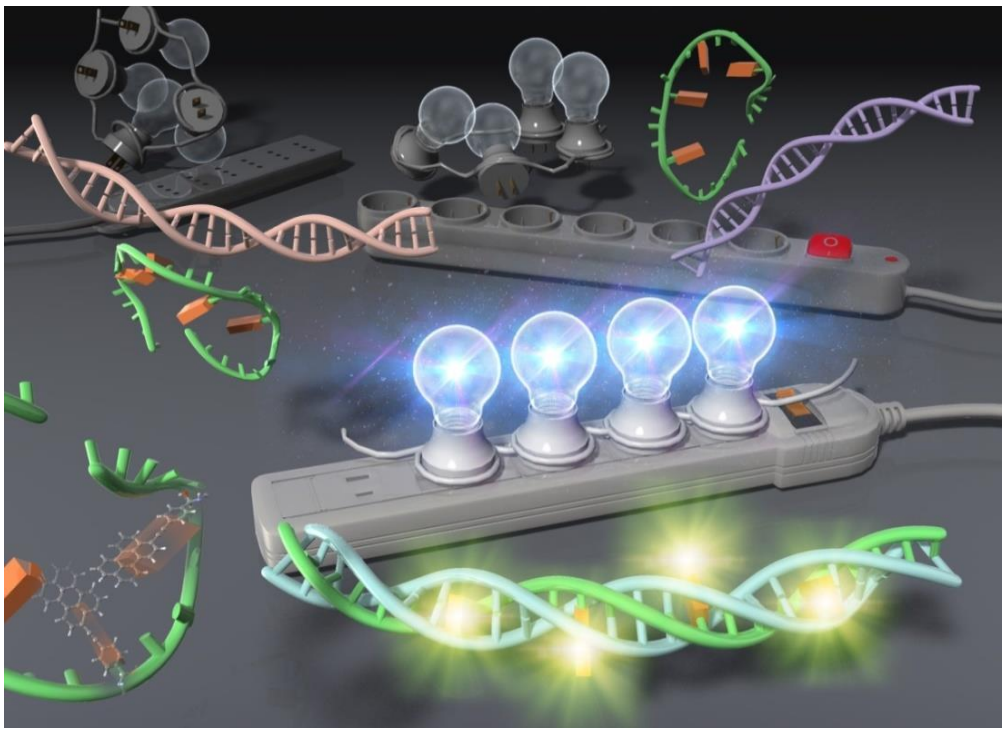

Figure 2.8.1 Graphic illustration of triplex forming linear probe.

2.9 Appendix

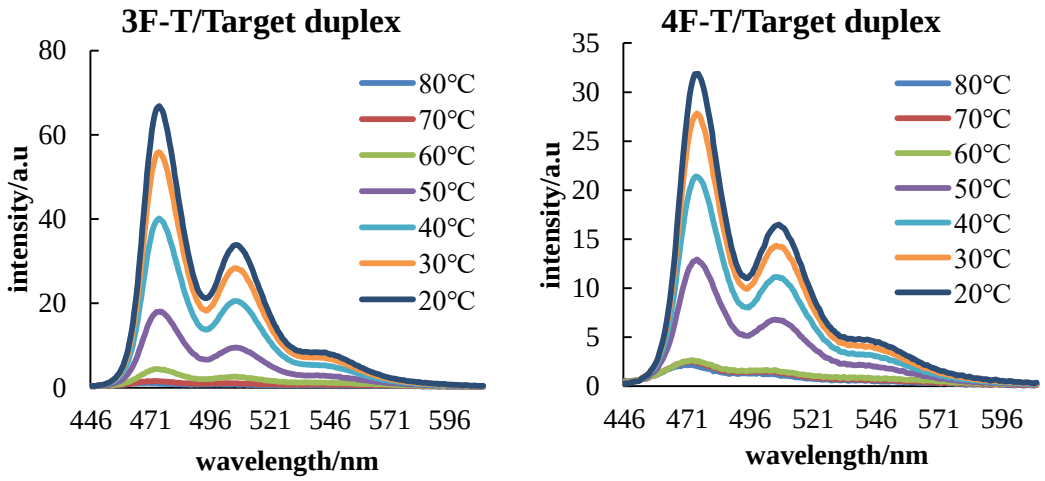

Figure S2.3.1 Fluorescence emission of each linear probe (1F-T, 2F-T, 3F-T, 4F-T) at triplex formation. Conditions: Excitation wavelength: 440nm; Linear probe 1.0 μM, DNA-A 1.0 μM, DNA-T 1.1 μM in 90mM TB buffer ([$MgCl_2$] = 10mM, pH 7.0).80-20 ℃.

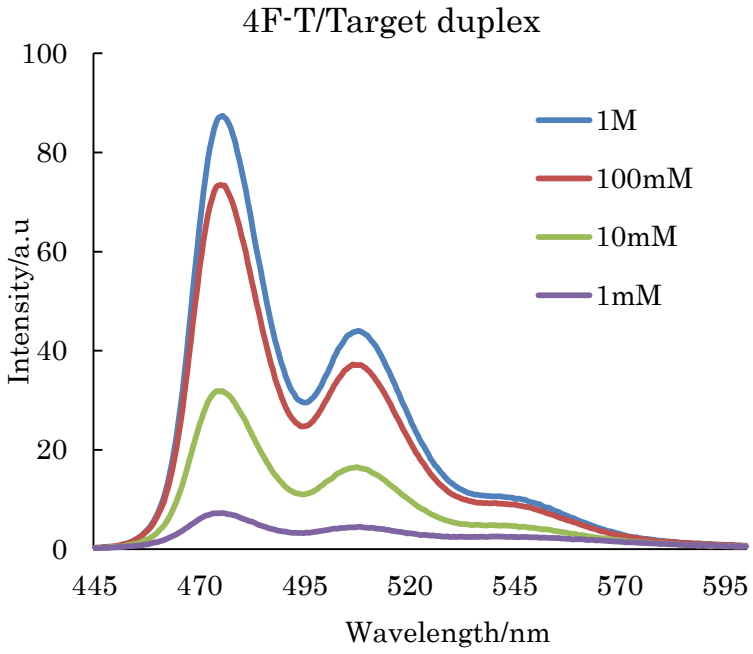

Figure S2.3.2 Fluorescence emission of each linear probe (4F-T) at triplex formation in different Mg^{2+} concentration. Conditions: Excitation wavelength: 440nm; Linear probe 1.0 μM, DNA-A 1.0 μM, DNA-T 1.1 μM in 90mM TB buffer ([$MgCl_2$] = 1, 10, 100, 1000mM, pH 7.0). 20 ℃

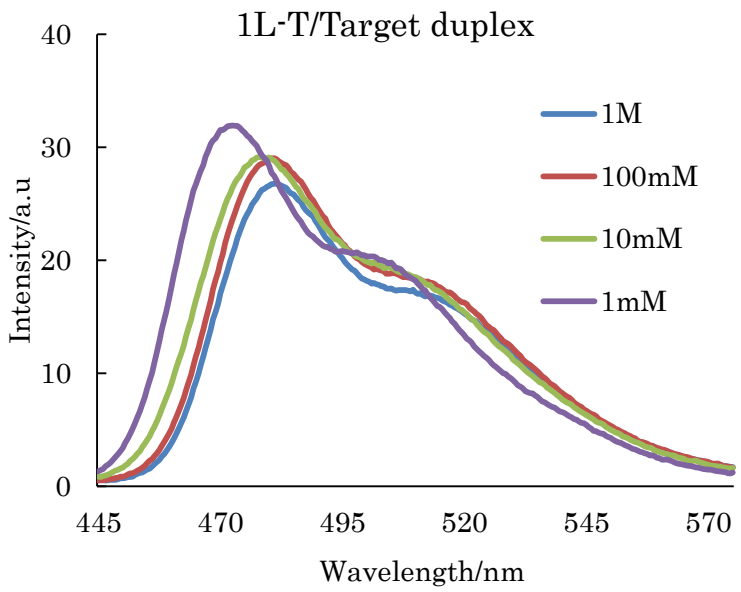

Figure S2.4.1 Fluorescence emission of each linear probe (1L-T) at triplex formation in different Mg^{2+} concentration. Conditions: Excitation wavelength: 455nm; Linear probe 1.0 μM, DNA-A 1.0 μM, DNA-T 1.1 μM in 90mM TB buffer ([$MgCl_2$] = 1, 10, 100, 1000mM, pH 7.0). 20 ℃

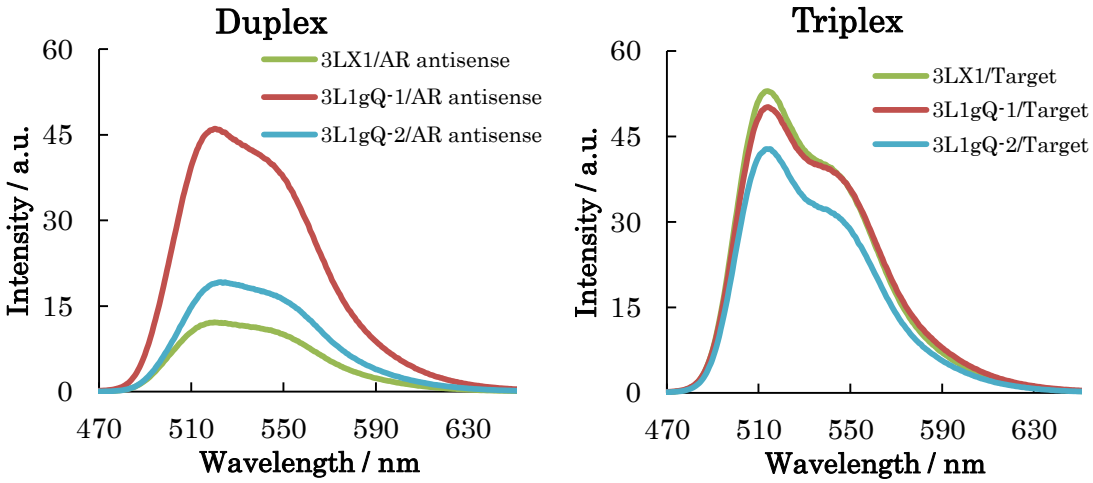

Figure S2.5.1 Fluorescence spectra of linear probe for AR dsDNA detection (3LX1, 3L1gQ-1, 3L1gQ-2). Left: Duplex; Right: Triplex. Conditions: Excitation wavelength: 455nm; Linear probe 1.0 uM, AR antisense 1.0 μM, AR sense 1.1 μM in 90mM TB buffer ([$MgCl_2$] = 100mM, pH 7.0). 20 ℃

AR antisense **AR sense**	**5'-CTACTAAAGAAGAAAAGAGAGAAGAATC-3'** **3'-GATGATTTCTTCTTTTCTCTCTTCTTAG-5'**
3L1gQ-1	5'-LTTTLCTTLCTTTTCgQTCTCTT-3'
AR mRNA	5'-AAGAGAGAAAAGAAGAAA-3'

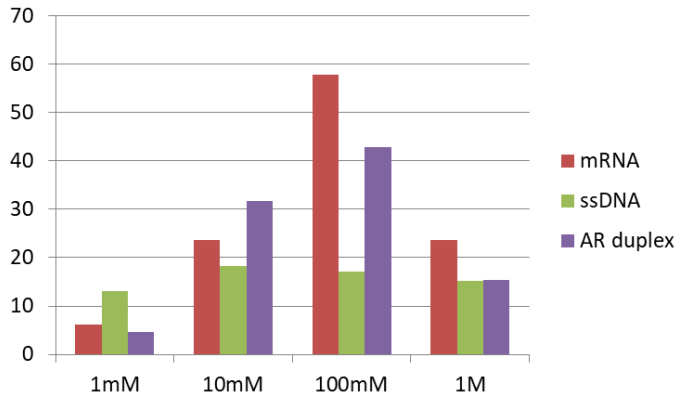

Figure S2.6.1 Comparison of fluorescence emission intensities among different targets (mRNA, ssDNA, AR duplex). Conditions: Excitation wavelength: 455nm; Linear probe 1.0 μM, AR mRNA 1.0 μM, AR antisense 1.0 μM, AR sense 1.1 μM in 90mM TB buffer ([$MgCl_2$] = 100mM, pH 7.0). 20 ^{o}C.

Protocol 1 for transformation

Subcloning Competent E.coli Transformation Protocol (C2988)

1. Thaw a tube of NEB 5-alpha Competent E. coli cells on ice until the last ice crystals disappear. Mix gently and carefully pipette 50 µl of cells into a transformation tube on ice.

2. Add 1-5 µl containing 100 pg-1 µg of plasmid DNA to the cell mixture. Carefully flick the tube 4-5 times to mix cells and DNA. Do not vortex.

3. Place the mixture on ice for 30 minutes. Do not mix.

4. Heat shock at exactly 42°C for exactly 30 seconds. Do not mix.

5. Place on ice for 5 minutes. Do not mix.

6. Pipette 950 µl of room temperature SOC medium into the mixture.

7. Place at 37°C for 60 minutes. Shake vigorously (250 rpm) or rotate.

8. Warm selection plates to 37°C.

9. Mix the cells thoroughly by flicking the tube and inverting, then perform several 10-fold serial dilutions in SOC.

10. Spread 50-100 µl of each dilution onto a selection plate and incubate overnight at 37°C. Alternatively, incubate at 30°C for 24-36 hours or 25°C for 48 hours.

Protocol 2 for DNA purification

Dr. GenTLE™ Precipitation Carrier

1. Add 0.1 volume of 3 M Sodium Acetate (pH 5.2) to the nucleic acid sample*1 and vortex.

2. Add 4 µl*2 of Dr. GenTLE Precipitation Carrier and vortex.

3. Add 2.5 volumes of ethanol and vortex.

4. Centrifuge at 12,000 rpm at 4℃ for 15 min.

5. Discard the supernatant.

6. Rinse the pellet with 70% ethanol 700uL and centrifuge again at 12,000 rpm under 4℃ for 5 min.

7. Discard the supernatant and dry.

8. Dissolve the pellet in sterile purified water or TE buffer.

Protocol 3 for agarose gel electrophoresis

1. Add loading buffer to each of your DNA samples. (DNA: purple loading buffer: Sterile water＝1: 2: 3)

2. Once solidified, place the agarose gel into the gel box (electrophoresis unit).

3. Fill gel box with 1xTAE until the gel is covered.

4. Carefully load a molecular weight 2-log ladder into the first lane of the gel.

5. Carefully load your samples into the additional wells of the gel.

6. Run the gel at 100 V until the dye line is approximately 75-80% of the way down the gel. A typical run time is about 40 mins, depending on the gel concentration and voltage.

7. Turn OFF power, disconnect the electrodes from the power source, and then carefully remove the gel from the gel box.

8. Using the device that has UV light, visualize your DNA fragments. The fragments of DNA are usually referred to as 'bands' due to their appearance on the gel.

Protocol 4 for transfection of constructed plasmid

1. Adherent cells: One day before transfection, plate 0.5-2x10^5 cells in 500 μl of growth medium without antibiotics so that cells will be 70-90% confluent at the time of transfection. Suspension cells: Just prior to preparing complexes, plate 4-8x10^5 cells in 500 μl of growth medium without antibiotics.

2. For each transfection sample, prepare complexes as follows:

a. Dilute DNA in 50 μl of Opti-MEM I Reduced Serum Medium without serum (or other medium without serum). Mix gently.

b. Mix lipofectamine 2000 regents gently before use, then dilute the appropriate amount in 50 μl of Opti-MEM I Medium. Incubate for 5 minutes at room temperature. Note: Proceed to Step c within 25 minutes.

c. After the 5-minute incubation, combine the diluted DNA with diluted Lipofectamine 2000 (total volume = 100 μl). Mix gently and incubate for 20 minutes at room temperature (solution may appear cloudy). Note: Complexes are stable for 6 hours at room temperature.

3. Add the 100 μl of complexes to each well containing cells and medium. Mix gently by rocking the plate back and forth.

4. Incubate cells at 37°C in a CO_2 incubator for 18-48 hours prior to testing for transgene expression. Medium may be changed after 4-6 hours.

5. For stable cell lines: Passage cells at a 1:10 (or higher dilution) into fresh growth medium 24 hours after transfection. Add selective medium (if desired) the following day.

Protocol 5 Fluorescence in situ hybridization (FISH)

1. Proper number of cells ($4x10^4$) to cover glass was placed in 12-well plate, incubated by 500 µL Dulbecco's Modified Eagle Medium (DMEM).

2. Incubate cells at 37°C in a CO_2 incubator for 24 hours.

3. Remove solution from the well, wash twice with 1x phosphate buffered saline (PBS). Fix cells in 500 µL PFA-PBS (formalin).

4. Discard PFA-PBS, add 500 µL PTGN (G: 10 mM glycine; N: NaN_3; T: 0.1 % Triton™ X-100; P: 1X PBS), incubate for 5 mins. Then, place the cover glass on wet paper towel.

5. Place 100 µL PGN containing 200 pmol linear probe on the cover glass, incubate 1 hour under 37°C.

6. Place cover glass into well and rinse twice with PGN.

7. Place 10 µL MoWiOL on the glass plate. Cover glass taken from the well is embedded on the glass plate, and incubates overnight in the dark.

2.10 Reference

[1] S. Rhee, Z. J. Han, K. Liu, H. T. Miles, D. R. Davies, *Biochemistry* **1999**, *38*, 16810–16815.

[2] J. Y. Chin, E. B. Schleifman, P. M. Glazer, *Front. Biosci. 12* **2007**, *12*, 4288–4297.

[3] M. P. Knauert, P. M. Glazer, *Hum. Mol. Genet.* **2001**, *10*, 2243–2251.

[4] J. L. Mergny, J. S. Sun, M. Rougée, T. Montenay-Garestier, J. Chomilier, C. Hélène, F. Barcelo, *Biochemistry* **1991**, *30*, 9791–9798.

[5] T. Foster, K. Kasper, *Z. Phys. Chem.* **1954**, *1*, 275.

[6] W. Tan, K. Wang, T. J. Drake, *Curr. Opin. Chem. Biol.* **2004**, *8*, 547–553.

[7] B. N. G. Giepmans, S. R. Adams, M. H. Ellisman, R. Y. Tsien, *Science (80-.).* **2006**, *312*, 217–224.

[8] Y. Hong, J. W. Y. Lam, B. Z. Tang, *Chem. Commun.* **2009**, 4332–4353.

[9] H. Asanuma, M. Akahane, R. Niwa, H. Kashida, Y. Kamiya, *Angew. Chemie - Int. Ed.* **2015**, *54*, 4315–4319.

[10] Y. Chen, K. Murayama, H. Kashida, Y. Kamiya, H. Asanuma, *Chem. Commun.* **2020**, *56*, 5358–5361.

[11] H. Kashida, N. Kondo, K. Sekiguchi, H. Asanuma, *Chem. Commun.* **2011**, *47*, 6404–6406.

[12] M. K. Graham, T. R. Brown, P. S. Miller, *Biochemistry* **2015**, *54*, 2270–2282.

[13] A. Suzuki, T. Yanaba, I. Saito, Y. Saito, *ChemBioChem* **2014**, *15*, 1638–1644.

Chapter 3. Hybridization Chain Reaction Composed of Acyclic Xeno Nucleic Acid

3.1 Introduction

3.1.1 DNA circuit

By utilizing a simple concept of strand displacement,[1] circuit consists of a serious of DNA strands implement functional algorithm in molecular level (Figure 3.1.1). DNA circuits have been widely facilitated over digital circuit computation,[2][3][4][5] biomolecular sensing,[6][7][8] chemical synthesis,[9] protein polymerization,[10] and nano-machines.[11][12] The circuit has been achieved via an orthogonality based on sequence complementarity for duplex formation. However, under complex condition some mismatched base-pairs were acceptable for duplex formation in long DNA sequences, only giving slight destabilization.

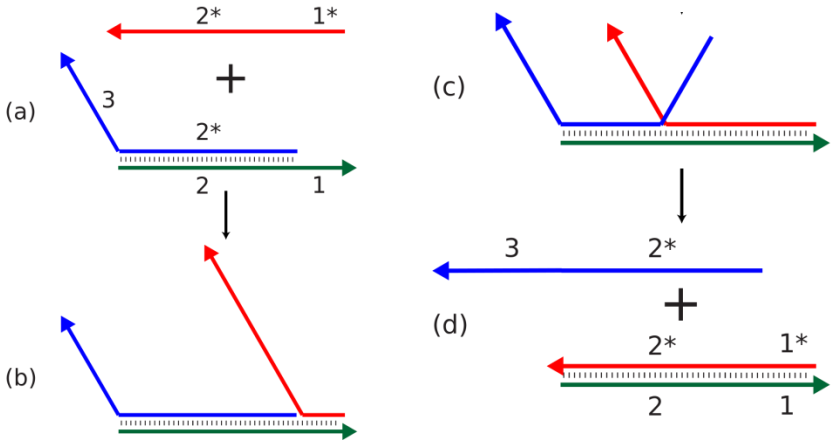

Figure 3.1.1 Basic concept of strand displacement, form (a) to (d). DNA duplex with overhang (strand number 1) of template strand (colored in green) could hybridized to the fuel strand (red) from 1*, which has longer complementary part than output strand (blue). Then fuel strand gradually invades the output/template duplex, overcoming the energy barrier. At last, fuel strand forms stable duplex with template strand, resulting in release of output strand.

In addition, partially complementary sequences can interact with each other to form unintended duplex, triplex, quadruplex, and other high-ordered structures, which

severely disturb the design of the circuit. Such incomplete orthogonality limits the development of complicated DNA circuit system. To expand the circuit system, use of orthogonal artificial nucleic acids would have a great potential.

3.1.2 D-*a*TNA see-saw circuit

Previously, we have attempted an orthogonal see-saw circuit consist of D-*a*TNA (Figure 3.1.2a), which was artificial nucleic acids: D-*a*TNA input was released via strand displacement of RNA and SNA/D-*a*TNA input duplex.[13] Furthermore, D-*a*TNA input conducted D-*a*TNA see-saw gate, releasing the output strand which was modified by Cy3 fluorophore. Since D-*a*TNA cannot form homo duplex to RNA, the orthogonal detection of RNA achieved.

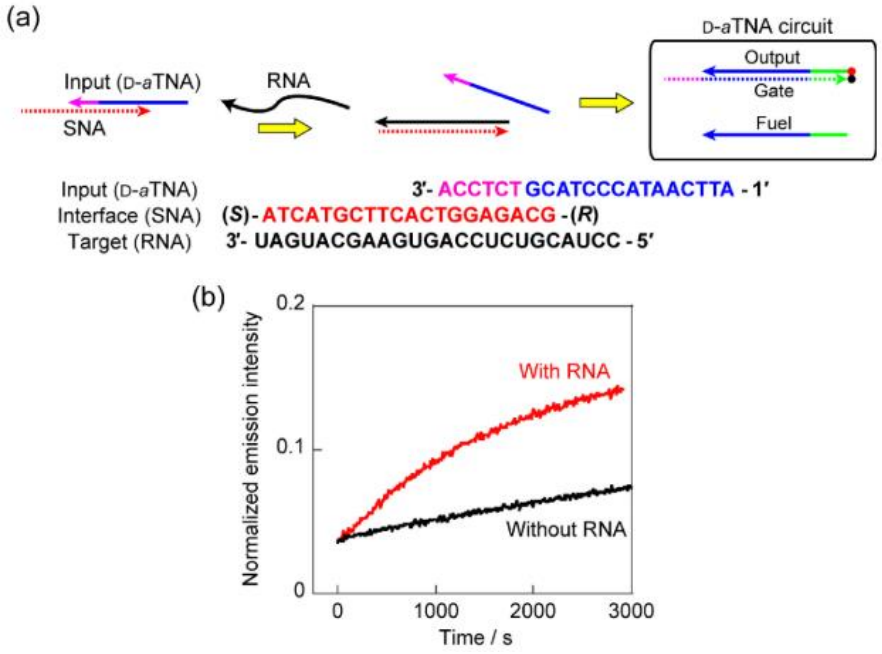

Figure 3.1.2 RNA-mediated activation of D-*a*TNA circuit via an SNA interface. (a) schematic of the conversion of RNA to D-*a*TNA input via SNA and the sequences used. The SNA prevents activation by D-*a*TNA input in the absence of RNA. Addition of RNA allows release of D-*a*TNA input to activate the circuit. (b) Signal generation of D-*a*TNA circuit with SNA interface in the presence (red) and absence (black) of target RNA.

As a result (Figure 3.1.2b), at the presence of target RNA, specific fluorescence was observed, whereas the reaction without RNA exhibited limited fluorescence. However, the leakage in the reaction was significant, and the kinetics of designed signal amplification was slow. Therefore, it is necessary to develop a highly efficient XNA circuit for orthogonal RNA detection.

3.2 Method

3.2.1 Hybridization chain reaction

Hybridization chain reaction (HCR) might be the most-used DNA circuits for biosensing due to ease of synthesis: only two distinct hairs-pin (HP) strands needs to be designed (HP1 and HP2 in Figure 3.2.1).[14] Under well sequence design, HP forms energy barrier for oligomerization, while this phenomenon will be broken in addition of complementary input strand. Details of signal amplification mechanism are illustrated in the Figure 3.2.1: HP2 modified with fluorophore and quencher was quenched in the single-stranded state. In addition of input strand, because of toehold design in HP1, strand displacement occurs, forming input/HP1 duplex. Then, the overhang of duplex will further cause strand displacement on the HP2, resulting in a long duplex product and the fluorescence recovers due to the separation of fluorophore and quencher. Notably, previous products also can be extended by HP1 due to the complementary sequence design at the overhang. Therefore, cascade reaction was conducted. Base on small amount of input strands, long DNA duplex products with exponential amplification of fluorescence could be observed.

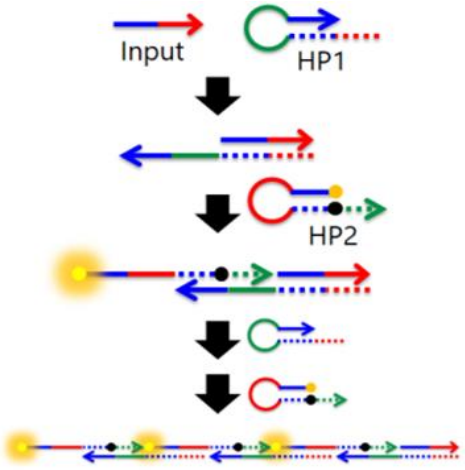

Figure 3.2.1 Illustration of HCR circuit

For DNA-based HCR circuit, however, there are several key challenges: 1. Background leakage due to spurious hybridization events often occur in the absence of the trigger strand, unless the stem in the hair-pin is designed pretty long (normally, more than 12-mers). 2. Although long stem can maintain hairpin metastability, the separation also relatively becomes difficult, which results in an extremely long reaction time (1-2 days) in the HCR circuit. 3. Natural DNA will easily be recognized by deoxyribonuclease. Herein application of DNA-HCR was limited such as living cell

visualization.

3.2.2 Orthogonal platform composed of acyclic nucleic acid

Artificial nucleic acids with modification on the mainchain scaffold have been referred to as xeno-nucleic acid (XNA). Several orthogonal XNAs that cannot hybridize to DNA and RNA have been also reported.[15][16][17][18] Induction of inversed helicity is an effective approach to facilitate the orthogonality. For example, right-handed D-DNA and left-handed L-DNA does not cross-hybridize with each other even though the sequences were complementary.[19] Ly et al. reported gamma-peptide nucleic acid (γPNA), a helicity can be controlled by a chiral center at the γ-position on the backbone.[20][21] Right-handed γPNA cross-hybridizes with D-DNA and D-RNA, whereas Left-handed one does not. Hetero duplex between right-handed γPNA and left-handed γPNA is also impossible. Such helical orthogonality promises a parallel processing of DNA circuit and orthogonal XNA circuit at the same time.

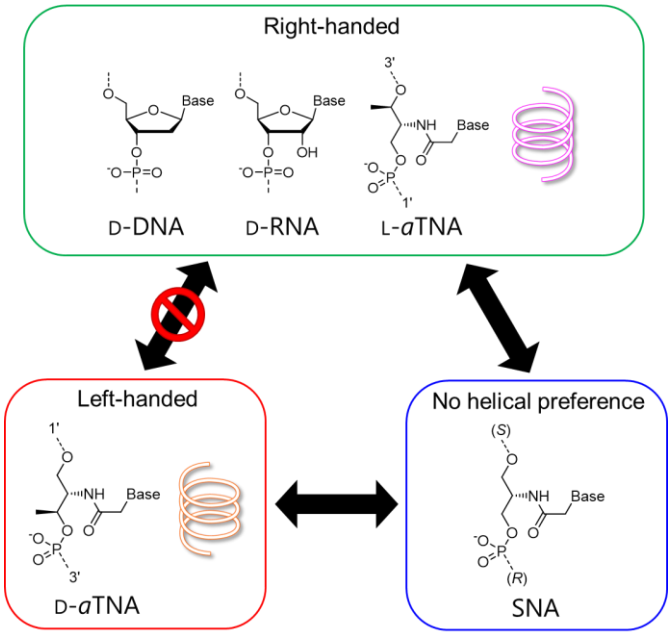

Figure 3.2.2 Chemical structures, helicity, and compatibility on hybridization of DNA, RNA, D-*α*TNA, SNA and L-*α*TNA. Oligonucleotides belonging to right-handed group can form homo- and hetero-duplex among them, while D-*α*TNA with left-hand helicity is orthogonal to them. SNA has achiral symmetrical scaffold with no helical preference can hybridize with both oligonucleotides belonging to right- and left-handed helicities.

Previously, our group has also developed an XNA platform with high orthogonality: D-threoninol nucleic acid (D-*α*TNA), L-threoninol (L-*α*TNA), and serinol nucleic acid (SNA). As Figure 3.2.2 showed, because of conformational compatibility, left-handed

D-*a*TNA was orthogonal to right-handed D-DNA, D-RNA, and L-*a*TNA. Besides, SNA composed symmetric linker with no helical preference, could act as interface that enabled translation of D-RNA information to D-*a*TNA circuit. Herein we would like to construct HCR circuit base on XNA, enabling signal amplification of D-RNA in simplified sequence design, strong nuclease tolerance, high orthogonality, and fast kinetics.

3.3 SNA-HCR circuit

3.3.1 SNA-HCR with short stem/toehold

We developed the XNA-HCR circuit from SNA. Table 3.3.1 indicated the sequence design of SNA-HCR circuit. Base on a part of target microRNA-20a (miR20a, 17-mer from 3'-end was selected as target region), we designed two SNA hair-pin strand (HP1, HP2) in different length of toehold and stem (5-7, 5-6, 6-7, respectively). Notably, the delta G (gibbs free energy) were primarily confirmed by Oligoanalyzer Tool.

Table 3.3.1 Sequence design of SNA-HCR 5-7, 5-6, 6-7. Calculated delta G (kcal/mol) was listed on the right. RNA with purple font represented complementary sequences to SNA. Red, blue and green font in SNA hair-pin strand represented the stem and toehold.

miR-20a (23 mer) (from 3')		
5'-UAAAGUGCUUAUAGUGCAGGUAG-3'		
HP1 R- CGAATATCACGTCCATCGGAATGATGGAC-*S*	*5-7*	*-6.02*
HP2 S- CCTTA**M**CTACCTGTAGTGCAGGTAG**Y**-*R*		*-6.55*
5'-UAAAGUGCUUAUAGUGCAGGUAG-3'		
HP1 R- CGAATATCACGTCCATCGGAATGATGGA-*S*	*5-6*	*-4.43*
HP2 S- CCTTA**M**CTACCTAGTGCAGGTAG**Y**-*R*		*-4.76*
5'-UAAAGUGCUUAUAGUGCAGGUAG-3'		
HP1 R- CGAATATCACGTCCATCGGAATAGATGGAC-*S*	*6-7*	*-5.43*
HP2 S- CCTTAT**M**CTACCTGATAGTGCAGGTAG**Y**-*R*		*-5.04*
Y = Cy3, M = Methyl Red		

Notably, HP1 was designed with an extra overhang (orange and red parts) at R-terminal, which was assumed to stabilize the affinity to miR20a. Herein the cascade reaction was slightly different to the traditional one: extra overhang would stretch out of the product (Figure 3.3.1a). HP2 was modified with Cy3 fluorophore and Methyl Red

quencher (Figure 3.3.1b), which was general pair for static quenching. Like the molecular beacon, HP2 was supposed to be quenched while input did not exist, whereas the fluorescence recovered in the cascade reaction.

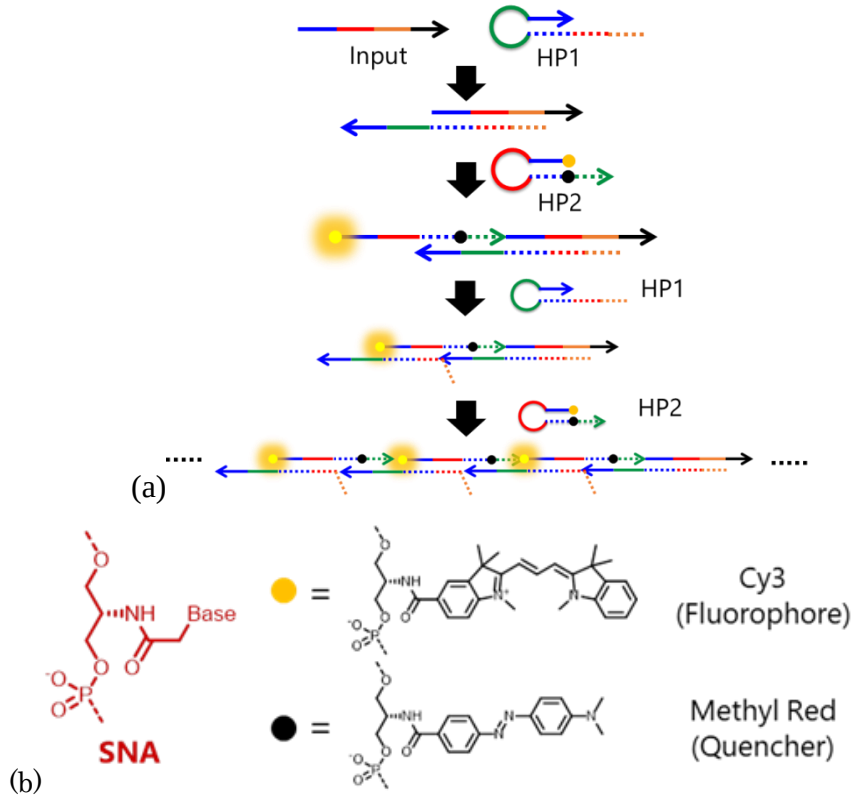

Figure 3.3.1 (a) Schematic of SNA-HCR targeting miR20a (S5-7, S-5-6, S-6-7). (b)Chemical structures of fluorophore Cy3 and quencher Methyl Red in the SNA hairpin.

Firstly, to confirm the hair-pin structure, the fluorescence spectra of HP2 were monitored with annealing process. We assumed the stem in SNA hairpin would unwind under high temperature and exhibit the maximum fluorescence emission, which could serve as reference for further evaluation. However, SNA HP2 in 20 ^{o}C showed highest fluorescence intensity, fluorescence intensity decreases along with increasing temperature. Similar spectra were recorded among S-5-6, S-5-7, and S-6-7 HP2 (Figure 3.3.2a-c, respectively). We contributed the problem to the ultra-high melting temperature in the SNA stem, herein it could be emphasized that hairpin structure has formed.

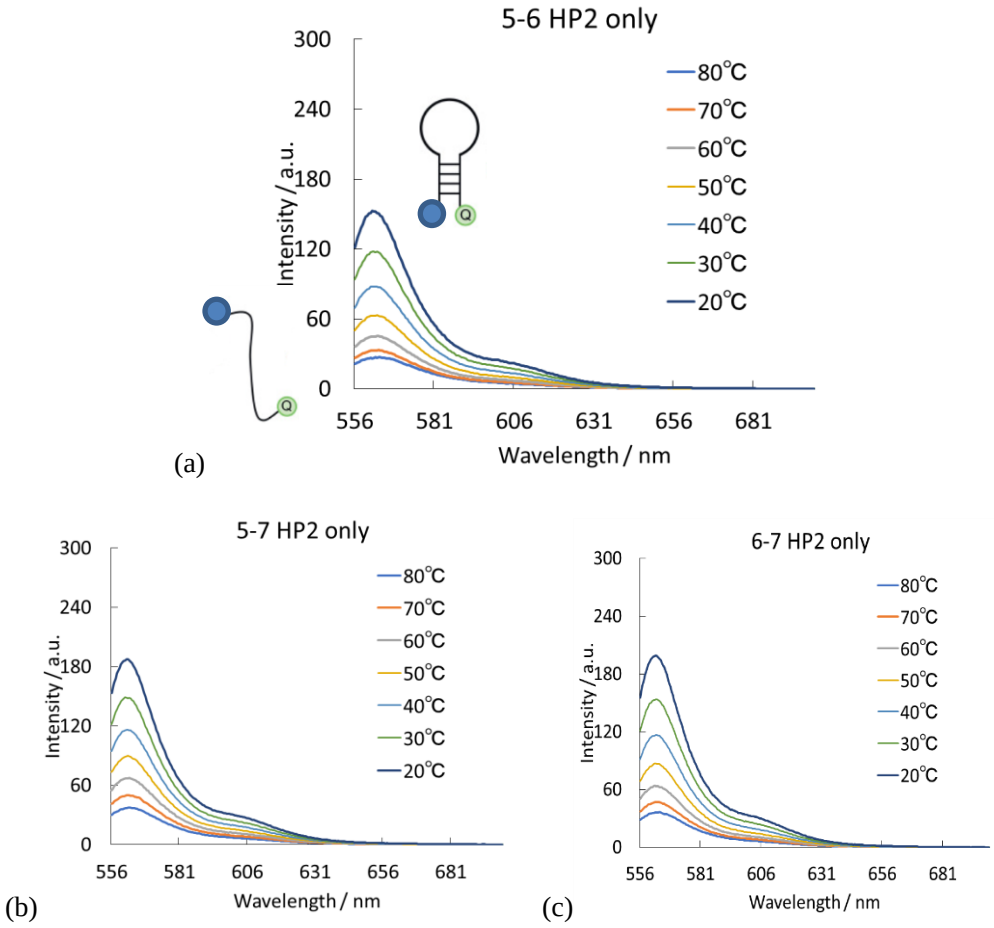

Figure 3.3.2 Temperature-interval fluorescence spectra of (a) S-5-6 HP2, (b) S-5-7 HP2, and (c) S-6-7 HP2. 100 nM indicated HP2 in 10 mM phosphate buffer containing 100 mM NaCl, pH=7.0, 80 ^{o}C-20 ^{o}C, Ex.= 546nm ; for interval spectra: Em.= 556 nm-700 nm.;

Next the kinetics of SNA-HCR (500 nM HP1 and HP2 in 10 mM phosphate buffer containing 100 mM NaCl) with/without 100 nM miR20a were subsequently measured by monitoring the fluorescence emission of Cy3 at 562 nm (Figure 3.3.3). As a result, in absence of miR20a, no leakage was observed for S-5-6 and S-5-7, whereas S-6-7 exhibited significant leakage, which was likely caused by the relatively long toehold. At presence of miR20a, all the SNA-HCR exhibited weak emission in 4000s, even 1 equiv. amount (500 nM) of miR20a was added in S-5-7. Since the maximum of fluorescence emission has not been determined, there are two possible reasons: 1. hairpin have not quenched sufficiently, thereby suppressing the ratio of signal/leak; 2. The SNA-HCR were slow, which was time consuming before reaching the equilibrium.

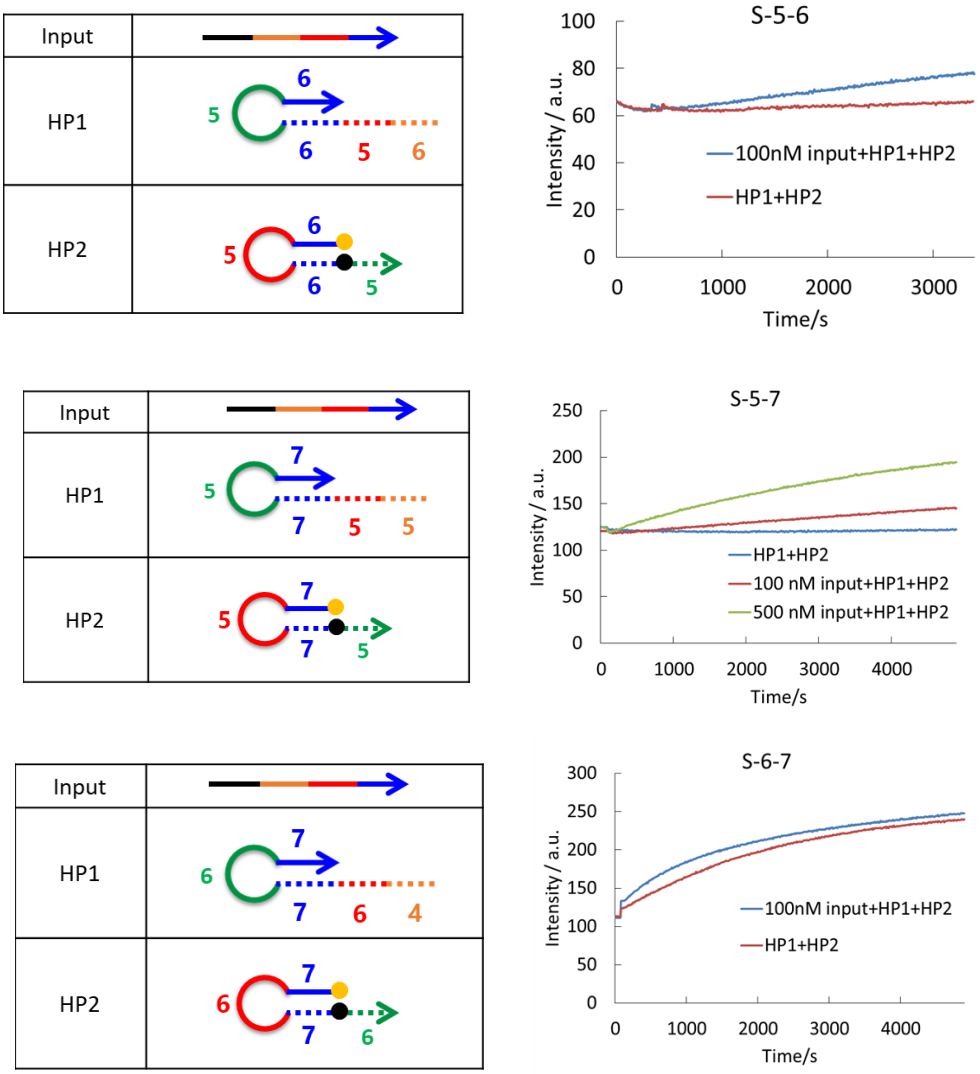

Figure 3.3.3 Fluorescence-time of S-5-6, S-5-7, and S-6-7 100 nM miR20a and 500 nM indicated HP1, HP2 in 10 mM phosphate buffer containing 100 mM NaCl, pH=7.0, 37 ^{o}C, Ex.= 546nm ; Em.= 562 nm.

Products of SNA-HCR were characterized in PAGE (Figure 3.3.4). In the solution containing HP1 and HP2, consistent with the kinetics, S-6-7 caused huge leakage with deep bands upper to the substrate. S-5-7 and S-5-6 cause relatively less unspecific cascade reaction. Noted that band which was a little bit higher than substrate was supposed as circular products. After adding miR20a strands, S-5-7 and S-6-7 formed long duplex product at top of the gel. Unfortunately, product in S-5-6 was not very clear, indicating slow kinetics.

Take an overall consideration, S-5-7 preformed the best among the SNA-HCR with short stem/toehold. Since the products in the agarose gel were pre-incubated overnight, we held the view that the kinetics of SNA-HCR was slow.

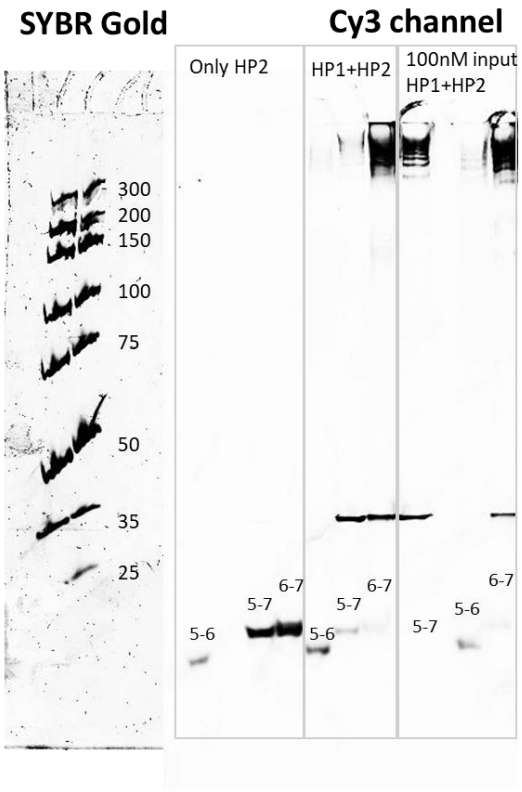

Figure 3.3.4 PAGE analyses of SNA-HCR procducts. From left to right, first part: 100 bp marker stained by SYBR Gold, second part: solution containing only HP2, third part: leakage in cascade reaction, fourth part: emission in the cascade reaction. 100 nM miR20a and 500 nM indicated HP1, HP2 in 10 mM phosphate buffer containing 100 mM NaCl, pH=7.0. Ex.= 532nm. 15% AA.

3.3.2 SNA-HCR with long stem/toehold

We reason the high background emission was caused by insufficient stability in the HP2 with short stem, herein we next lengthen the stem/toehold in the SNA-HCR to suppress background emission of HP2. S-9-8, S8-9, and S10-7 was further prepared for detection of miR20a. This time, no extra toehold in HP1 was designed (Figure 3.3.2), which was assumed as a positive factor for accelerating the kinetics of HCR.

Table 3.3.2 Sequence design of SNA-HCR 9-8, 8-9, 10-7. Calculated delta G (gibbs free energy) were listed on the right. RNA with purple font represented complementary sequences to SNA. Red, blue and green font in SNA hair-pin strand represented the stem and toehold.

miR-20a (23 mer) (from 3')		
5'-UAAAGUGCUUAUAGUGCAGGUAG-3'		
HP1 R-	CGAATATCA CGTCCATC AGAATACAG GATGGACG-*S 9-8*	*-7.82*
HP2 S-	TCTTATGTC**M**CTACCTGC GCTTATAGT GCAGGTAG**Y**-*R*	*-8.86*

HP1 R- CGAATATC ACGTCCATC GAATACAG GATGGACGT-*S* *8-9* *-8.27*

HP2 S- CTTATGTC**M**CTACCTGCA GCTTATAG TGCAGGTAG**Y**-*R* *-7.85*

HP2 S- CTTATGTC**MM**CTACCTGCA GCTTATAG TGCAGGTAG**Y**-*R* *8-9 2M*

HP1 R- CGAATATCAC GTCCATC TAGAATACAG GATGGAC-*S* *10-7* *-5.08*

HP2 S- ATCTTATGTC**M**CTACCTG GCTTATAGTG CAGGTAG**Y**-*R* *-4.98*

Y = Cy3, M = Methyl Red

Similarly, we firstly determined the hair-pin conformation of HP2. Figure 3.3.5 showed the fluorescence-temperature curve, the fluorescence intensity at low temperature firstly decreased and increase and form a sigmoid curve around 80 ^{o}C, which was regarded as the unwinding of stem. We reasoned the low fluorescence intensity at high temperature to insufficient unwinding, due largely to high thermal satiability in the stem.

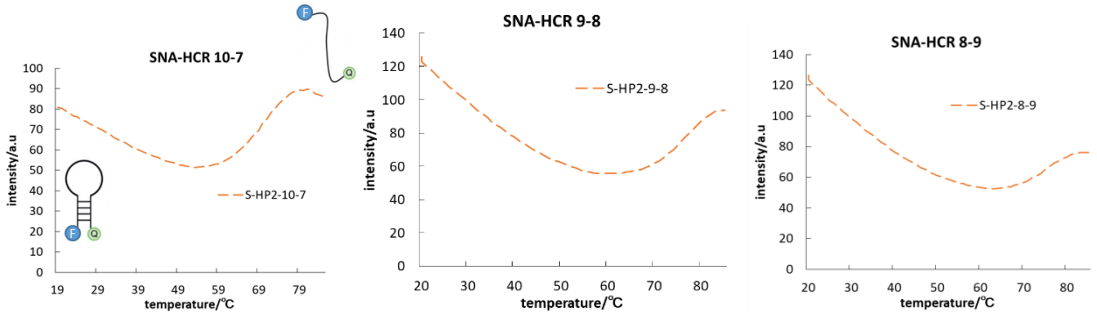

Figure 3.3.5 Fluorescence-temperature curve of S-10-7, S-9-8, and S-8-9 HP2. 500 nM indicated HP2 in 10 mM phosphate buffer containing 100 mM NaCl, pH=7.0, 37 ^{o}C, Ex.= 546nm ; Em.= 562 nm.

Kinetics of SNA-HCR by monitoring fluorescence emission was measured (Figure 3.3.6). This time, as our expectation, the signal amplification was accelerated, although background emission was still high. S-10-7 exhibited highest rate in the reaction, however, the leak was significant due to its long toehold. S-9-8 exhibited relatively slow rate in both leak and emission, while S-8-9 showed the weakest leakage and emission in the reaction. The leakage was not desirable, herein we concluded the optimal design in the SNA-HCR might be design in the long hairpin with relatively longer toehold than stem. However, the efficiency of cascade reaction was not enough: maximum intensity in S-10-7 circuit was assumed as 100% efficiency, herein the kinetics in both S-8-9 and S-9-8 circuits were slow. Although the kinetics could be accelerated by addition of an equivalent amount of miR20a (1 μM, Figure S3.3.1), since the HCR was a signal amplification circuit, it was desirable for developing fast circuit within small amout of

input strands.

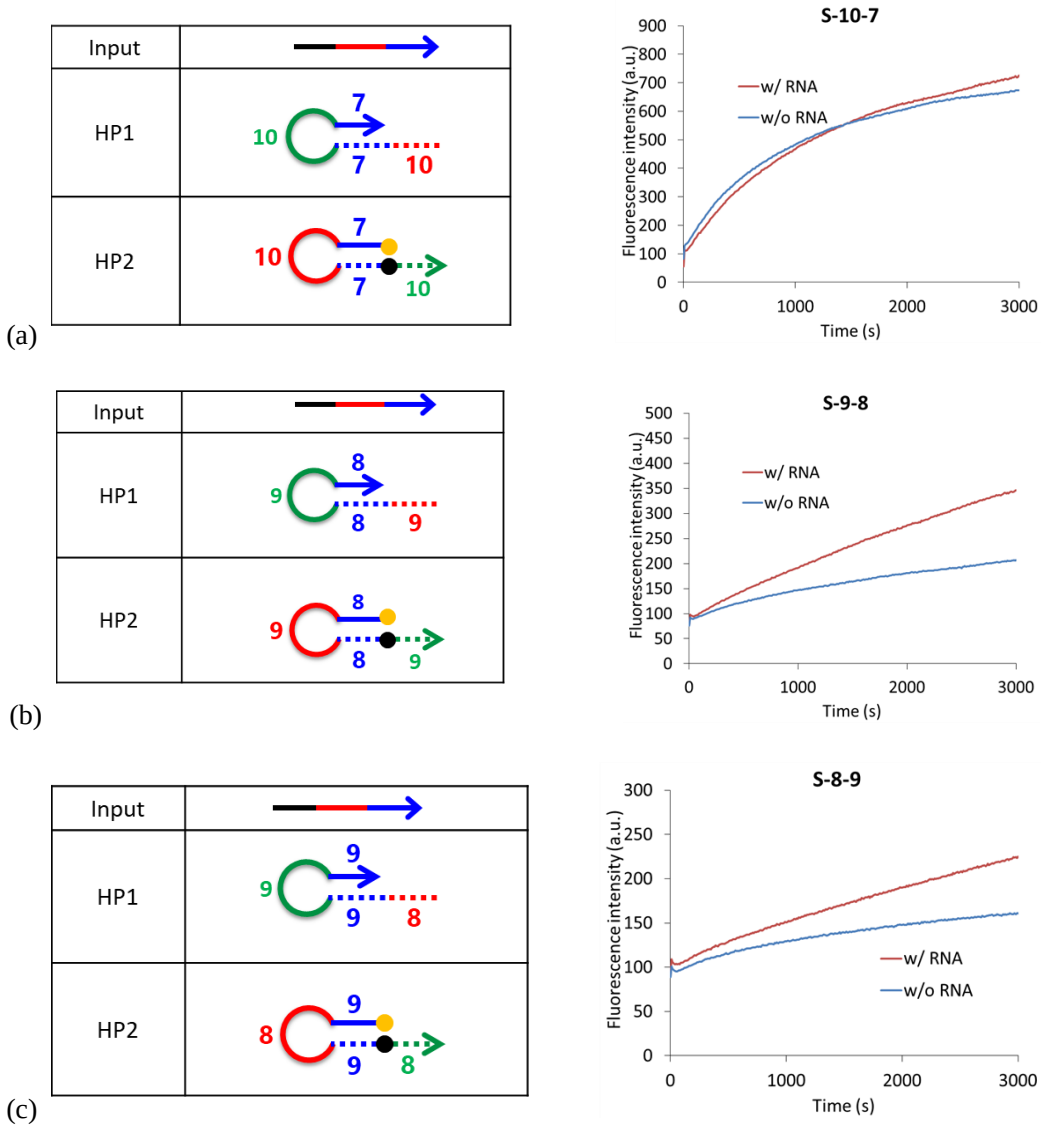

Figure 3.3.6 Fluorescence-time of (a) S-10-7, (b) S-9-8, and (c) S-8-9. 100 nM miR20a and 1 μM indicated HP1, HP2 in 10 mM phosphate buffer containing 100 mM NaCl, pH=7.0, 37 ^{o}C, Ex.= 546nm; Em.= 562 nm.

Products of SNA-HCR were characterized in PAGE (Figure 3.3.7). In S-10-7, we found most of the HP2 was consumed even miR20a has not added into the reaction. While the concentration of miR20a increased, specific products at top of the PAGE increased. In S-9-8, consistent with the kinetics refer to the fluorescence emission, leakage relatively decreased, and specific products increased with increasing amount of miR20a. S-8-9 with more concentration gradients has been confirmed, although leakage was weak. The band at the bottom of PAGE was the deepest, indicating unreacted HP2 after overnight incubation.

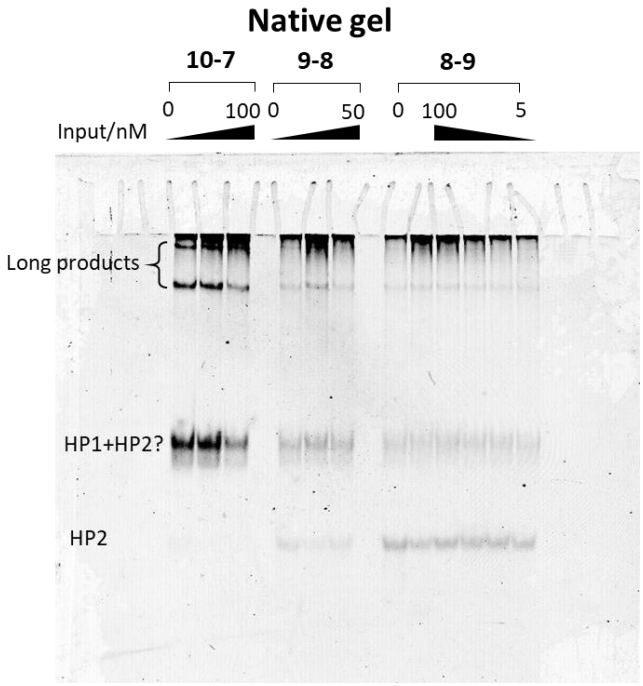

Figure 3.3.7 PAGE analyses of SNA-HCR procducts. From left to right, first part:S-10-7 conducted by 0, 50, 100 nM miR20a, respectively. Second part: S-9-8 conducted by 0, 10, 50 miR20a, respectively. Third part: S-8-9 conducted by 0, 100, 50, 25, 10, 5 nM miR20a, respectively. 500 nM indicated HP1, HP2 in 10 mM phosphate buffer containing 100 mM NaCl, pH=7.0. Ex.= 532nm. 15 % AA.

Optimal condition of SNA-HCR has also been determined (Figure 3.3.8). Reaction under 50 ^{o}C leaded to dehybridization of RNA/HP1, resulting in fast leakage. Reaction under 37 ^{o}C and 25 ^{o}C was suitable for SNA-HCR, although the kinetics was slow. Discussion among different concentration of NaCl has also done. As a result, reaction exhibited fast rate in 100 mM compared to the kinetics under condition containing 50 mM NaCl. In buffer containing 1M NaCl, unfortunately, kinetic was extremely slow even miR20a was inputted, the reason was unknown. Refer to the phenomena, SNA-HCR in the buffer containing 100 mM NaCl under 37 ^{o}C was regarded as the optimal condition.

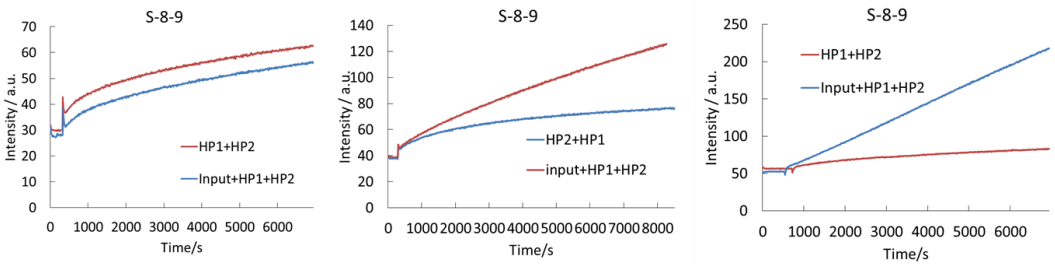

(a)

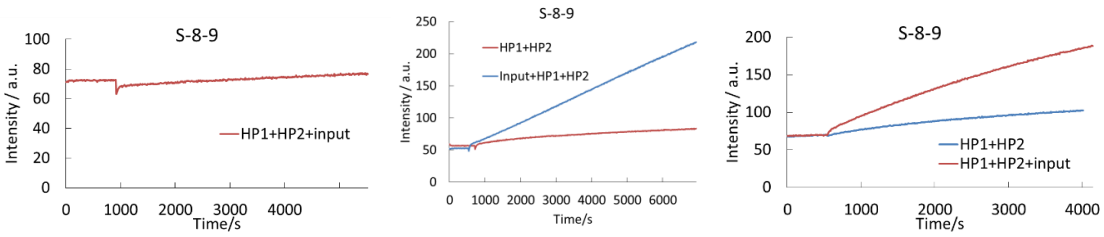

Figure 3.3.8 Fluorescence-time of S-8-9 under (a) 50 °C, 37 °C, and 25 °C, respectively. (b) 10 mM phosphate buffer containing 1M, 100 mM, and 50 mM NaCl, respectively. Conditions: 100 nM miR20a and 500 nM indicated HP1, HP2, pH=7.0, Ex.= 546nm; Em.= 562 nm.

In conclusion, although SNA-HCR 8-9 performed well, the high background emission and slow rate in the reaction remained, cascade reaction hardly reached the equilibrium, and further optimization was needed.

Based on the S-8-9, we incorporated one more methyl red (S-8-9 2M in Table 3.3.2), in order to suppress background emission in advance. This time before the purification of HPLC, I have roughly purified it by the PAGE. Kinetic was showed in the Figure 3.3.9 on the left. Unfortunately, almost same background emission was found, and the signal amplification become harder to be observed than S-8-9, even in addition of an equal amount of miR20a was inputted (500 nM).

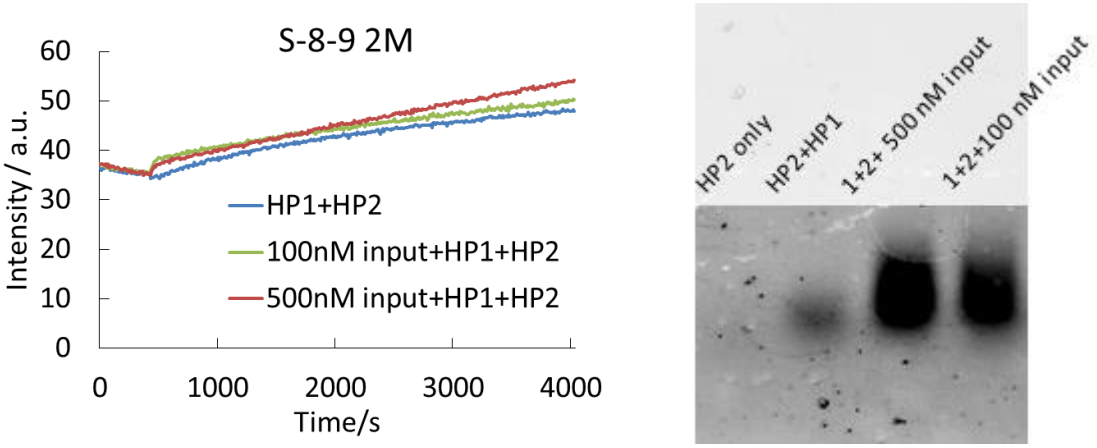

Figure 3.3.9 Fluorescence change over time and agarose gel (3 w/v%) of S-8-9 2M HCR reactions. Conditions: 100 mM NaCl in 10 mM phosphate buffer, pH=7.0, 25 °C, [HP1] =[HP2] = 0.5 μM, Ex.= 546 nm; Em. =562 nm. Agarose gel (3 w/v%) was run under 100 V for 30 min.

In the agarose gel analysis (Figure 3.3.9 on the right) which has a high resolution of long duplex products. In contrast to the fluorescence-time kinetics, we found S-8-9 2M seemed go well and form a huge band (lane 3-4) in comparison of the leak (lane 2) and the blank (lane 1). Since the sample was incubated overnight after before the gel was

run. We confirmed the problem in SNA-HCR circuit is caused by the slow reaction between SNA and RNA. Hence, we measured spectra of previous SNA-HCR again (samples was stored for a long period of time). This time all the samples have shown acceptable emission intensity (data not shown). In a conclusion, the SNA-HCR requires a long time for completing the reaction.

3.3.3 Kinetic analysis

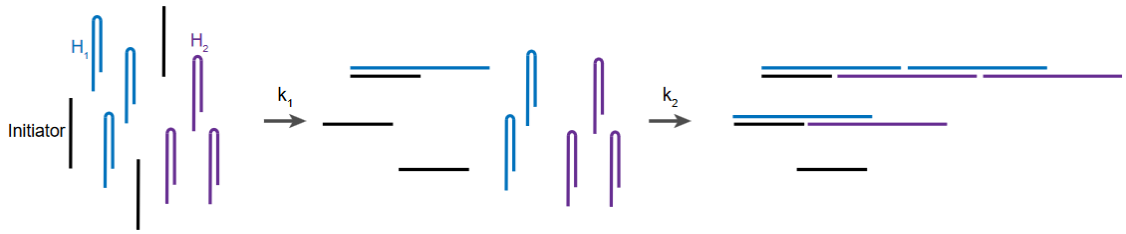

Figure 3.3.10 Schematic of HCR. k_1, k_2 represent to the rate constant of initiation and propagation in the HCR.

Other works on the process of HCR has also shown the reason (Figure 3.3.10): HCR was mainly composed of initiation phase and propagation phase with rate constant k_1 and k_2.[22] Herein, for SNA-HCR, we reason the problem to low rate constant of intiation (k1<<k2), indicating the hybridization between SNA and RNA was much weaker than homo SNA. As a result, SNA hairpins preferred to enlongate the product, rather than be initiated by RNA input. Herein only small amout of RNA could be reacted, efficient concentration decreased. Follow this assumption, we claimed the SNA input could threoritically accelerate the reaction which provided almost same rate consant bewteen initiation and propagation phase.

Table 3.3.3 Sequence design of SNA input.

miR-20a (23 mer) (from 3')
5'-UAAAGUGCUUAUAGUGCAGGUAG-3'
SNA input
S- TAAAGTGCTTA TAGTG CAGGTAG –*R*

We ordered SNA input which has same sequence to the miR20a and evaluated the performance in SNA-HCR (Table 3.3.3). Compare to the kinetics which was conducted by miR20a, addition of SNA input greatly accelerated the reaction rate of both the HCR 8-9 and 8-9 2M. Although background emission was still high, because of relatively strong emission, ratio of signal/background increased (Figure 3.3.11). Our assumption has been confirmed that slow detection for RNA target was cause by the lag in the initiation phase of HCR.

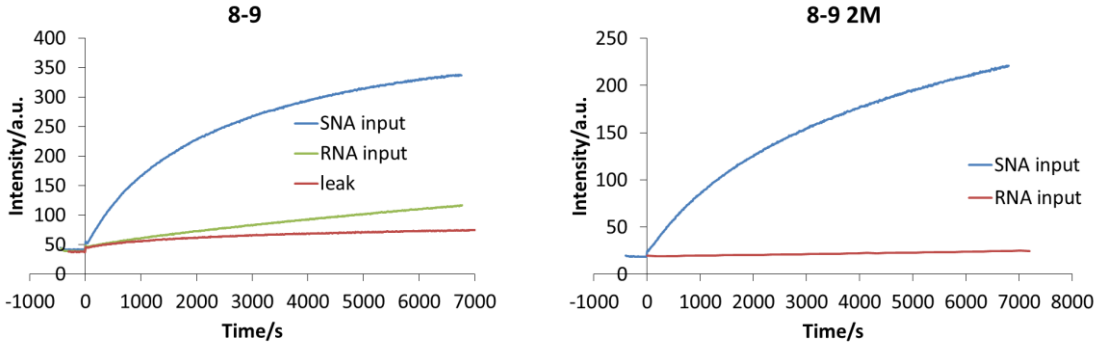

Figure 3.3.11 Kinetics of SNA-HCR initiated by SNA inputs, RNA inputs (miR20a), or no inputs (leak). Conditions: [HP1] =[HP2] = 0.5 μM, [Indicated input]= 0.1 μM. 100 mM NaCl in 10 mM phosphate buffer, pH=7.0, 37 °C.

Therefore, the kinetics of SNA-HCR circuit for RNA detection will be accelerated if we can enhance the hybridization between SNA-HP1 and miR20a in the initiation phase. One possible solution is addition of Maruyama polymer, which has been proved to be powerful chaperone for nucleic acid. Positive charge of L-lysine backbone in maruyama polymer neutralizes negative charge of phosphate group in the DNA and SNA, thereby catalyzing the strand exchange reaction by reducing the counter ion concentration (Figure 3.3.12).[23] We next attempted SNA-HCR with addition of Maruayama polymer PLL-*g*-Dex 30k90D. The results showed below in Figure 3.3.13):

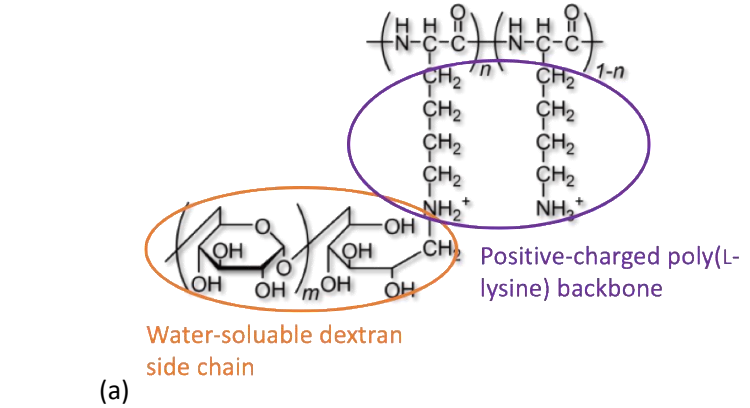

(a)

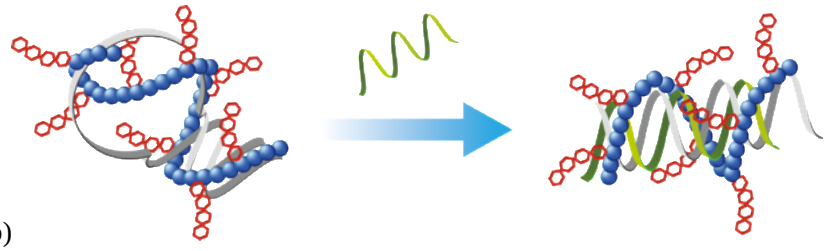

(b)

Figure 3.3.12 (a) Chemical structure of PLL-*g*-Dex. Water-soluble side chain is introduced to increase

the solubility of polymer-DNA complex in solution. (b) PLL-*g*-Dex forms complex with DNA through static interaction thus negative-charged DNA phosphate backbone is neutralized.

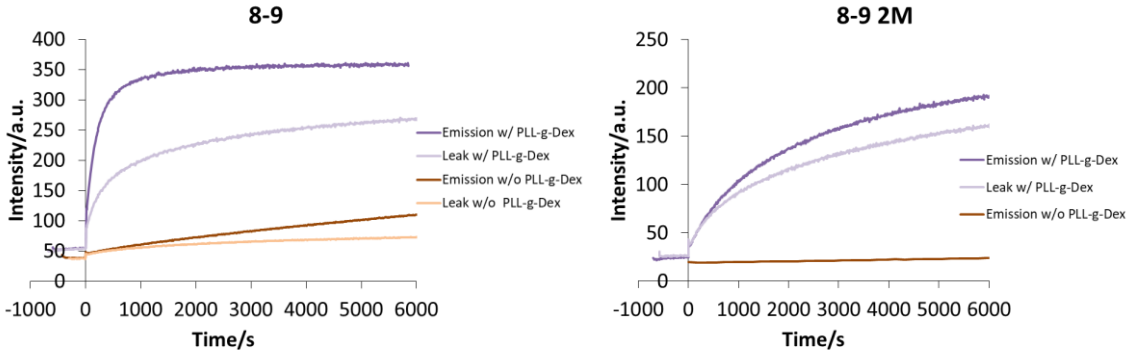

Figure 3.3.13 Detect target RNA with addition of PLL-g-Dex. Conditions: [HP1] =[HP2] = 0.5 μM, [InputRNA]= 0.1 μM. 100 mM NaCl in 10 mM phosphate buffer, pH=7.0, 37 ^{o}C. PLL-g-Dex (15k90d) was added with [N]:[P]=2:1.

Here, comparing to the previous kinetics in the RNA detection, addition of maruyama polymer greatly accelerated the rate constant of reaction, even faster than homo SNA HCR circuit (SNA input). However, at the same time the leak has also become significant. Seems that Maruyama polymer unspecifically enhance the strand exchange both on SNA-SNA and SNA-RNA. In conclusion, it was interesting that maruyama polymer could catalyze the HCR, further optimization of experimental conditions were needed.

3.3.4 FRET SNA-HCR

As a possible solution, we next deigned fluorescence resonance energy transfer (FRET)-HCR. Cy5 and Cy3 were modified in HP1 and HP2 respectively (Chemical structure of Cy5 was shown in Figure 3.3.14). Before conducting reaction, two fluorophore works individually, whereas the FRET occurs in the long duplex product of cascade reaction. For the FRET-HCR, since it does not have background emission, we assume it will solve the problem of high background emission. Moreover, hairpin with no quencher enables short stem which was supposed to accelerate the kinetics of initiation. The design showed below in Table 3.3.4.

Table 3.3.4 Sequence design of FRET-HCR 5-7 and 4-6

miR-20a (23 mer) (from 3’)
5’-UAAAGUGCUUAUAGUGCAGGUAG-3’
F5-7 HP1 R- CGAATATCACGTCCATCGGAATGATGGAC**-Cy5** *-S*

F5-7 HP2 S- CCTTA CTACCTG TAGTG CAGGTAG**Y**-*R*

F4-6 HP1 R- CGAATAGCACTCCATCGGAAGATGGA-**Cy5** -*S*

F4-6 HP2 S- CCTT CTACCT GTGC AGGTAG**Y**-*R*

Y = Cy3

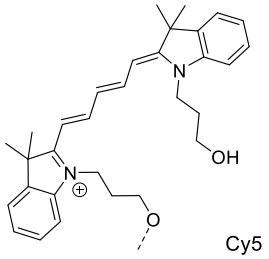

Figure 3.3.14 Chemical structure of Cy5 in the FRET-SNA-HCR.

To determine the maximum emission of FRET-SNA-HCR circuit, reaction was firstly conducted by SNA input detection. As a result, design 5-7 has showed a fast FRET emission, whereas the design 4-6 has not. While solution was excited by 546 nm-laser, which was not included in the absorbance of Cy5, emission of Cy3 in the 5-7 FRET SNA-HCR decreased in 150 mins, resulting in extra emission of Cy5 in the spectra (Figure 3.3.15). Calculated FRET efficiency (E) from the emission change in the donor (design 5-7, E=1-F_D'/F_D, where F_D' and F_D are the donor fluorescence intensities with and without an acceptor respectively.), the E=63.2 %. Which seemed reasonable since same interval in DNA will leads efficiency to 67%. However, under this efficiency, the emission measured from the accepter Cy5 was weak, which might be caused by weak detecting ability of fluorescence machine in the long wavelength. More discussion was needed to confirm the reason for weak emission from acceptor.

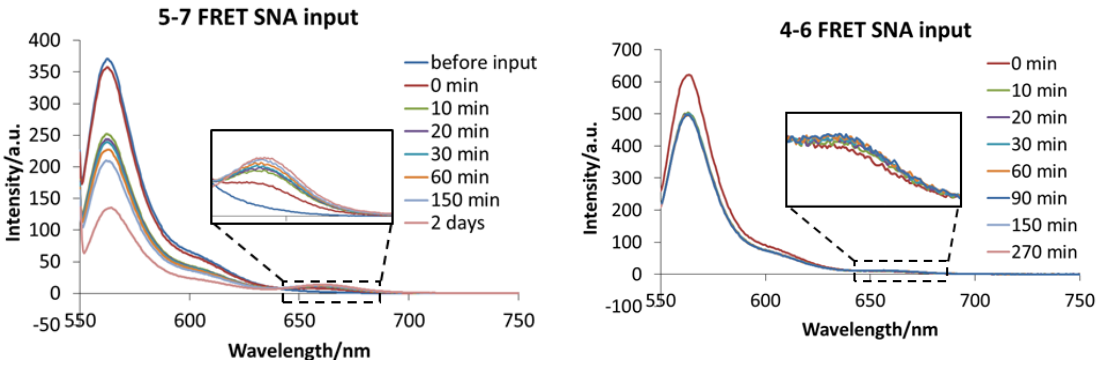

Figure 3.3.15 Fluorescence spectra of SNA FRET-HCR. Conditions: [HP1] =[HP2] = 0.5 μM, [Input SNA] = 0.1 μM. 100 mM NaCl in 10 mM phosphate buffer, pH=7.0, 37 °C.

Next, we tested the FRET 5-7 HCR for RNA detection (Figure 3.3.16). Unfortunately,

although detection of SNA input was fast, the detection of RNA was still slow. It has a slow initiation in the first few minutes and took about 1 day before reaching the equilibrium, which was also caused by the slow kinetics of SNA/RNA strand displacement.

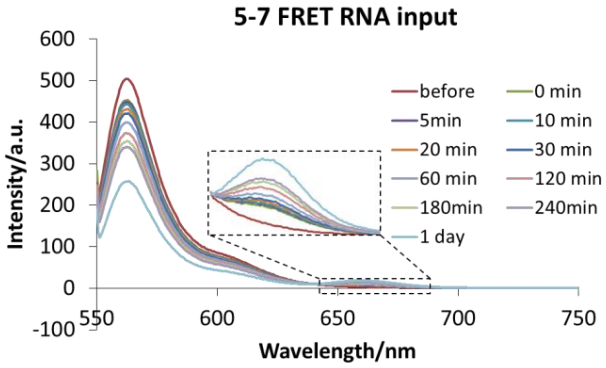

Figure 3.3.16 Design of FRET-HCR and their fluorescence spectra. Conditions: [HP1] =[HP2] = 0.5 μM, [Input RNA] = 0.1 μM. 100 mM NaCl in 10 mM phosphate buffer, pH=7.0, 37 °C.

We subsequently confirmed this assumption by measuring the melting temperature (T_m) among the stem of hairpins. In Figure S3.3.2, most of the stems have ultra-high thermal stability with T_m around 80 °C, even for short hairpin with 6 bp stem. Although the toehold was designed in the hairpin, the affinity of SNA-HP1/RNA duplex was too low to launch the cascade reaction (Figure 3.3.17).

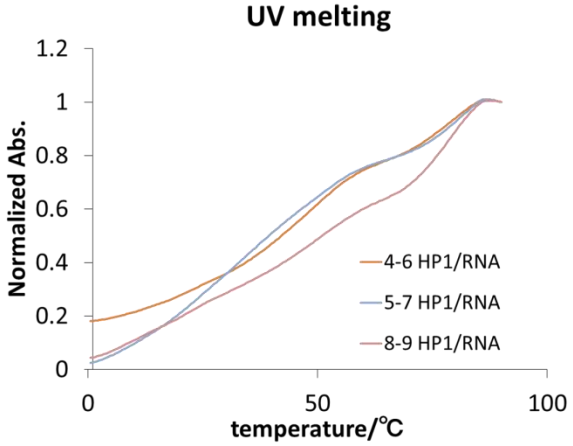

T_m	duplex	stem
46 hp1/RNA	47.5	79.1
57 hp1/RNA	34.1	82.4
89 hp1/RNA	51.2	79.9

Figure 3.3.17 UV melting of SNA hairpin and SNA-RNA duplex. Conditions: 100 mM NaCl in 10 mM phosphate buffer, pH=7.0, 90-0 °C, [HP1] =[RNA]= 1.0 μM.

Finally, products of FRET SNA-HCR (5-7) in RNA detection were analyzed in agarose gel (Figure 3.3.18) As a result, reaction containing F-5-7 HP1 formed large amount of long duplex products with Cy5 emission (lane 3). At the same time, emission

of Cy3 decreased a lot at the same location, indicating the occurrence of FRET. Moreover, content of F-5-7 HP2 containing Cy3 decreased a lot at bottom of the gel, indicating high yield of the reaction. In contrast, reaction containing 5-7 HP1 without modification of Cy5 has not caused FRET, only products with Cy3 emission were visualized (lane 4). Although the rate of reaction has not satisfied us a lot, we claimed that the FRET-SNA 5-7 was conducted properly as our expectation.

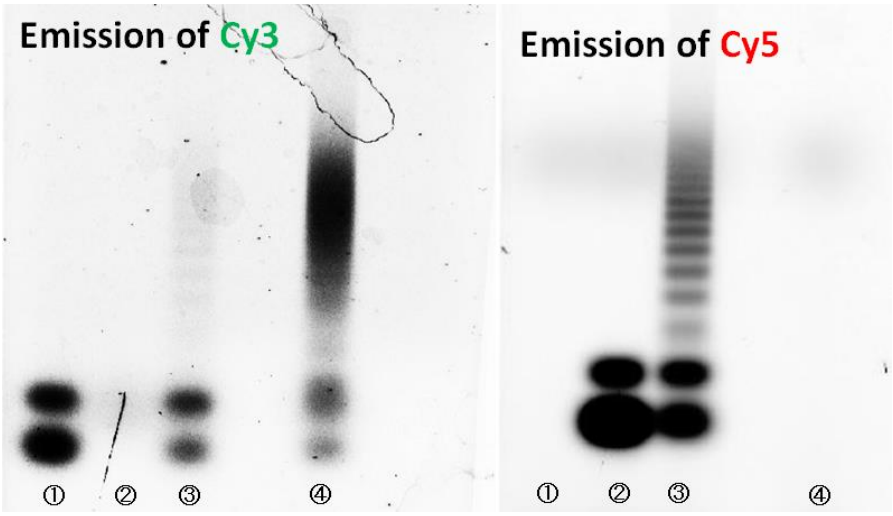

Figure 3.3.18 Products of HCR (reacted overnight) have showed in 3 w/v % agarose gel. Left image indicated emission of Cy3, right image indicated emission of Cy5. Sample containing only F-5-7 HP2 (lane1), only F-5-7 HP1 (lane2), SNA input+ F-5-7 HP1+ F-5-7 HP2 (lane 3), miR20a+ 5-7 HP1+ F-5-7 HP2 (lane 4) were analyzed. [miR20a] =0.1 µM, [Indicated HP] =0.5 µM. pH=7.0, 37 °C.

3.3.5 SNA-mediated SNA-HCR circuit

We have confirmed the reason of slow kinetic, which was caused by low rate in the initiation phase. Except for shorten stem in the hairpin, we considered an SNA-interfaced SNA-HCR circuit as another possible solution for accelerating initiation in the HCR (Figure 3.3.19): target RNA was firstly pre-annealed with a designed SNA interface, after that, SNA/RNA duplex would subsequently serve as initiator for cascade reaction. We assume the strong base-pairing interaction of homo SNA was able to lead fast initiation.

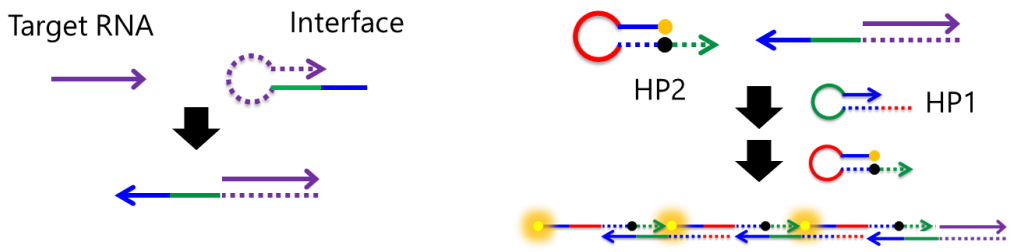

Figure 3.3.19 Experimental protocol for SNA-interfaced SNA-HCR circuit.

Sequence design was shown in Table 3.3.5, based on the S-8-9 HCR circuit, 22-mer model target RNA and SNA interface strand were designed. SNA interface with complementary part to target RNA was designed in hair pin structure with 8-mer stem to ensure detection *in vitro*. Herein, 17-mer overhang at S-terminal of SNA/RNA duplex was supposed to launch the HCR circuit from S-8-9 HP2.

Table 3.3.4 Sequence design of SNA interface and SNA-8-9 HP2 containing NMR.

Target RNA 5'-GACAUAAG AGAUGGAACGAUAG -3'
S-I1 R- CTGTATTC TCTACCTTGCTATC GAATACAG GATGGACGT –S
HP2 S- CTTATGTC**N**CTACCTGCA GCTTATAG TGCAGGTAG**Y**-*R* *8-9 NMR*
Y = Cy3, N = Nitro Methyl Red

This time we have newly designed a HP2 with modification of nitromethyl red (NMR in Figure 3.3.20, S-8-9 NMR) at same position to methyl red, refer to the calculation, NMR could provide stronger dynamic quenching due to its longer foster radius with cy3 than methyl red (Figure 3.3.21), we expected it could provide significant quenching effect and suppress background emission of SNA-HCR.

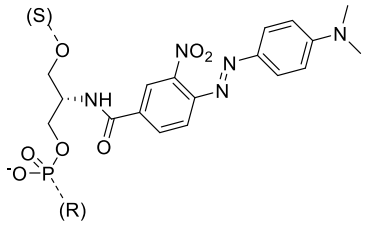

Figure 3.3.20 Chemical structure of NMR.

$$R_0 = 0.2108[J(\lambda)\kappa^2 n^{-4}\Phi_D]^{1/6}$$

n: Refractive index 1.4	Index in water
Φ_D: Quantum yield of the donor 0.41	Cy3
κ^2: Qrientation factor 2/3	Duplex
J(λ): Spectral overlap integral	

$$\Phi_T = \frac{1}{1 + (R/R_0)^6}$$

R:25.7 Å(Cy3-MR)

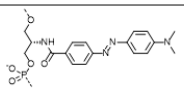

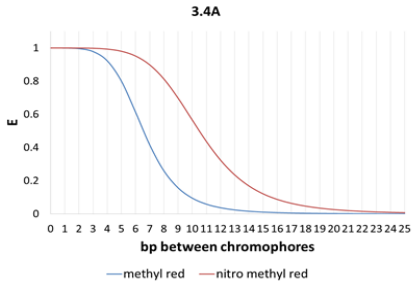

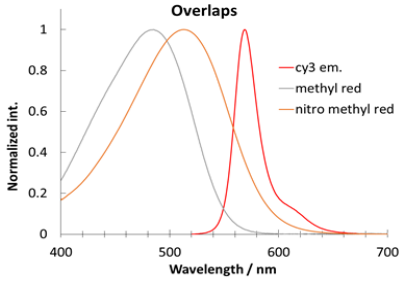

Figure 3.3.21 Calculation of FRET radius between Cy3 and quenchers (methyl red, NMR). Base pair interval in SNA was hypothesized to 3.4 angstrom.

The kinetic of circuit was monitored by the fluorescence-time curve of Cy3 emission. We have measured fluorescence emission with annealing process and without annealing process. As the result showed in Figure 3.3.22 on the left, whatever the RNA and interface has annealed or not, addition of interface HP has greatly speeded up the HCR circuit. At the same time, no significant leakage was observed.

Refer to agarose gel (Figure 3.3.22 on the right), almost all substrate (S-8-9 HP2) was consumed, indicating high efficiency of SNA-mediated SNA-HCR reaction. Notably, although no toehold was designed between SNA interface and target RNA, the reaction also conducted with similar efficiency to the group within pre-annealing process. We reason it to the hybridizing pattern between RNA/SNA, which was started from the loop of the hairpin.

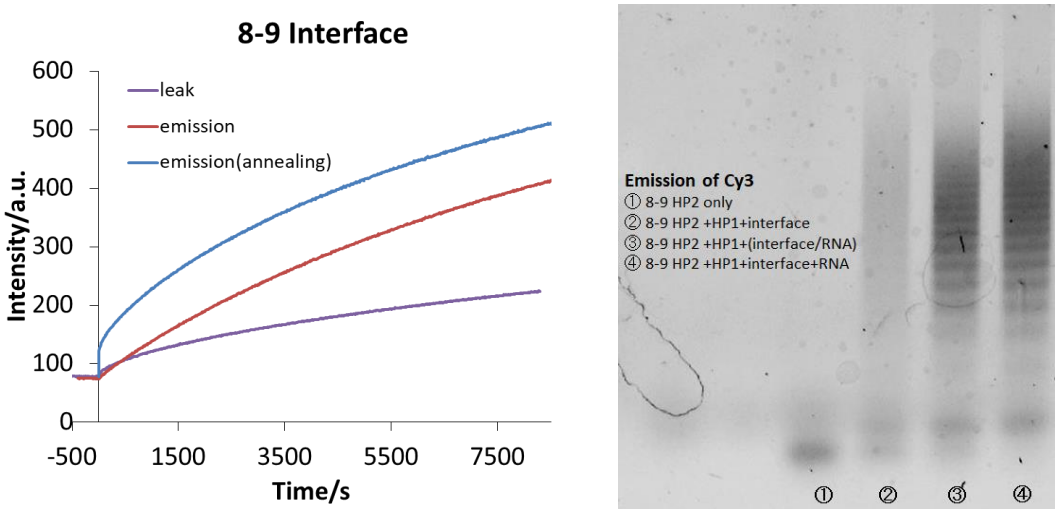

Figure 3.3.22 Fluorescence emissions in HCR. Conditions: 100 mM NaCl in 10 mM phosphate buffer, pH=7.0, 25°C, [HP1] =[HP2] = 0.5 μM, [RNA]=[Interface]=0.1 μM Ex.= 546 nm (on the left). On the right, products of HCR (reacted overnight) have showed in 3 w/v% agarose gel.

Similar results have also observed in 8-9 HP2 2M: Compare to previous (w/o interface) measurement which we could even hardly start HCR (Figure 3.3.23 on the left). Existence of SNA interface caused strong emission, at the same time, leak of it could rarely be observed, which was consistent to the kinetics in SNA-mediated SNA-8-9.

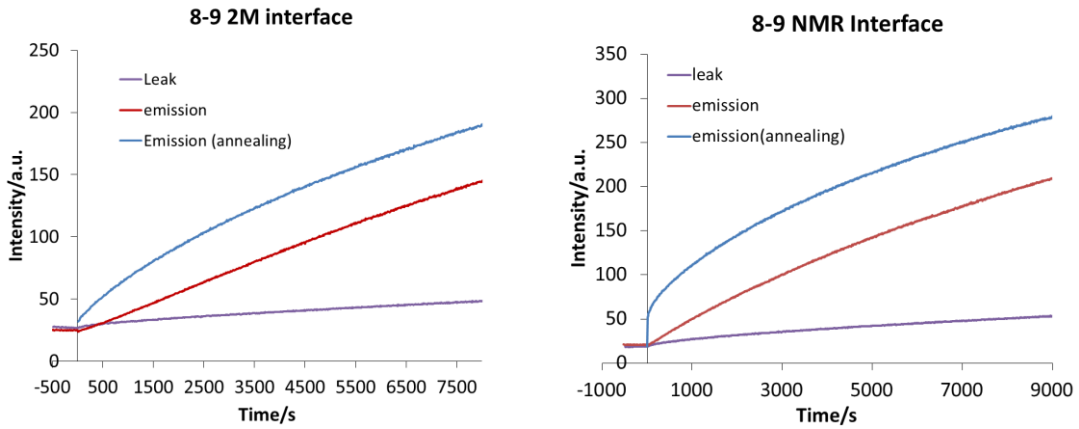

Figure 3.3.23 Fluorescence emissions in SNA mediated SNA-8-9 and SNA-8-9 NMR HCR. Conditions: 100 mM NaCl in 10 mM phosphate buffer, pH=7.0, 25°C, [HP1] =[HP2] = 0.5 μM, [Target RNA]= [S-I1] = 0.1 μM Ex.= 546 nm.

We have further evaluated the HP2 with incorporation of NMR. As the result showed in Figure 3.3.23 on the right, incorporation of NMR has slightly suppressed background (from 70 to 20) and the leak in the HCR has also been suppressed. Although S-8-9 NMR exhibited best performance among all the design, improvement was not significant. Therefore, HP2 in the HCR circuit still needs to be improved.

In conclusion, we have verified our assumption, and successfully accelerated the kinetics of SNA-HCR by incorporating SNA-interface for RNA detection.

3.4 SNA-mediated L-*a*TNA HCR circuit

To further strengthen the detecting ability of HCR circuit, we next expanded the scope of nucleic acid from SNA to other artificial nucleic acid. We have designed a SNA-mediated L-*a*TNA HCR circuit. Sequence designed was shown in Table 3.4.1.

Table 3.4.1 sequence design for L-*a*TNA HCR circuit

miR20a	3'-GAUGGACGUGAUAUUCGUGAAAU-5'
S-I2	*S*-TCAGATC GTGCTTCTACCTGCACTATAAGCAC-*R*
Lhp1	1′-**Y**CTAGACTGATGTTAGTCTAG**M**CACGAA-3′
Lhp2	3′-TCAGATCGTGCTTGATCTGACTACAA-1′
Y = Cy3, M = Methyl Red	

There were two reasons for amplifying signal by L-*a*TNA: 1. Background in SNA HP was hardly suppressed, we attribute the problem to flexible scaffold in SNA, which caused insufficient static quenching. We supposed the hard L-*a*TNA scaffold with methyl group could fixed the position of fluorophore and quencher, result in low

background emission. 2. Ly's group has reported strong relevance between oligonucleotides' conformational compatibility and kinetics in the HCR. Refer to our previous report, SNA serves as an ideal material for propagating chirality due to its flexible and achiral scaffold, which indicates the preorganization for overhang of S-I1/miR20a in right-handed bound state prior to the recognition.[24] Therefore, we assume L-aTNA which forms right-handed duplex will further accelerate HCR circuit. L-aTNA hairpin (Lhp1) with toehold/stem length of 6-7 has been designed and synthesized.

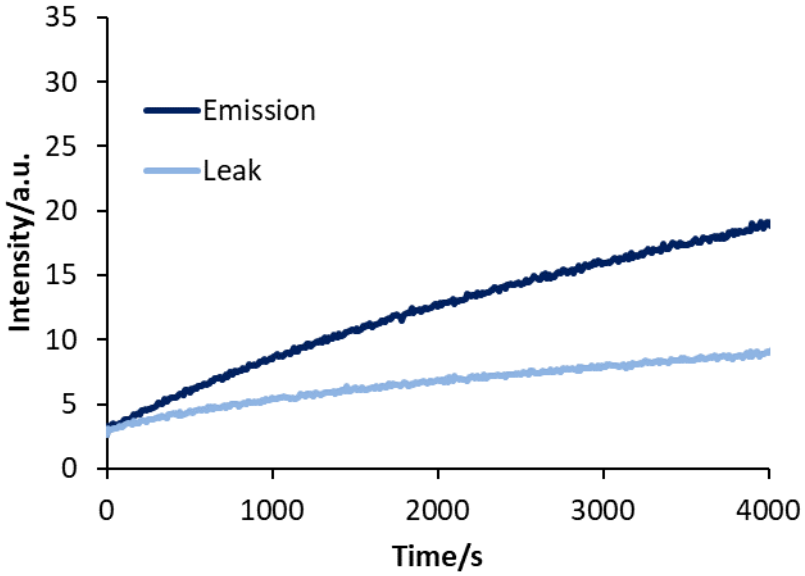

Figure 3.4.1 Fluorescence emission in the process of HCR. Deep and light blue represent the emission and leak in the HCR, respectively. Conditions: ex.=546 nm, em. = 562 nm. 100 nM mir20a, S-I2 and 500 nM Lhp1, Lhp2. 10 mM phosphate buffer (NaCl= 100 mM), pH 7.0, 37 ^{o}C.

As our expectation, under 100 mM NaCl, background emission (emission of XNA-HCR at 0s) had significantly been suppressed comparing to similar modification in S-8-9 (Figure 3.4.1, background intensity from 70 to 4). However, at presence of miR20a, the kinetics was slow. We next increased the concentration of cation (Na^{2+}), which was assumed to accelerate the kinetics by suppressing the electronic repulsion, like Maruyama polymer.

As our expectation, SNA-mediated L-*a*TNA HCR amplified signal rapidly under 1M NaCl, reaching equilibrium within 4000 seconds, whereas SNA HCR circuit had not achieved (Figure 3.4.2). At absence of miR20a, comparing to the leakage containing Lhp1 and Lhp2, the leakage containing S-I2 was magnified (Figure S3.4.1). We reason the problem to fragile stem in S-I2, which was not desirable for RNA detection.

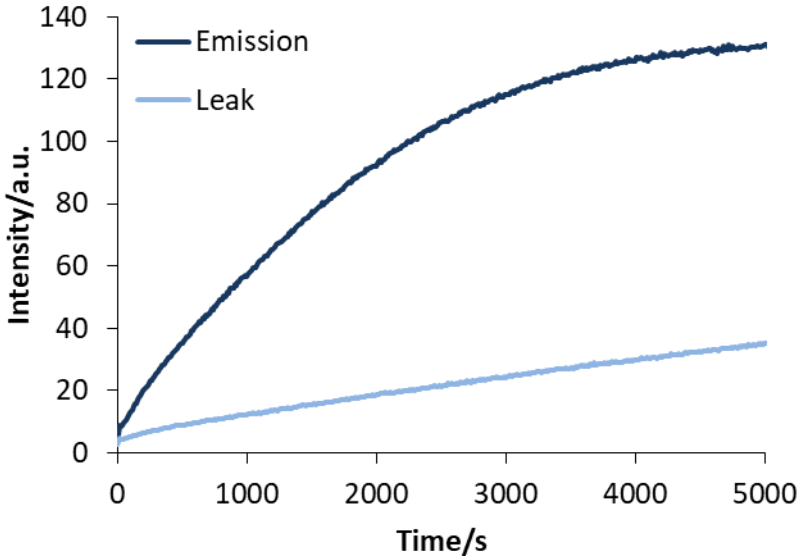

Figure 3.4.2 Fluorescence emission in the process of SNA-mediated L-*α*TNA HCR. Deep and light blue represent the emission and leak in the HCR, respectively. Conditions: ex.=546 nm, em. = 562 nm. 100 nM miR20a, S-I2 and 500 nM Lhp1, Lhp2. 10 mM phosphate buffer (NaCl= 1 M), pH 7.0, 37 ^{o}C.

Gel electrophoresis analysis was shown in Figure 3.4.3. High kinetics of HCR caused fast consuming of LHP1 at the bottom. As a result, many bands of HCR products were found in lane 4, whereas the leakage was not such significant in the gel (lane 3). It proves the feasibility of SNA-mediate L-*α*TNA HCR circuits targeting RNA.

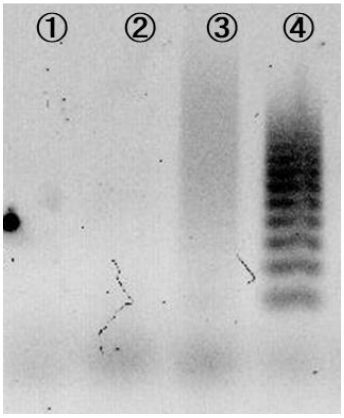

Figure 3.4.3 Agarose gel of SNA-mediated L-*α*TNA HCR under overnight incubation. Lane 1: Lhp1 only, lane 2-4 showed products of HCR. (Lane 2: Lhp1+ Lhp2, lane 3: S-I2+ Lhp1+ Lhp2, lane 4: miR20a+S-I2+ Lhp1+ Lhp2. Conditions: 100 nM miR20a and S-I2, 500nM Lhp1, Lhp2 for reaction time of 12 hours, 3% agarose gel at 100V for 30 min.)

3.5 SNA-mediated D-*α*TNA HCR circuit

3.5.1 Extended stem in SNA interface

Previously, we have confirmed the feasibility of SNA as interface to translate information from RNA to *a*TNA. Next, we expanded the scope of XNA-HCR to D-*a*TNA circuit. Since left-handed D-*a*TNA was highly orthogonal to right-handed RNA. D-*a*TNA circuit was assumed to work well under complex condition like biopsy, avoiding unintended cross-hybridization. Herein we have designed SNA-mediate D-*a*TNA HCR circuit for RNA detection. This time, for ease of synthesis, D-*a*TNA HCR with modification of Cy3 and Methyl Red with toehold/stem length of 6-7 was chosen for cascade amplification, which has been well evaluated in our laboratory. Base on it, SNA interfaces (S-I3, S-I3-1, and S-I3-2) and 23-mer model target RNA were designed (Table 3.5.1). Notably, S-I3-1 and S-I3-2 with 1-mer and 2-mer extended stem were designed, aiming to stabilized SNA hairpin thereby avoiding extra leakage in the detection.

Table 3.5.1 Sequence design for D-*a*TNA HCR circuit

Target RNA:	5'-GAUGCAGGUGAUAUUCCAUAGCU-3'
S-I3	*R*-TCATCGA TACCTTCTACGTCCACTATAAGGTA-*S*
S-I3-1	*R*-TCATCGA TACCTTCTACGTCCACTATAAGGTAT-*S*
S-I3-2	*R*-TCATCGA TACCTTCTACGTCCACTATAAGGTATC-*S*
Dhp1	1' –**Y**AGCTACTGATGTTAGTAGCT**M**ATGGAA-3′
Dhp2	3'-TCATCGATACCTTTCGATGACTACAA -1′
Y = Cy3, M = MethylRed	

As a control group, D-*a*TNA circuit conducted by D-*a*TNA input strand prepared for basic characterization for the leakage and emission of the circuit (Figure S3.5.1). Figure 3.5.1 showed the kinetics of SNA-mediate D-*a*TNA HCR circuit. In contrast to SNA-mediate L-*a*TNA circuit, addition of SNA interface strand has not cause extra leakage compared to that of interface-free D-*a*TNA HCR circuit, with maximum leakage intensity around 30. Out of our expectation, this time translation of SNA form RNA to D-*a*TNA has not gone well: reaction processed in slow pace even in the presence of S-I3/Target RNA, finally resulting in weak emission which was comparable to the leakage within only S-I3.

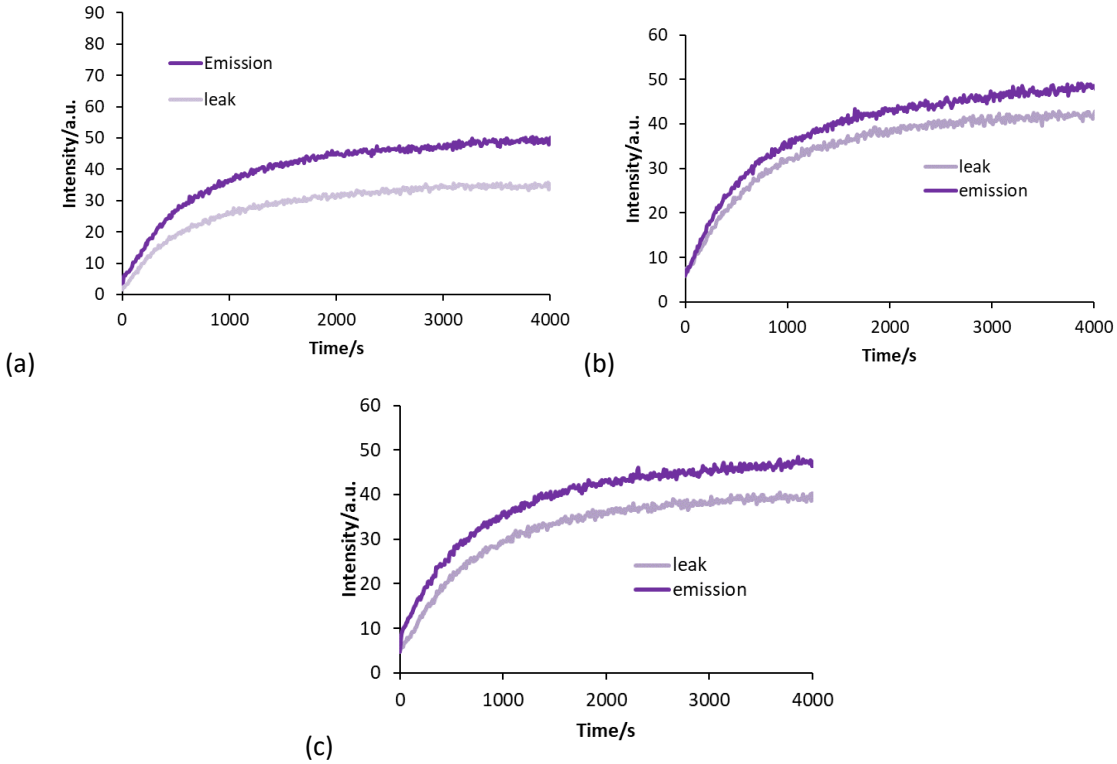

Figure 3.5.1 Fluorescence emissions of SNA-mediated D-*a*TNA HCR circuit. Deep and light purple represent the emission and leak in the HCR, respectively. 20 nM target RNA, indicated interface (a) S-I3, (b) S-I3-1 and (c) S-I3-2. 100nM Dhp1, Dhp2. 10 mM phosphate buffer (NaCl= 1M).

3.5.2 Incorporation of C3-spacer

We reasoned that the low yield of SNA-mediate D-*a*TNA circuit resulted from propagation of helicity. RNA/SNA-interface complex caused propagation of right-handed helicity from RNA/SNA duplex into overhang input, which reduced the rate of binding to the left-handed D-*a*TNA HCR. A similar phenomenon has also been confirmed in other nucleic acids, like PNA.[25] Thus, the helical mismatch between the initiator complex and the D-*a*TNA hairpin likely led to the slow reaction.

The helicity propagation in SNA is guided by the base stacking. Herein we further incorporated 1-mer and 2-mer C3-spacer (synthesis scheme shown in Figure S3.5.2) to SNA interface (S-I3-s1 and S-I3-s2, respectively. Table 3.5.2) between the overhang part and RNA-complementary part at R-terminal. We assume C3-spacer (structure was shown in Figure 3.5.4) would suppress helicity propagation, thereby accelerating the strand displacement between SNA and D-*a*TNA.

Table 3.5.2 Sequence design for D-*a*TNA HCR circuit with SNA spacer

S-I3-s1	*R*-TCATCGA TACCTTSCTACGTCCACTATAAGGTA-*S*
S-I3-s2	*R*-TCATCGA TACCTTSSCTACGTCCACTATAAGGTA-*S*
Y = Cy3, M = MethylRed	

As result shown in Figure 3.5.2, incorporation of C3-spacer significantly enhanced signal amplification of D-*a*TNA HCR circuit. With number of C3-spacer increased, the rate of reaction also increased. Finally, for S-I3-s2, signal amplification in HCR reached the equilibrium in 1500 seconds, while significant extra leakage was not observed comparing to the reaction containing S-I3.

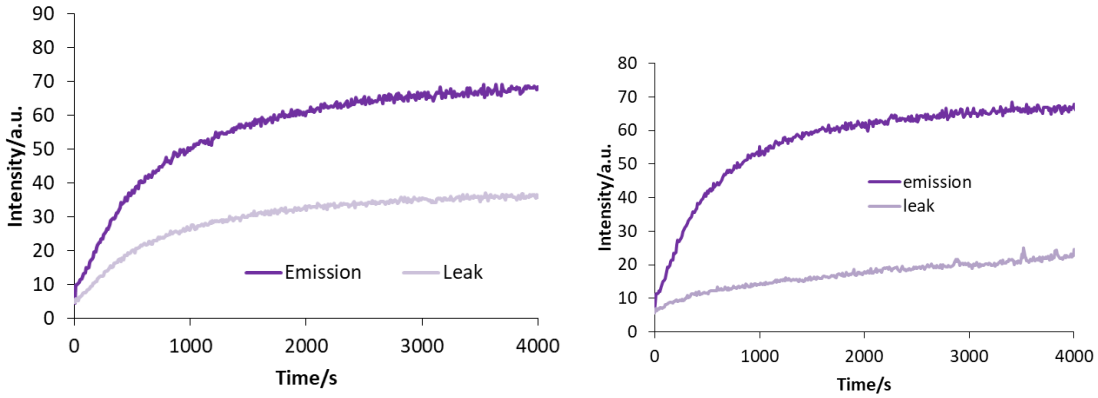

Figure 3.5.2 Fluorescence emission of SNA-mediate D-*a*TNA HCR circuit. Deep and light purple represent the emission and leak in the HCR, respectively. Conditions: ex.=546 nm, em. = 562 nm.20 nM RNA2, (a) S-I3-s1 and (b) S-I3-s2. 100nM DHP1, DHP2. 10 mM phosphate buffer (NaCl= 1M), pH 7.0, 37 °C.

In the agarose gel analysis (Figure 3.5.3), comparing to the products of D-*a*TNA HCR circuit containing S-I3 (lane3), deepened band clearly revealed accelerating effect that caused by incorporation of spacers in the interface (lane 5, 7). Similarly, high efficiency in the reaction has also been confirmed by evaluating the consumption of D-*a*TNA HP1. In conclusion, we have confirmed our assumption and successfully accelerated the strand displacement between RNA/SNA initiator and D-*a*TNA HCR circuit, result in high efficiency of orthogonal signal amplification.

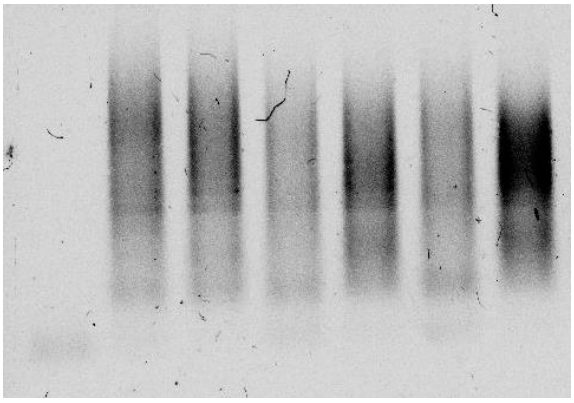

Figure 3.5.3 Agarose gel analysis of SNA-mediate D-*a*TNA HCR circuit. From left to right, Lane 1: Dhp1, Lane 2: S-I3+Dhp1+Dhp2, lane 3: RNA+S-I3+Dhp1+Dhp2, lane 4: S-I3-s1+Dhp1+Dhp2, lane 5: RNA+S-I3-s1+Dhp1+Dhp2, lane 6: S-I3-s2+Dhp1+Dhp2, lane 7: RNA+S-I3-s2+Dhp1+Dhp2. Conditions: 20 nM for target RNA and indicated interface, 100nM for Dhp1, Dhp2 for reaction time of 12 hours, 3 w/v% agarose gel at 100V for 25 min.)

3.5.3 Further incorporation of Nitro Methyl Red

Relatively high leakage in the D-*a*TNA circuit was still a problem for RNA detection. To further improve it, refer to previous work in our laboratory, Mr. Nagao had developed D-*a*TNA circuit with low leakage, which was modified by NMR instead of methyl red. As a result, optimal D-*a*TNA HCR which was conducted by D-*a*TNA input had achieved high signal/leakage ratio and fast kinetics, which had been confirmed by fluorescence-time curve and agarose gel analysis (Figure S3.5.3). Moreover, since D-*a*TNA could not be recognized by nuclease, D-*a*TNA circuit had been characterized with high nuclease tolerance in 10% Fetal Bovine serum (FBS) solution, whereas DNA hairpin was soon digested and exhibited high unspecific emission (Figure S3.5.4).

Table 3.5.3 Sequence design of SNA-mediate D-*a*TNA HCR circuit targeting model RNA2

Target RNA 2	5'-GAUGCAGGUGAUAUUCCAUAGCU-3'
S-I0s	*R*-TCAGACT TACCTTCTACGTCCACTATAAGGTA-*S*
S-I1s	*R*-TCAGACT TACCTTSCTACGTCCACTATAAGGTA-*S*
S-I2s	*R*-TCAGACT TACCTTSSCTACGTCCACTATAAGGTA-*S*
S-I3s	*R*-TCAGACT TACCTTSSSCTACGTCCACTATAAGGTA-*S*
DT-H1	1' –**Y**TCAGACTGATGTTAGTCTGA**N**ATGGAA-3′
DT-H2	3'- TCAGACTTACCTTAGTCTGACTACAA -1′
S= C3-spacer Y= cy3 N= nitro methyl red	

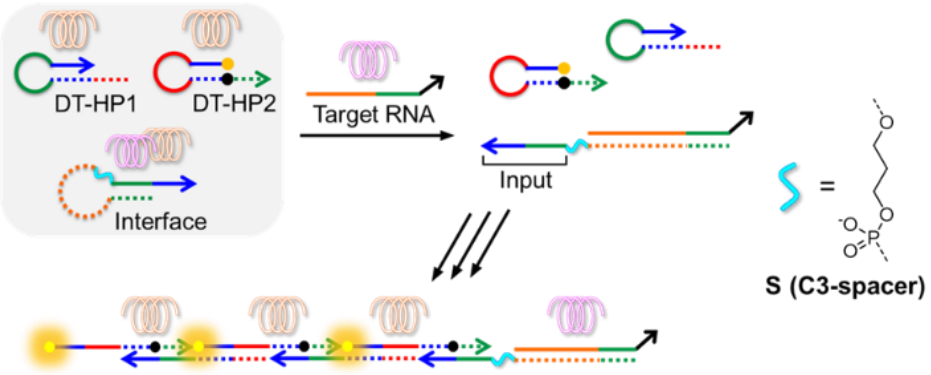

Figure 3.5.4 Schematic of SNA-mediate D-aTNA HCR circuit for RNA detection.

Experimental protocol was same, which was shown in Figure 3.5.4. All the sequences designs were shown in Table 3.5.3, sequence of DT-H1 (DT-HP1 in the Figure 3.5.4) and DT-H2(DT-HP2 in the Figure 3.5.4) has same ratio of stem/loop to pervious hairpins (Dhp1, Dhp2), only serval bases have changed. 4 SNA interface strands were prepared, with 0, 1, 2, and 3 C3-spacers (S-I1s, S-I2s, S-I3s, respectively) between the SNA-overhang and RNA-recognition region to confirm the usefulness of C3-spacer for accelerating signal amplification of D-*a*TNA circuit.

The T_m values of the S-I(n)s stem and of the S-I(n)s/RNA duplex (n=0-4) were very high, over 54 ^{o}C (Figure S3.5.5). Herein these structures are stable under the conditions of circuit operation. Kinetics was shown in Figure 3.5.5. The reaction containing SNA interface with no C-3 spacer exhibited slow kinetics, signal was amplified slowly and hard to reach the equilibrium. As a result, normalizing the emission intensity by the maximum intensity in the reaction containing S-I3s, the reaction efficiency was 30 %, which was very low. With number of C3-spacer increased in the SNA interface, the kinetics gradually increased, like our expectation. Finally, the SNA with 3 C3-spacer exhibited highest rate and efficiency in the reaction, although S-I3s slightly caused extra leakage. Reaction containing S-I2s and S-I1s exhibited limited extra leakage, which was desirable. Take an overall consideriation, SNA-mediate D-*a*TNA HCR circuit for orthogonal RNA detection, S-I2s was regarded as the optimal interface strand due to its fast kinetic with low leakage.

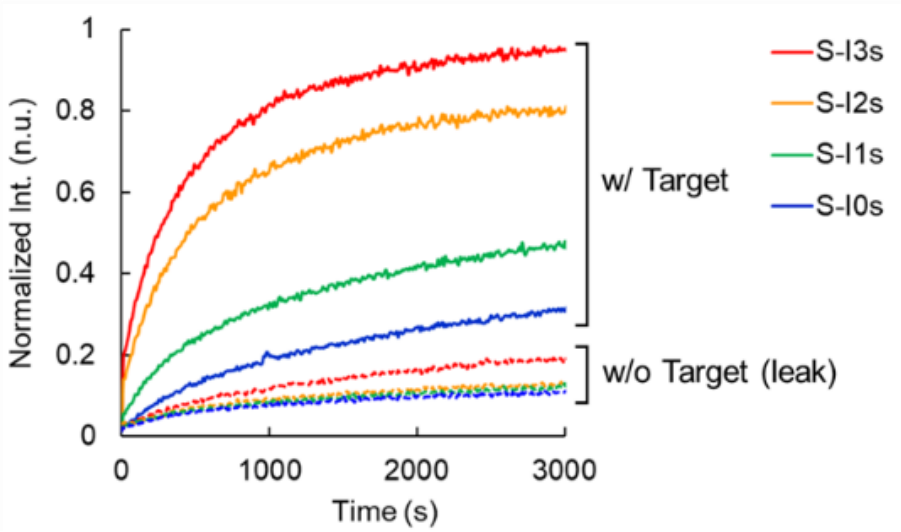

Figure 3.5.5 Kinetics of D-*a*TNA HCR triggered by of the indicated SNA interface and target RNA. Conditions: 37 °C, 10 mM phosphate buffer, 1.0 M NaCl, pH 7.0, 100 nM each hairpin, 20 nM indicated SNA interface, and 20 nM target RNA. Intensities are normalized by maximum intensity of reaction within 0.2 eq corresponding input.

Kinetic without pre-annealing of SNA interface/Target RNA 2 was also be evaluated in Figure 3.5.6. Although we have not designed a toehold for strand displacement between target RNA and SNA interface, addition of RNA in the solution containing SNA interface, DT-H1, and DT-H2 still launched the HCR circuit, due largely to the starting point of reaction on the loop of SNA interface. The kinetics was slower than the reaction conducted by pre-annealed SNA interface/RNA, 25% yields decreased for each SNA interface, respectively. Herein, we have achieved one-step detection for RNA, indicating potential usefulness of this orthogonal signal amplification system for further application, like cell-imagination.

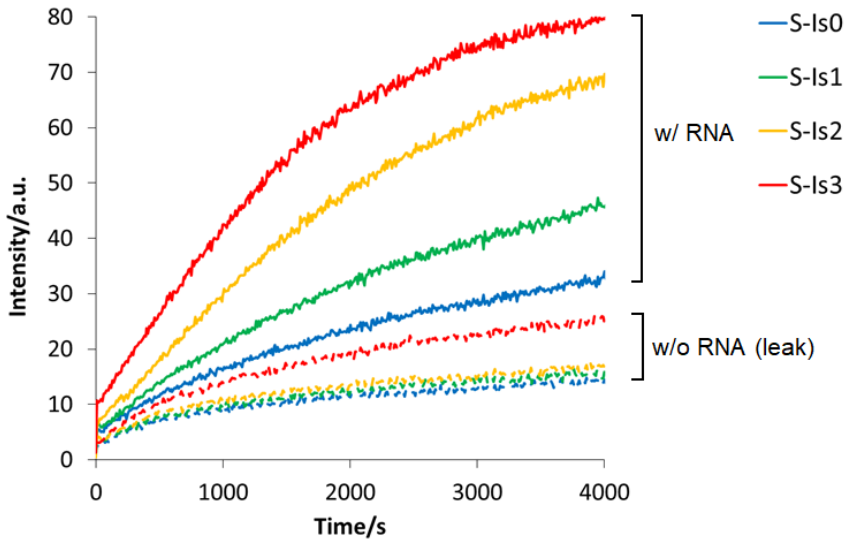

Figure 3.5.6 Kinetics of D-*a*TNA HCR trigger by 20 nM indicated SNA interface and 20 nM target RNA. Target RNA added to the solution including SNA interface, DT-H1, and DT-H2. Conditions: 37 °C, 10 mM phosphate buffer, 1.0 M NaCl, pH 7.0, 100 nM each D-*a*TNA hairpin. Intensities are normalized by maximum intensity of reaction within 0.2 eq corresponding input.

3.5.4 Detecting limitation

As an important factor for fluorescent probe, we finally evaluated detection limitation of SNA-mediate D-*a*TNA circuit. Target RNA2 in different concentrations were pre-annealed with 20 nM S-I2s (constant concentration ensure ease of comparison, since S-I2s was proved to cause no extra leakage), then 100 nM DT-H1 and DT-H2 were added to the solution. As the result shown in Figure 3.5.7, kinetics exhibited concentration dependency: the high RNA concentration was, the fast kinetics in the orthogonal reaction would achieve. Because of relatively higher leakage under high concentration of Na^+, RNA less than 500 pM was hard to be detected by the signal amplification system.

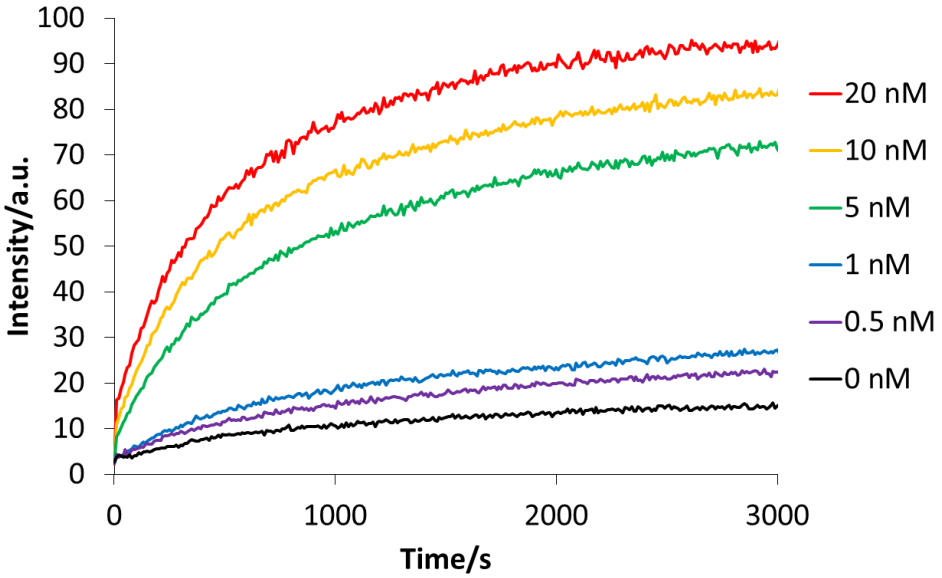

Figure 3.5.7 Kinetics of SNA-mediated D-*a*TNA HCR circuits triggered by different concentration of Target RNA in 10 mM phosphate buffer (NaCl = 1.0 M). Conditions: indicated concentration of Target RNA, 20 nM S-I2s and 100 nM each D-*a*TNA hairpin.

3.6 Dual OR logic gate

3.6.1 Orthogonality confirmation of *a*TNA-HCR circuit

As an attempt, we subsequently developed an orthogonal HCR platform consist of *a*TNA. Sequence designed shown in Table 3.6.1, based on optimal D-*a*TNA HCR circuit, we newly purchased L-aTNA HCR circuit in same sequence to D-*a*TNA HCR (LT-H1, LT-H2, LT-Input). Since L-*a*TNA formed right-handed duplex, it supposed to be orthogonal to D-*a*TNA HCR circuit and conducted individually. Moreover, we designed an SNA input strand, which was supposed to launch both D-*a*TNA and L-*a*TNA circuit, due to its non-helical preference in hybridization. Chemical structures of the fluorophore and quencher shown in Figure 3.6.1 (Cy3 in D-*a*TNA HCR circuit and NMR in both D-*a*TNA and L-*a*TNA circuit, structure of Cy5 has shown before).

Table 3.6.1 Sequence design of *a*TNA dual OR logic gate

S-Input:	(R)- TTGTAGTCAGACT -(S)
DT-Input:	3'-TTGTAGTCAGACT-1'
DT-H1:	1'-AACATCAGTCTGATTCCATTCAGACT-3'

DT-H2:	3’ -AAGGTA**N**AGTCTGATTGTAGTCAGACT-**Y**-1’
LT-Input:	1’-TTGTAGTCAGACT-3’
LT-H1:	3’-AACATCAGTCTGATTCCATTCAGACT-1’
LT-H2:	1’ -AAGGTA**N**AGTCTGATTGTAGTCAGACT-**Cy5**-3’

Y = Cy3, N =Nitro MethylRed

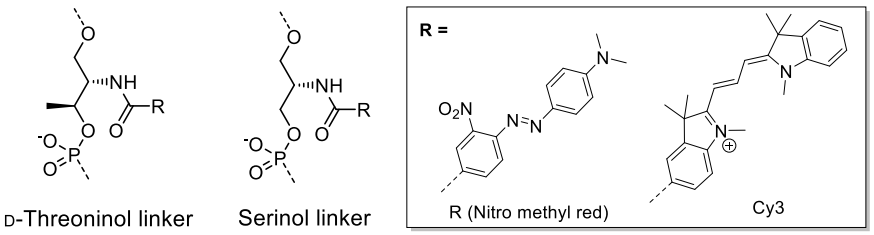

Figure 3.6.1. Chemical structures of Cy3, Cy5, and R (Nitro methyl red). For incorporation of R and Cy3, D-Threoninol linker and serinol was used for D-*a*TNA HCR and L-*a*TNA HCR, respectively.

Firstly, the T_m values of *a*TNA hairpins (LT-H1 and DT-H1, Figure S3.6.1) were determined by fluorescence melting temperature. As a result, both *a*TNA hairpin exhibited very high T_m (over 80 ^{o}C), which could hardly be measured in the fluorescence machine.

Then, we discussed the orthogonality of *a*TNA HCR individually. For the kinetic in Figure 3.6.2 on the left, in the solution containing L-*a*TNA HCR circuit (100 nM LT-H1 and LT-H2), 10 nM different inputs were added to launch the cascade reaction (SNA, D-*a*TNA, L-*a*TNA input). As a result, the L-*a*TNA and SNA conducted the L-*a*TNA HCR circuit by monitor the fluorescence emission Cy5, in contrast, because D-*a*TNA was orthogonal to L-*a*TNA. Even though they are sequence complementary, the emission was still hard to be recognized, which was almost same comparing to the blank group without any input strand in the solution.

Moreover, for D-*a*TNA HCR circuit, similar result was confirmed (Figure 3.6.2 on the right). The orthogonal L-*a*TNA input strand could not conduct the signal amplification of Cy3, whereas SNA and D-*a*TNA input successfully launched the reaction with fast kinetics of fluorescence amplification. As a result, both D-*a*TNA and L-*a*TNA showed a fast kinetics, reaching the equilibrium within 1200 s, which was caused by high rate of strand displacement in initiation phase.

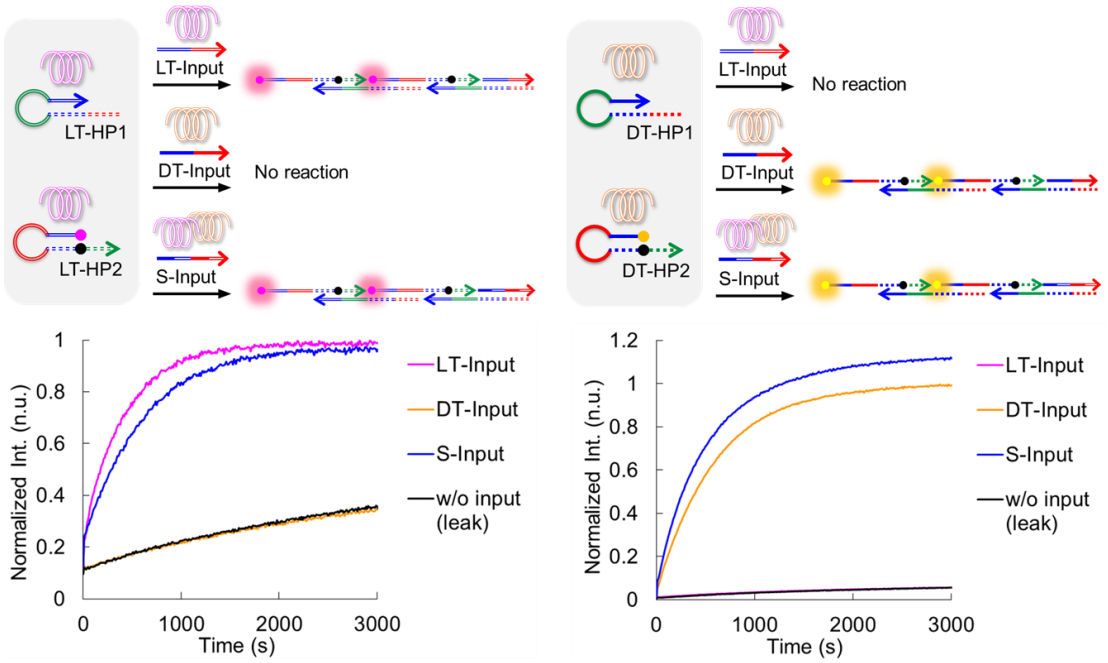

Figure 3.6.2 Fluorescence emissions in the process of HCR. 20 nM indicated input (S-input, LT-input, DT-input), 100nM indicated hcr hairpin (LT-H1+LT-H2 or DT-H1+DT-H2). 10 mM phosphate buffer (NaCl= 1M). Intensities are normalized by maximum intensity of reaction within 0.2 eq corresponding input.

In the agarose gel analysis (Figure 3.6.3, lane 1-8), the distribution of products was consistent to the kinetics of fluorescence emission: comparing to the leak in lane 2 (leak in the L-*a*TNA HCR circuit), in the L-*a*TNA, addition of SNA and L-*a*TNA input caused a high yield of HCR reaction, with many bands containing Cy5 emission upon the substrate (lane 3 and 5). One thing needed to be mentioned that L-*a*TNA caused a high leakage both in the gel and time trace of Cy5 fluorescence, which was possibly caused by large Cy5 molecule. In contrast, no product was visualized in addition of D-*a*TNA input (lane 4). Products of D-*a*TNA HCR in lane 6-8 was similar, comparing to the leak in lane 1, D-*a*TNA and SNA input conducted the HCR circuit (lane 7 and 8), whereas no products was founded in the group within L-*a*TNA input (lane 6).

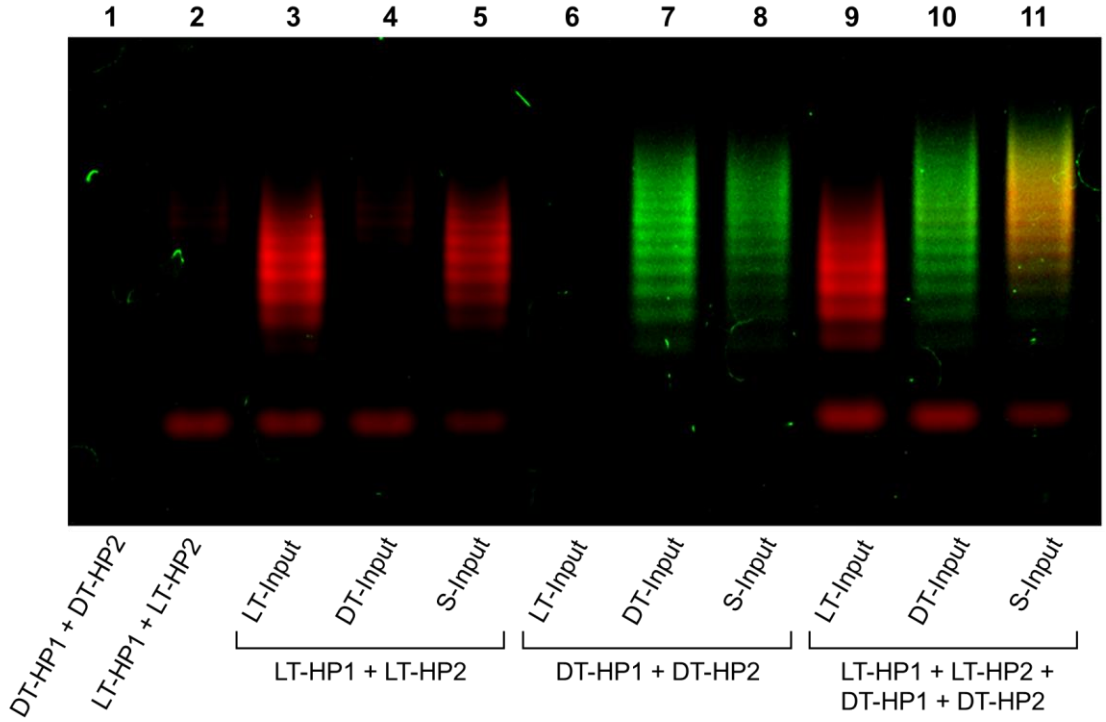

Figure 3.6.3 Agarose gel analysis (3 w/v%) of HCR product after 1h incubation under 37 °C. Lane1, D-*a*TNA hairpins without input; Lane2, L-*a*TNA hairpins without input; Lane 3-5; L-*a*TNA hairpins with indicated input; Lane 6-8, D-*a*TNA hairpins with indicated input; Lane 9-11; mixture of both D- and L-*a*TNA hairpins with indicated input.

3.6.2 Mixed *a*TNA-HCR circuit

Furthermore, orthogonality was confirmed at the existence of both L- and D-*a*TNA HCR. SNA, D-*a*TNA, and L-*a*TNA input were added to the mixture of *a*TNA HCR circuits (100 nM LT-H1, LT-H2, DT-H1, DT-H2, Figure 3.6.4a).

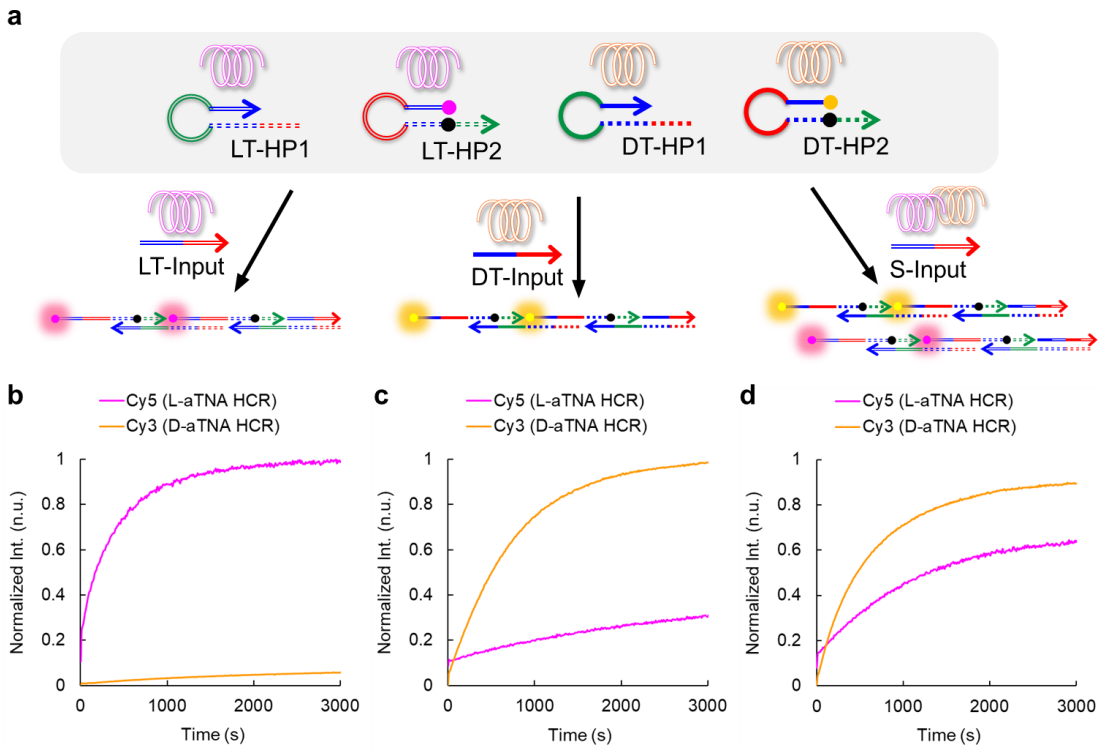

Figure 3.6.4 (a) Schematic illustration of mixed *a*TNA HCR circuit conducted by XNA input strands. (b)Fluorescence emissions in the process of HCR. 20 nM indicated input (S-input, LT-input, DT-input), 100nM L/D hcr hairpin (LT-H1+LT-H2 and DT-H1+DT-H2). 10 mM phosphate buffer (NaCl= 1M). Intensities are normalized by maximum intensity of reaction within 0.2 eq corresponding input.

Emissions in the HCR were normalized by the maximum emission in corresponding 0.2 nM *a*TNA inputs. As a result, signal was again amplified specifically: L-*a*TNA input conducted only L-*a*TNA HCR circuit (Figure 3.6.4b), D-*a*TNA input conducted only D-*a*TNA HCR circuit (Figure 3.6.4c), while SNA input conducted both *a*TNA HCR circuits (Figure 3.6.4d). Amplification kinetics in the presence of S-Input were slower than in the presence of LT-Input and DT-Input strands. We hypothesize that this was due to the competition between HCR circuits, which decreased the effective concentration of initiator for each HCR. Note that total concentration of the circuits (DT-HP plus LT-HP) was doubled in experiments with both *a*TNA hairpins with respect to experiments with individual circuits (Figures 3.6.2), whereas the concentration of S-Input was the same.

Product characterized using agarose gel electrophoresis was consistent with the kinetics (Figure 3.6.3, lane 9-11). Mixed *a*TNA HCR circuits amplified the specific signal to corresponding XNA inputs. These results confirm the remarkably high orthogonality between L-*a*TNA and D-*a*TNA in the HCR circuits and demonstrate that SNA communicates with both L-*a*TNA and D-*a*TNA. This system can be described as

dual OR gate circuits that output two signals responding to input XNAs (Figure 3.6.5 on the left). As the truth table has shown (Figure 3.6.5 on the right), different pattern of output will be confirmed in respond to XNA input strands.

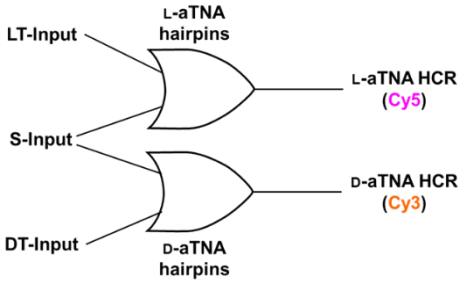

Inputs			Outputs	
LT-Input	DT-Input	S-Input	L-aTNA HCR	D-aTNA HCR
0	0	0	0	0
1	0	0	1	0
0	1	0	0	1
0	0	1	1	1

Figure 3.6.5 Design of dual OR logic gate and the truth table.

3.7 Summary

In conclusion, we have successfully established a platform of acyclic XNA targeting natural RNA.

Firstly, we developed SNA HCR circuit targeting miR20a. Due to strong base-paring interaction, differ to DNA-HCR circuit with at least 12-mer stem which was time consuming, the SNA with short stem/toehold length of 9-8 was designed. For the direction of design of SNA HCR circuit, relatively long stem was recommended. During the detection, because of the great different between SNA/RNA duplex and SNA stem. We found the initiation phase was slow, resulting in weak signal amplification. Then we further incorporated SNA interface which was pre-annealed with miR20a. As our expectation, SNA overhang greatly accelerated the initiation of HCR.

Secondly, we subsequently developed SNA-mediate L-*a*TNA HCR circuit to improve for detection of miR20a. L-aTNA with shorter stem/toehold with length of 6- 7 was further designed. L-*a*TNA in relative high stability in L-*a*TNA/SNA hetero-duplex was compatible to SNA toehold in RNA detection, besides, right-handed bounded state of L-*a*TNA was conformational complementary to SNA overhang in SNA/RNA duplex which was pre-organized to right-handed state. As a result, under high concentration of Na^+, L-*a*TNA exhibited high rate of signal amplification, reaching the equilibrium within 4000 s.

Although D-*a*TNA in left-handed duplex is highly orthogonal to natural nucleic acid, SNA-mediate D-*a*TNA HCR circuit targeting natural RNA was evaluated. We characterized the D-*a*TNA HCR at first, proving high nuclease-resistance and yield in the HCR circuit. Because of helicity propagation, right-handed over in SNA hardly conducted the left-handed D-*a*TNA circuit. Herein we further incorporated C3-spacer to SNA interface, which successfully inhibited the propagation of helicity. The more spacers were modified in the interface, the faster signal amplification could be visualized. As a result, within 2 spacer, S-I2s could effectively transmitted the information of RNA to the D-*a*TNA HCR circuit within about 1500 seconds.

To best of our knowledge, this is the first report for hetero-chiral HCR circuit for detection of RNA. High orthogonality and nuclease-resistance enable minimization cross-hybridization of unspecific genetic materials in the future visualization *in vivo*. Overall, this work has revealed the potential of acyclic nucleic acid including SNA, L-*a*TNA and D-*a*TNA, which could serve as material of molecular organization and assembly for executing molecular process in biological system.

3.8 Appendix

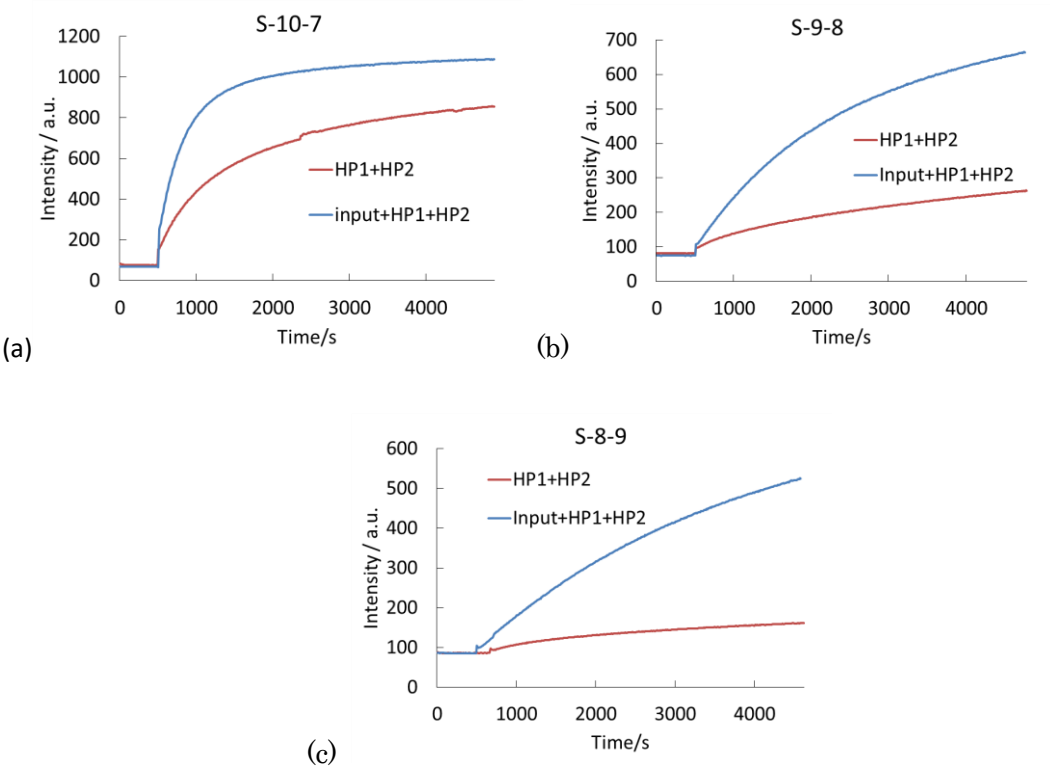

Figure S3.3.1 Kinetics of (a) S-10-7, (b) S-9-8, and (c) S-8-9 circuits triggered by miR20a. 1 μM miR20a and 1 μM indicated HP1, HP2 in 10 mM phosphate buffer containing 100 mM NaCl, pH=7.0, 37 °C, Ex.= 546nm; Em. = 562 nm.

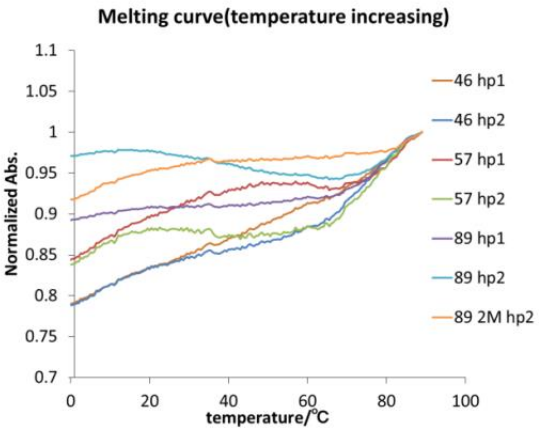

	Tm
46 hp1	78.7
46 hp2	76.6
57 hp1	83.8
57 hp2	77.8
89 hp1	78.9
89 hp2	82.4

Figure S3.3.2 UV melting curves of SNA hairpins. Conditions: 100 mM NaCl in 10 mM phosphate buffer, pH=7.0, 90-0 °C, [HP1] =[RNA]= 0.5 μM. T_ms were average of heating and cooling absorbance melting curves.

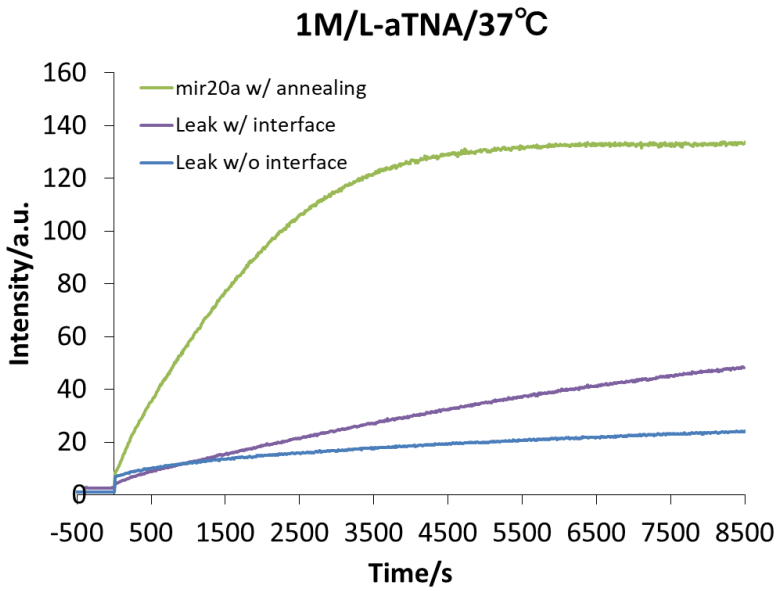

Figure S3.4.1 Fluorescence emission in the process of HCR. Green, purple and blue line represent to the experimental group within mir20a/S-I2 duplex input, leak within S-I2 and leak without S-I2, respectively. 100nM indicated input and 500 nM LHP1, LHP2. 10 mM phosphate buffer (NaCl= 1 M).

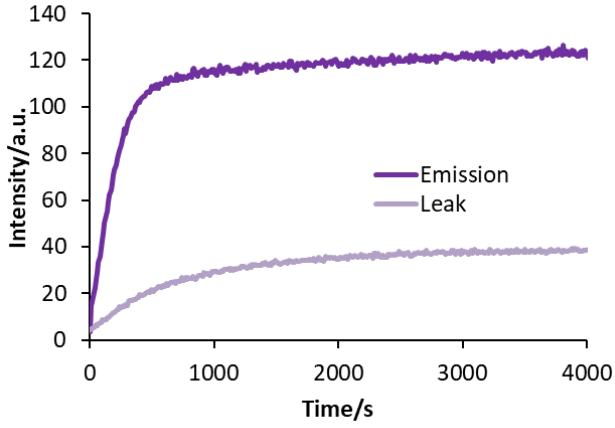

Figure S3.5.1 Fluorescence emission in the process of HCR. Deep and light purple represent the emission and leak in the HCR, respectively. 20 nM target Dinput1 (1'-AGCTACTGATGTT-3'), 100nM DHP1 and DHP2. 10 mM phosphate buffer (NaCl= 1M).

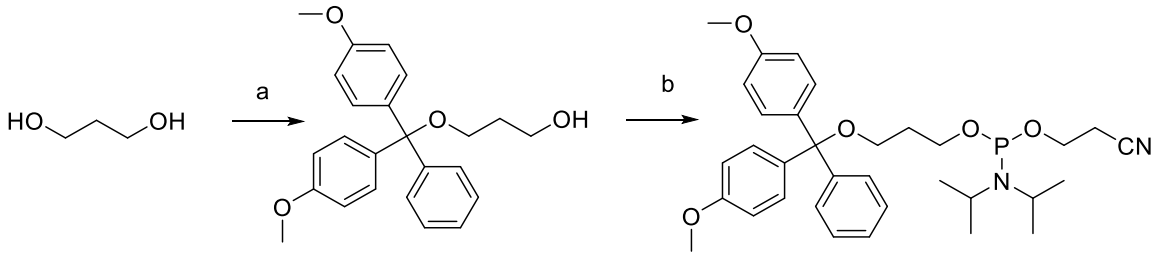

Figure S3.5.2 Synthesis of C3-spacer. a) DMT-Cl, dry pyridine r.t. 4h. Column chromophotograph (chloroform: hexane: trimethylamine=50:50:3). b) 2-Cyanoethyl Diisopropylchlorophosphoramidite under 30min ice bath and 1h r.t. column chromophotograph (ethyl acetate: hexane: trimethylamine=17:84:3). Total yield: 54%.

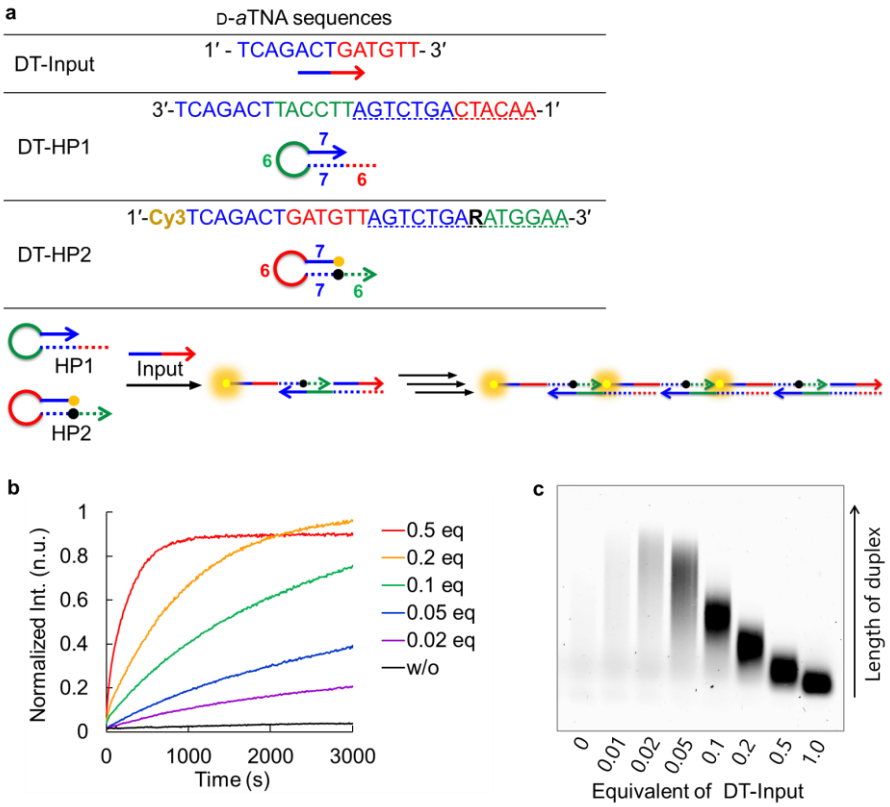

Figure S3.5.3 (a) Sequence design and schematic illustration of D-*a*TNA HCR circuit. (b) Time trace of signal generated from D-*a*TNA HCR triggered by DT-Input with indicated equivalents of each hairpin. Conditions: 37 °C, 10 mM phosphate buffer, 100 mM NaCl, pH 7.0, 100 nM DT-HP1, 100 nM DT-HP2. Fluorescence intensity was normalized by the maximum emission of the *a*TNA HCR trigger by 20 nM DT-Input. (c) Agarose gel analysis (2 w/v%) of the D-*a*TNA HCR product after 2 h with indicated amount of DT-Input. Intensities are normalized by maximum intensity of reaction within 0.2 eq corresponding input.

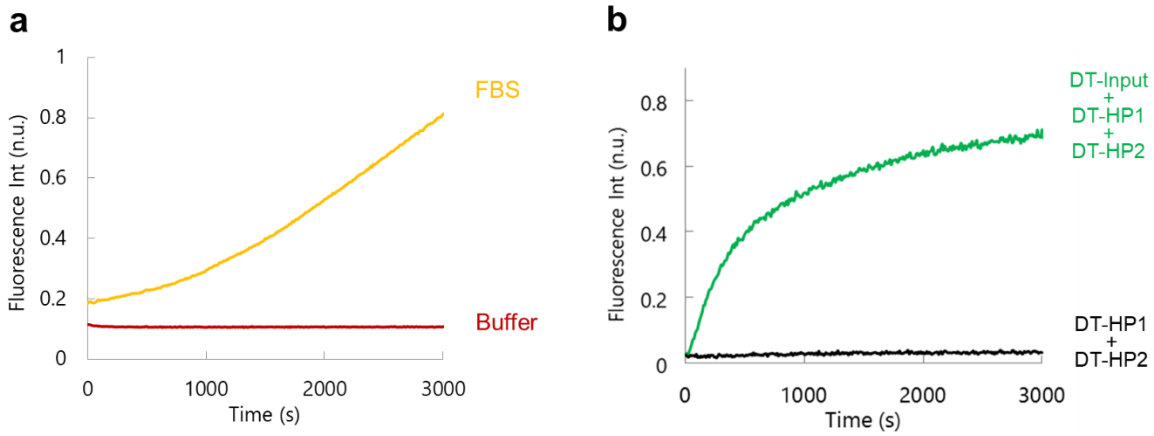

Figure S3.5.4 (a) Normalized fluorescence emission of 100 nM DNA-hairpin (5'-**Cy3**-CTAGACTCATGTTAGTCTAG**N**CACGTA-3') in 10% Fetal Bovine serum (FBS, orange line) and 10 mM phosphate buffer (NaCl= 100 mM, red line). (b) Kinetics of D-*a*TNA HCR circuits triggered by 10 nM DT-input in 10% FBS. Intensities are normalized by maximum intensity of reaction within 0.2 eq corresponding input.

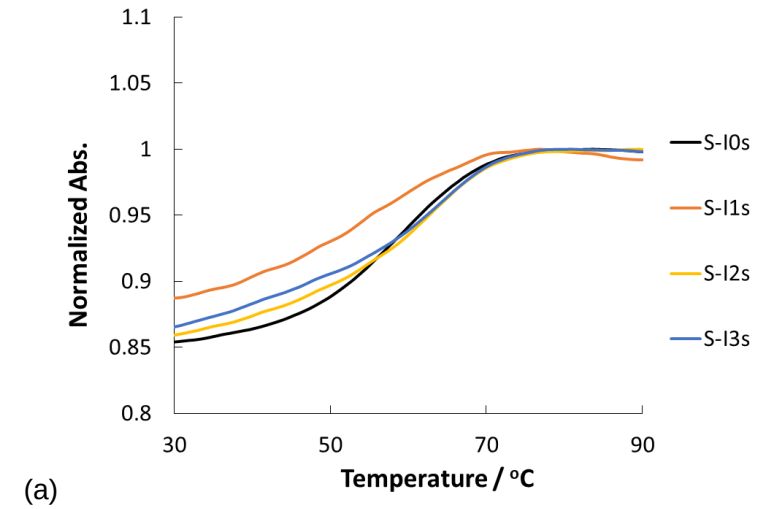

(a)

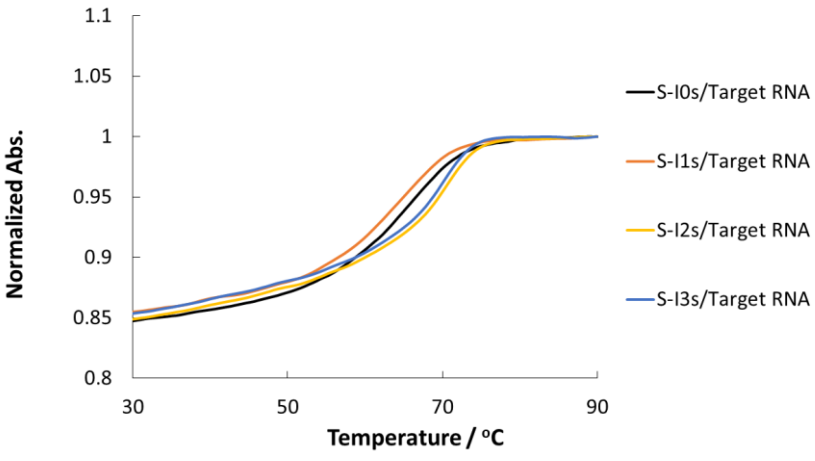

(b)

Figure S3.5.5 UV-melting curves of SNA interface (S-I(n)s) and S-I(n)s/RNA duplex. Conditions: [S-I(n)s] = [Target RNA] = 2.0 µM in 10 mM phosphate buffer ([NaCl] = 1.0 M). T_m of S-I(n)s and S-I(n)s/RNA : 59.6 °C and 65.8 °C (n=0), 54.7 °C and 64.8 °C (n=1), 63.2 °C and 70.4 °C (n=2), 63.9 °C and 69.9 °C (n=3).

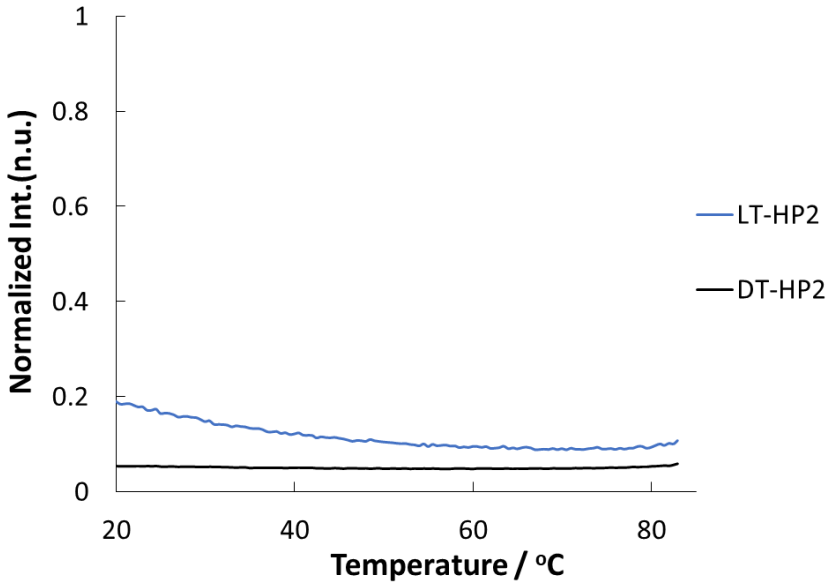

Figure S3.6.1 Fluorescence-temperature melting curves of LT-HP2 and DT-HP2. Conditions: [DT-HP2] = [LT-HP2] = 100 nM in 10 mM phosphate buffer ([NaCl] = 200 mM), pH 7.0. Fluorescence intensity was normalized to the maximum emission after saturation of the reaction in the presence of 20 nM corresponding *α*TNA input strand. Intensities are normalized by maximum intensity of reaction within 0.2 eq corresponding input.

3.9 Reference

[1] F. C. Simmel, B. Yurke, H. R. Singh, *Chem. Rev.* **2019**, *119*, 6326–6369.

[2] K. Sakamoto, H. Gouzu, K. Komiya, D. Kiga, S. Yokoyama, T. Yokomori, M. Hagiya, *Science (80-.).* **2000**, *288*, 1223–1226.

[3] B. Yordanov, J. Kim, R. L. Petersen, A. Shudy, V. V. Kulkarni, A. Phillips, *ACS Synth. Biol.* **2014**, *3*, 600–616.

[4] G. Seelig, D. Soloveichik, D. Y. Zhang, E. Winfree, **2006**, *314*, 1585–1589.

[5] E. E. Watson, S. Angerani, P. M. Sabale, N. Winssinger, *J. Am. Chem. Soc.* **2021**, *143*, 4467–4482.

[6] F. Xuan, I. M. Hsing, *J. Am. Chem. Soc.* **2014**, *136*, 9810–9813.

[7] D. Y. Zhang, S. X. Chen, P. Yin, *Nat. Chem.* **2012**, *4*, 208–214.

[8] S. Angerani, N. Winssinger, *J. Am. Chem. Soc.* **2020**, *142*, 12333–12340.

[9] W. Meng, R. A. Muscat, M. L. McKee, P. J. Milnes, A. H. EL-Sagheer, J. Bath, B. G. Davis, T. Brown, R. K. O'Reilly, A. J. Turberfield, *Nat. Chem.* **2016**, *8*, 542–548.

[10] J. R. McMillan, O. G. Hayes, J. P. Remis, C. A. Mirkin, *J. Am. Chem. Soc.* **2018**, *140*, 15950–15956.

[11] B. Yurke, A. J. Turber, A. P. M. Jr, F. C. Simmel, J. L. Neumann, *Nature* **2000**, *406*, 605–608.

[12] F. Wang, C. H. Lu, I. Willner, *Chem. Rev.* **2014**, *114*, 2881–2941.

[13] K. Murayama, R. Nagao, H. Asanuma, *ChemistrySelect* **2017**, *2*, 5624–5627.

[14] R. M. Dirks, N. A. Pierce, *Proc. Natl. Acad. Sci. U. S. A.* **2004**, *101*, 15275–15278.

[15] J. C. Chaput, P. Herdewijn, *Angew. Chemie - Int. Ed.* **2019**, *58*, 11570–11572.

[16] K. Murayama, H. Asanuma, *ChemBioChem* **2021**, *22*, 2507–2515.

[17] V. B. Pinheiro, P. Holliger, *Curr. Opin. Chem. Biol.* **2012**, *16*, 245–252.

[18] C. J. Leumann, *Bioorganic Med. Chem.* **2002**, *10*, 841–854.

[19] S. Klußmann, A. Nolte, R. Bald, V. A. Erdmann, J. P. Fürste, *Nat. Biotechnol.* **1996**, *14*, 1112–1115.

[20] I. Sacui, W. C. Hsieh, A. Manna, B. Sahu, D. H. Ly, *J. Am. Chem. Soc.* **2015**, *137*, 8603–8610.

[21] W. C. Hsieh, G. R. Martinez, A. Wang, S. F. Wu, R. Chamdia, D. H. Ly, *Commun. Chem.* **2018**, *1*, Article number: 89.

[22] C. A. Figg, P. H. Winegar, O. G. Hayes, C. A. Mirkin, *J. Am. Chem. Soc.* **2020**, *142*, 8596–8601.

[23] W. J. Kim, Y. Sato, T. Akaike, A. Maruyama, *Nat. Mater.* **2003**, *2*, 815–820.

[24] H. Kashida, K. Nishikawa, W. Shi, T. Miyagawa, H. Yamashita, M. Abe, H. Asanuma,

Chem. Sci. **2021**, *12*, 1656–1660.

[25] N. Kundu, B. E. Young, J. T. Sczepanski, *Nucleic Acids Res.* **2021**, *49*, 6114–6127.

List of related publications

"A triplex-forming linear probe for sequence-specific detection of duplex DNA with high sensitivity and affinity"

Chen, Y.; Murayama, K.; Kashida, H.; Kamiya, Y.; Asanuma, H.

Chem. Commun. **2020**, *56*, 5358-5361. DOI: 10.1039/D0CC01865A

Selected as a "Back Cover"

"Signal Amplification Circuit Composed of Serinol Nucleic Acid for RNA Detection"

Chen, Y.; Murayama, K.; Asanuma, H.

Chem. Lett. **2022**, Accepted

"Orthogonal amplification circuits composed of acyclic nucleic acids enable RNA visualization"

Chen, Y.; Nagao, R.; Murayama, K.; Asanuma, H.

J. Am. Chem. Soc. Submitted

List of related presentations

Chen, Y., "Liner Probe for Direct Visualization of Duplexed DNA", Nagoya Univ.-Tshinghua Univ.-Toyota Motor Corp.-Hokkaido Univ. Joint. Symposium (NTTH 2019), Hakodate(Japan), July 29-31, 2019

Chen, Y.; Murayama, K.; Asanuma, H. "Sensitive triplex-forming linear probe tethering perylene derivatives for duplex DNA detection with high affinity", The International Chemical Congress of Pacific Basin Societies 2021. (Pacifichem 2021), Online, December 16-21, 2021

Acknowledgement

At the end of the thesis, I would like to appeal my pleasure to all the people who has supported me since I studied abroad.

I thank Dr. Hiroyuki Asanuma, who is my supervisor. He is a strange but good guy, except for pointing the direction of my research work, he taught me how to think logically for the experiments, and how to express my perspective properly to other researchers clearly. He helped me a lot in my third year of doctoral course. I could not graduate smoothly without his quick response and kind help.

I thank Dr. Keiji Murayama, who is my secondary supervisor. He is an omnipotent person who can solve (almost) all the problems from the repairment of machine to the design of experiments in Asanuma lab. I think he is an inborn researcher, who is smart, patient, and always devote himself to science. Besides, he has a very nice sense in both science and aesthetic. He also helped me a lot at end of my doctoral course, especially in the revision of the paper.

I thank Dr. Hiromu Kashida and Dr. Yukiko Kamiya. They have given me lots of advises in the development of linear probe. Their perspective in the physical-chemistry and cellular biology really helped me a lot.

I also thank my co-workers, especially the people in Asanuma lab, Yu Arimura, Tomonari Mizuno, Noriko Yokoda, Yuki Shigematsu, and Yuta Kokubo. Although I could hardly speck Japanese, they helped me with Japanese through the daily conversation, hope we can meet each other again in the future. Yuhei Yamano taught me the skills in the chemical synthesis, which really helped me as an undergraduate student major in bioinformatics. Zehua Liu and I have kept a long relationship in the lab, we helped each other in the research, I really hope his work would go well in the future.

My special thank is given to LOTTE Co., Ltd. Scholarship and Graduate Program of Transformative Chem-Bio Research (GTR), without those financial support I cannot focus on the research during the doctoral course.

Finally, I would like to thank my father and mother. They always stand behind me during my graduate life, their understanding and supports are the largest motivation of me.